INSTITUTO DE PESQUISAS ENERGÉTICAS E NUCLEARES

Autarquia Associada à Universidade de São Paulo

Towards new therapeutic strategies for cutaneous leishmaniasis

FERNANDA VIANA CABRAL

A thesis submitted to obtain the degree of Doctor in Science in Nuclear Technology - Materials

Advisor:
Prof. Dr. Martha Simões Ribeiro

São Paulo
2021

INSTITUTO DE PESQUISAS ENERGÉTICAS E NUCLEARES

Autarquia Associada à Universidade de São Paulo

Towards new therapeutic strategies for cutaneous leishmaniasis

Versão Corrigida
Versão Original disponível no IPEN

FERNANDA VIANA CABRAL

A thesis submitted to obtain the degree of Doctor in Science in Nuclear Technology - Materials

Advisor:

Prof. Dr. Martha Simões Ribeiro

São Paulo

2021

Como citar:

VIANA CABRAL, F. ***Towards new therapeutic strategies for cutaneous leishmaniasis***. 2021. 123 f. Tese (Doutorado em Tecnologia Nuclear), Instituto de Pesquisas Energéticas e Nucleares, IPEN-CNEN, São Paulo. Disponível em: ‹http://repositorio.ipen.br/› (data de consulta no formato: dd/mm/aaaa)

Ficha catalográfica elaborada pelo Sistema de geração automática da Biblioteca IPEN, com os dados fornecidos pelo(a) autor(a).

Viana Cabral, Fernanda
Towards new therapeutic strategies for cutaneous leishmaniasis / Fernanda Viana Cabral; orientadora Martha Simões Ribeiro. -- São Paulo, 2021.
123 f.

Tese (Doutorado) - Programa de Pós-Graduação em Tecnologia Nuclear (Materiais) -- Instituto de Pesquisas Energéticas e Nucleares, São Paulo, 2021.

1. Cutaneous leishmaniasis. 2. Photodynamic therapy. 3. Nitric oxide . 4. Chitosan nanoparticles. 5. OLEDs. I. Simões Ribeiro, Martha , orient. II. Título.

ACKNOWLEDGEMENTS

I would like to thank God without whom nothing is possible.

I would like to thank my parents, Olavo and Sylma, for supporting me emotionally and financially so that I may pursue my higher education. I would like to express my deep gratitude to my partner, Armando, for his love, support, and for always encouraging me to do my best.

I extend my gratitude to my supervisor and friend Prof. Dr. Martha Simões Ribeiro for all scientific and emotional support, ideas, suggestions, encouragement through all these years and for giving me the opportunity to conduct my thesis. My project wouldn't have been completed without all her help.

I would like to express my sincere gratitude to Prof. Dr. Terry K. Smith for all the help, support and for giving me the opportunity to work in his lab, allowing me to learn and expand my skills.

I sincerely thank Prof. Dr. Ifor D.W. Samuel for the learning experience, for giving me the chance to take part in the OLEDs project, which I am sure will be helpful throughout my career.

I am also thankful to Prof. Dr. Mauro Javier Cortez for allowing me to work in his lab where I was able to carry out my research project. I also appreciate all support, professional advice and expertise.

I would like to thank Prof. Dr. Amedea B. Seabra for all collaboration, expertise, ideas and providing the nanoparticles.

I am also thankful to Prof. Dr. Silvia Reni Bortolin Uliana for guidance, support and providing the *Leishmania* strains.

I would like to acknowledge my friends and colleagues from my research group in Brazil, Tania, Camila Ramos, Ismael, Mayara, Carol, Saulo, Caetano, Camila Salvego, and also my friends and colleagues in the UK, Michela, Saydulla, Cheng, Louise, Simon, Will, Leigh-Ann, Sarah, Rebecca and Rachel who have supported and encouraged me.

I would like to thank all my friends and family for being so understanding and supportive all these years. It’s comforting to know that I have such caring people surrounding me.

I would like to thank all the people at Center for Lasers and Applications at IPEN. I also would like to thank the laboratory animal facility at IPEN and CEFAP for all the help with animals.

I also acknowledge Conselho Nacional do Desenvolvimento Científico e Tecnológico (CNPQ). Comissão Nacional de Energia Nuclear (CNEN), à Coordenação de Aperfeiçoamento de Pessoal de Nível Superior (CAPES, #88887.364974/2019-00) and FAPESP for my scholarship and financial support.

Thank you!

“If I have seen further, it is by standing on the shoulders of Giants”

Isaac Newton,1675

Towards new therapeutic strategies for cutaneous leishmaniasis

FERNANDA VIANA CABRAL

ABSTRACT

Cutaneous leishmaniasis (CL) is a zoonotic disease developed by protozoa parasites of genus *Leishmania.* It promotes destructive and ulcerated lesions with limited treatment options. There is an urgent need for the development of topical, cost-effective and efficacious treatments with minimized side effects to treat affected patients. The parasite-host interaction is of great importance since *Leishmania* parasites survive and replicate within host macrophages. As phagocytic cells, the activated macrophages produce reactive oxygen species (ROS) and nitric oxide (NO), which are toxic to pathogens, hence preventing parasites proliferation. However, *Leishmania* parasites can evade the host immune response and subvert antimicrobial macrophage defenses, thereby surviving within these cells even in harsh conditions. Indeed, the role played by ROS and NO in the control of CL has been under debate over the past years, emerging as potential alternatives to tackle this important neglected disease. In this regard, we aimed to evaluate the role of both NO and ROS towards antileishmanial activity using two different therapeutic strategies: (1) nitric oxide-releasing chitosan nanoparticles (NONPs) and (2) antimicrobial photodynamic therapy (PDT). For this, we focused on development and investigation of the potential of NONPs *in vitro* and *in vivo* against *Leishmania amazonensis,* one of the causative agents of CL. To assess the role of ROS, photodynamic therapy was investigated against different *Leishmania* species. Firstly, we evaluated the potential of organic light-emitting diodes (OLEDs) as a novel light source to inactivate *in vitro* promastigotes of *L. major* and *L. amazonensis*, using three phenothiazine dyes: Methylene blue, new methylene blue and 1,9-dimethyl methylene blue (DMMB). Then, we addressed the underlying mechanisms of DMMB-PDT upon promastigotes of *L. amazonensis wild-type* (WT) and miltefosine-resistant (MFR) strains. DMMB-PDT effectiveness was also evaluated against intracellular amastigotes of WT and MFR together with cytotoxicity assay on mammalian cells. Our findings demonstrate that either NONPs or PDT are promising strategies to target CL and should be further explored for future preclinical and clinical trials.

Buscando novas estratégias terapêuticas para o tratamento de leishmaniose cutânea

FERNANDA VIANA CABRAL

RESUMO

Leishmaniose é uma zoonose desenvolvida por protozoários do gênero Leishmania. A leishmaniose cutânea (LC) abrange lesões destrutivas e ulceradas que podem evoluir para condições mais graves culminando em óbito dos hospedeiros. Tratamentos alternativos têm sido implementados com a finalidade de promover maior eficácia e menores efeitos colaterais aos pacientes. A interação patógeno-hospedeiro é de fundamental importância já que os parasitos se multiplicam no interior de macrófagos dos hospedeiros. Essas células são capazes de produzir grandes quantidades de oxigênio (ROS) e óxido nítrico (NO), promovendo a morte de diversos patógenos. Entretanto, esses protozoários são capazes de evadir o sistema imune do hospedeiro sobrevivendo no interior dessas células mesmo em ambientes hostis. Dessa forma, o equilíbrio entre parasito e resposta imune do hospedeiro possui fundamental importância na susceptibilidade e resistência do indivíduo à infecção por *Leishmania.* De fato, ROS e NO possuem uma função muito relevante no controle da leishmaniose. Nesse contexto, nós nos propusemos a avaliar as funções de ambas as moléculas como potenciais agentes terapêuticos no combate à LC. No presente estudo foram sintetizadas nanopartículas contendo doadores de óxido nítrico (NONPs) e avaliadas na inativação *in vitro* e *in vivo* de *L. amazonensis.* Para avaliarmos o papel das ROS, os efeitos da terapia fotodinâmica (PDT) foram investigados contra diferentes espécies do protozoário. Inicialmente, avaliamos o potencial de LEDs orgânicos (OLEDs) como fonte de luz para PDT na inativação das espécies de *L. amazonensis* e *L. major* utilizando três fotossesibilizadores pertencentes à classe das fenotiazinas: Azul de metileno, novo azul de metileno e 1,9-dimetil azul de metileno (DMMB). Posteriormente investigamos os possíveis mecanismos de ação envolvidos na morte de promastigotas de *L. amazonensis WT* e resistentes à miltefosina (MFR). Finalmente, investigamos a eficácia do DMMB-PDT na morte de amastigotas intracelulares de *L. amazonensis* WT e MFR. Ensaios de citotoxicidade em fibroblastos e macrófagos também foram investigados. Nossos resultados demonstram que tanto as NONPs quanto a PDT são estratégias promissoras para o tratamento de LC, portanto, podem ser exploradas em futuros ensaios pré-clínicos e clínicos.

TABLE OF CONTENTS

1. INTRODUCTION

Leishmaniasis is a complex of tropical neglected diseases caused by multiple species of protozoan parasites of the genus *Leishmania spp.* which belongs to the family Trypanosomatidae.[1] It is a vector-borne disease with a worldwide distribution across nearly 100 endemic countries.[2] Since it is a poverty-related disease, it receives little attention from funding agencies or healthcare services.[3] However, it has been listed by World Health Organization (WHO) as one of the most important neglected disease for which the development of new treatments are urgently needed.[2]

Pentavalent antimonials have been the standard drug for over 60 years, and amphotericin B as a second-line treatment for unresponsive cases.[4,5] However, those treatments are based on a long-term intravenous regimen which are highly toxic and expensive, thereby resulting in poor patient compliance, treatment failure and selection of drug-resistant pathogens.[6] Miltefosine has been recently introduced as an oral antileishmanial agent, however, because of the decreased efficacy and increased relapse rate, its use has been restricted in several countries.[5,6]

Leishmania spp. comprise an extra and intracellular phase of life cycle, alternating between two morphological and biochemical distinct forms, defined as promastigotes and amastigotes.[2,7] The extracellular promastigote corresponds to a flagellated and motile form which develops within the gut of the sandfly vector. The disease is then transmitted by the bite of female phlebotomine sandflies during their bloodmeal, where metacyclic (infective stage) promastigotes are inoculated in the mammalian host.[7] Once inside the host, promastigotes are phagocytized and differentiated into amastigotes within phagocytic cells, mostly macrophages.[7,8] Amastigotes (interiorized flagellum) belong to the obligatory intracellular stage of parasites cycle, where they develop and proliferate by binary fission within phagolysosome-like structures, referred to as parasitophorous vacuole (PV) (Figure 1.1).[8]

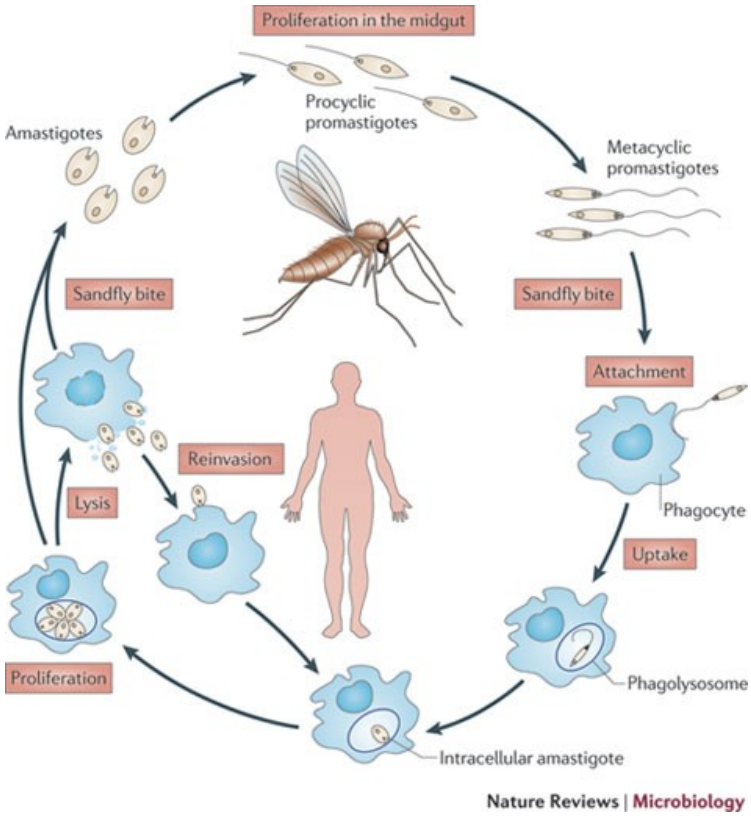

Figure 1.1. Life cycle of *Leishmania* parasites.[7]

1.1 Cutaneous leishmaniasis clinical presentations

There are two main clinical forms: Visceral leishmaniasis and cutaneous leishmaniasis (CL). The visceral form is potentially fatal, affecting internal organs such as the liver, spleen and bone marrow.[2] CL is not usually life-threatening, however, it may have an important psychological impact on patients, leading to serious social stigma.[2,9]

CL displays a wide spectrum of clinical manifestations, in which the most used classifications encompass (1) Localized cutaneous leishmaniasis (LCL), (2) mucocutaneous leishmaniasis (ML), and (3) diffuse cutaneous leishmaniasis (DCL).[10]

LCL clinical presentations range from a single papule at the site of infection to chronic ulcerative lesions with a raised outer border.[10] It might also be scaling with inflammatory exudate covered by a crust.[11] The disseminated form might be a variant clinical manifestation of LCL and is characterized by multiple lesions in two or more different parts of the body.[2]

ML is one of the most severe forms of CL and can be locally destructive to the nasopharyngeal mucosa, thereby promoting deformities on the face of affected individuals.[12,13] It is often referred to as metastatic CL due to the parasite dissemination from the original site of lesion to the oropharynx, nose and mouth via lymphatic and hematogenous system.[13] This clinical feature could potentially be life-threatening and is related to immunocompromised patients.[2]

The diffuse (DCL) presentation, also known as anergic CL, is linked to the lack of immune response, developing erythematous nodular lesions over the entire individual's body, including the face, resembling lepromatous leprosy.[2,12] Lymphedema and fever are symptoms usually observed, and these patients are unresponsive to current treatments in most of the cases.[13]

1.2 New World and Old World leishmaniasis

Leishmaniasis are also classified based on the geographic distribution, defined as New World and Old World leishmaniasis owing to the wide range of *Leishmania* species. The Old World comprises arid and semiarid countries in Asia, Africa, Middle East and Southern Europe.[1,13] New World CL are found in tropical and subtropical regions of South America, Central America and Mexico.[1]

The most common etiological agents of CL in the Old World comprise *L. major* and *L. tropica*.[1] They develop LCL and even though lesions might be self-healing, they often result in persistent scars.[2]

The most prevalent and infective species in the New World involve the *L. mexicana* complex (subgenus *Leishmania)*, including *L. (Leishmania) amazonsensis,* and *L. braziliensis* complex (subgenus *Viannia),* such as *L. (Viannia) braziliensis.*[1,2] The subgenus is defined according to the location where promastigotes develop and attach in the gut of sandflies vectors.[14] The *L. mexicana* complex undergo development in the midgut and foregut, whereas *L. braziliensis* complex develop only in the hindgut of sandflies.[14]

L. braziliensis promote LCL that can progress to the ML form due to an imbalanced immune response, which leads to an exacerbated Th1-type cell response and low number of parasites in the lesions.[2,7] Conversely, *L. amazonensis* can promote LCL and DCL. The latter is attributed to a low Th1-type and predominant Th2-type response.[7] The amastigote forms of *L. mexicana* complex

parasites are well-known for dwelling within large PVs containing a large number of parasites within the lesions.[15] It has been shown that large PVs enable amastigotes to survive even in inhospitable enviornments.[15,16]

1.3 The role of immune response in CL pathogenesis

The parasite-host interaction is of great importance since *Leishmania* parasites dwell and proliferate inside the host's macrophages.[17] As phagocytic cells, the activated macrophages produce reactive oxygen species (ROS) and reactive nitrogen species (RNS), such as nitric oxide (NO), which are highly toxic to pathogens, hence preventing parasites proliferation.[17,18]

The course of disease is determined since the early phase of infection by the host innate immune response with the rapid recruitment of neutrophils and inflammatory monocytes at the site of parasite inoculation.[7] Indeed, monocytes may differentiate into monocyte-derived dendritic cells and migrate to lymph nodes, which leads to a protective immune response Th1 cell type-mediated.[7,19] The cell-mediated response enables macrophage activation releasing NO and ROS, therefore conferring resistance to *Leishmania* infection.[7,20]

Conversely, Th2-type response encompass the humoral immunity or antibody-mediated immunity. It has been known as a non-protective response and it has been attributed to susceptibility to infection since macrophages are inhibited.[7,20,21]

Moreover, *Leishmania* species can also evade the host immune system and subvert antimicrobial macrophage defenses surviving within these cells even in harsh conditions.[22,23] It has also been shown that some *Leishmania* species may also play a role on the stimulation of Th2 cell response rather than Th1.[20,21]

Thus, the interplay between parasites and the host immune response is indispensable to determine resistance or susceptibility to *Leishmania* infection. Although this mechanism is best understood for animal models, it can help elucidate the complexity of Th1/Th2 paradigm over humans and *Leishmania* species.[7,21]

1.4 Nitric oxide and reactive oxygen species

The role played by NO and ROS in the control of CL has been under debate over the past years, both emerging as potential alternatives to tackle this important neglected disease.[18]

Nitric oxide is an important biological molecule responsible for several cellular signaling pathways, physiologic functions, and antimicrobial activities against a broad range of intracellular pathogens.[24] As mentioned earlier, NO production relies on activated macrophages induced by Th1 cell response. Proinflammatory cytokines, such as IFN-γ and TNF-α induce the expression of inducible nitric oxide synthase (iNOS), which converts L-arginine to L-citruline and NO.[18,24] Alternatively, Th2 type response leads to the expression of arginase, rather than iNOS, therefore L-arginine is used as a substrate for the synthesis of polyamines, which contributes for parasites proliferation (Figure 1.2).[25]

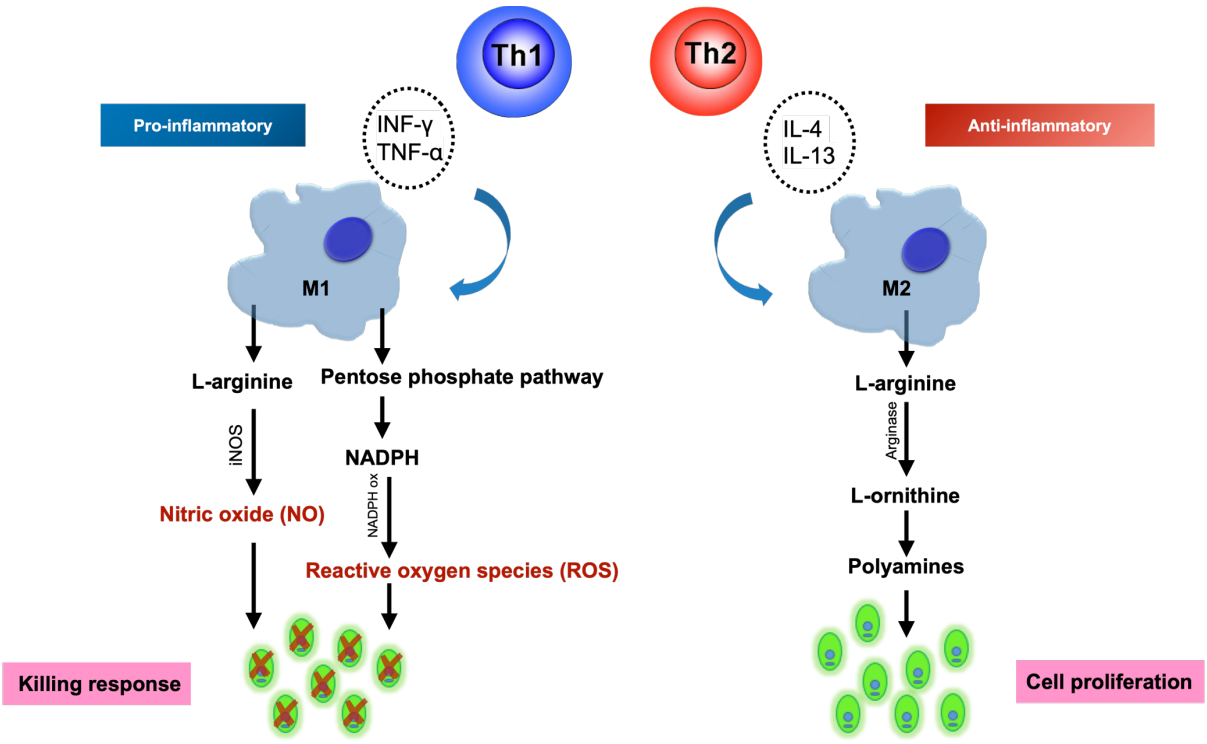

Figure 1.2. Th1 and Th2 paradigm and macrophage activation in *Leishmania* infection. Source: The author

As an important mediator of host defense, NO may have multiple antimicrobial mechanisms of action, damaging lipids, proteins and DNA.[26] It may react with the cellular nucleus causing deamination of DNA bases, and/or react with

metalloproteins particularly those containing iron, copper or zinc, leading to alterations in biological signaling pathways.[26,27] For example, the reaction of NO with cytochrome c oxidase is strongly involved in the inhibition of the mitochondrial electron transport chain.[26,28] NO may also react with other free radicals, such as superoxide (O_2^-) to form peroxynitrite ($ONOO^-$), a highly reactive molecule, therefore resulting in lipid peroxidation. $ONOO^-$ can also disrupt iron-sulfur (Fe-S) clusters, hence promoting mitochondrial dysfunction due to aconitase inactivation.[27] Additionally, protein tyrosine nitration and S-nitrosylation of cysteine residues are other possible NO reactions that may affect cell viability by changing protein structure and function at the molecular level.[27,28]

Reactive oxygen species are generated from respiratory burst NADPH-oxidase-dependent (NOX).[29] The reduction of molecular oxygen produces O_2^-, which can promptly dismutase to hydrogen peroxide (H_2O_2). H_2O_2 can also be converted to hydroxyl radicals ($^{\cdot}OH$) or peroxyl radicals ($^{\cdot}OOH$) in the presence of ferric iron (Fe^{3+}).[30] Other non-radical ROS, such as hypochlorite anion, (OCl^-) and singlet oxygen ($^1O_2$) might also be produced, even though these molecules are less common under physiological or pathological conditions.

ROS can be generated in response to the presence of different pathogens and once released in high amounts, it may cause significant oxidative stress, hence affecting lipids, proteins and DNA.[29,30] Therefore, both molecules may act as antimicrobial agents within macrophages, either alone or in combination in order to prevent pathogens proliferation.[30]

1.4.1 Nanoparticulated nitric oxide donors

Since NO is an endogenous molecule, its exogenous administration has been widely investigated as an alternative approach to kill *Leishmania* parasites.[31,32] However, because of its short half-life (1 to 5 s) *in vivo*, NO is easily inactivated in biological environments, particularly in the presence of hemoglobin and oxygen.[33] Therefore, nitric-oxide donors have emerged as a potential strategy to ensure NO storage and release for biomedical applications.[33,34]

The class of S-nitrosothiols (RSNOs) is among the low molecular weight endogenous NO donors with several biological functions.[34] It is usually generated by the nitrosation of free thiol groups in the presence of nitrous acid.[33,35] Nevertheless,

most of RSNOs are unstable and likely to be decomposed by heat, light and/or upon reactions with some metals ions, resulting in the NO spontaneous release.[34,36] Such uncontrolled NO release might increase cytotoxicity, hence leading to undesirable side effects.[33]

In this regard, nanomaterials have arisen as attractive platforms to ensure a gradual and controlled NO delivery.[37] Particularly, polymeric nanoparticles, such as chitosan, are advantageous for good biocompatibility, biodegradability, low toxicity and sustained NO release.[38,39] Chitosan-based nanoparticles have been used for different biomedical applications, including for amphotericin B encapsulation to inactivate *in vitro Leishmania* parasites.[40] Moreover, NO-releasing chitosan nanoparticles have also been shown to inactivate *Trypanosoma cruzi*, a protozoa parasite which belongs to the same family as *Leishmania*.[41] Thus, the encapsulation of nitric oxide donors into chitosan nanoparticles can be a promising strategy to treat CL with a great potential for biomedical applications.

1.4.2 Antimicrobial photodynamic therapy

Photodynamic therapy, also referred to as PDT, is a light-based therapy that combines simultaneously a light source, a photosensitizer and molecular oxygen to generate ROS to inactivate pathogens by oxidative stress.[42]

For PDT to be effective, the light source wavelength should match the absorption band of the photosensitizer.[43] The ground state dye absorbs the light-emitted photons and undergo a short-lived (nanoseconds) excited singlet state. In this state, one of the photosensitizer's electron is lifted to an orbital of higher energy without changing the direction of the electron spin.[43] The photosensitizer may further lose energy by fluorescence, or alternatively, in the excited singlet state undergo an intersystem crossing to generate a long-lived excited triplet state (microseconds), where the spin of excited electron is inverted.[44] The process is followed by the transition of the photosensitizer to the ground state (phosphorescence) or the excited triplet state dye may otherwise undergo Type I and/or Type II reactions.[44]

Type I pathway involves the transference of a proton or an electron to form radicals or radical ions.[45,46] This process may occur by a direct interaction of the excited triplet state photosensitizer with the substrate, such as cell membranes, molecules and ground state molecular oxygen to produce superoxide anion, H_2O_2,

·OH.[44,45] In the alternative Type II reaction the triplet state dye may transfer energy to molecular oxygen to generate $^1O_2$, which is a highly reactive species and readily oxidizes several biological molecules, including nucleic acids, amino acids and unsaturated fatty acids (Figure 1.3).[44,45]

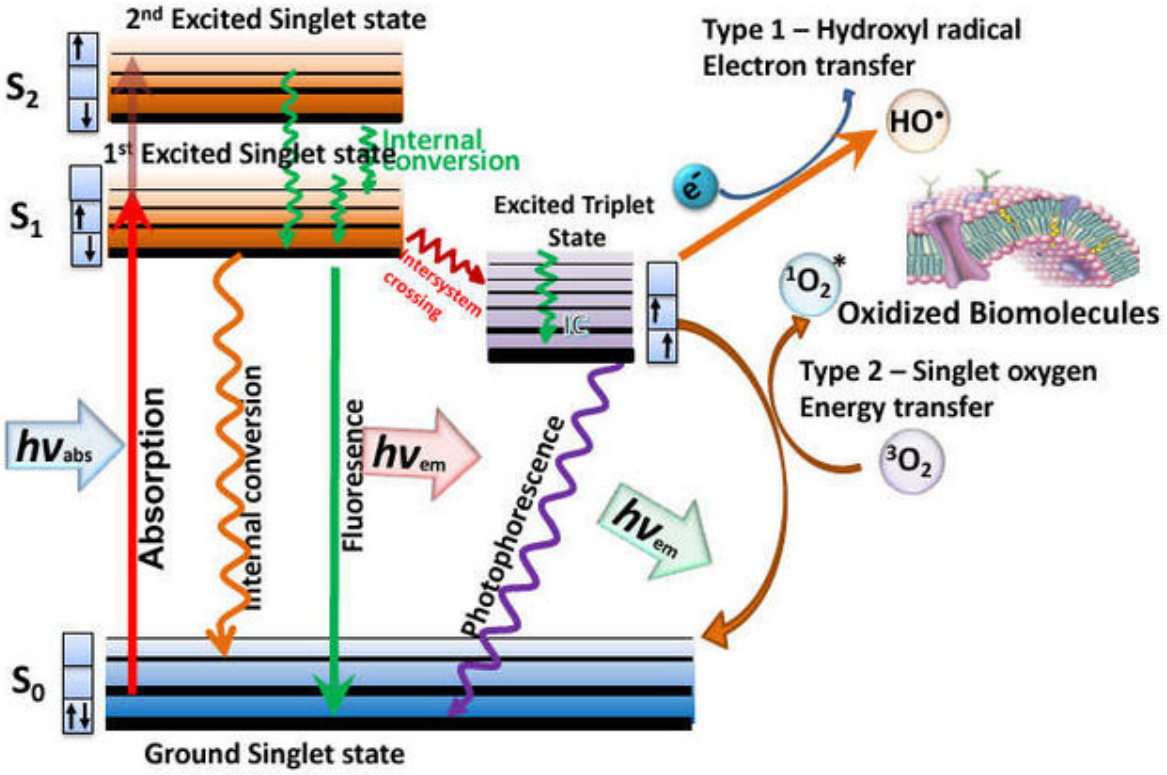

Figure 1.3. Jablonski diagram demonstrating the photochemical mechanisms of PDT.[46]

Antimicrobial PDT has been widely used to treat a broad spectrum of infectious diseases.[43] Phenothiazine dyes have shown to be effective in killing several *Leishmania* species *in vitro* and *in vivo*.[47-49] Methylene blue (MB) is the most widely used photosensitizer of this class, and it has demonstrated good activity to treat CL in preclinical and clinical trials.[50-52] It is able to generate high levels of ROS by both types of reaction, yielding nearly 50% of $^1O_2$. Moreover, the positive charge enables it to accumulate into cellular lysosome and mitochondria, therefore targeting multiples organelles.[53]

Other phenothiazine photosensitizers include 1,9-dimethyl methylene blue (DMMB) and new methylene blue. DMMB has been shown to produce 20% more $^1O_2$, and it less likely to be photobleached in relation to MB.[53] It has been recently introduced as an antimicrobial compound with great activity against a plethora of microorganisms.[54-56] However, its use against *Leishmania* parasites has never been reported. Thus, DMMB could be an attractive approach to potentiate PDT for CL treatment, thus improving parasites killing.

2. OBJECTIVES

In the present work, we aimed to assess the role of both, NO and ROS towards antileishmanial activity using two different therapeutic strategies: (1) nitric oxide-releasing chitosan nanoparticles and (2) antimicrobial photodynamic therapy. Therefore, this work has been divided into five specific objectives, as follows:

(1) To evaluate the *in vitro* potential of nitric oxide-releasing chitosan nanoparticles (NONPs) against *L. amazonensis,* one of the causative agents of CL.
(2) To evaluate the *in vivo* potential of nitric oxide-releasing chitosan nanoparticles (NONPs) against *L. amazonensis* on infected BALB/c mice.
(3) To evaluate organic light-emitting diodes (OLEDs) as a novel light source to inactivate two *Leishmania* species *in vitro*: *L. major* and *L. amazonensis,* an Old World and New World *Leishmania* species, respectively.
(4) To evaluate the effects of photodynamic therapy (PDT) using the photosensitizer 1,9-dimethyl methylene blue (DMMB) against promastigotes of *L. amazonensis wild-type* (WT) and miltefosine-resistant (MFR) strains, addressing the possible underlying mechanisms of PDT action upon both parasites.
(5) To evaluate DMMB-PDT effectiveness against intracellular amastigotes of *L. amazonensis wild-type* (WT) and miltefosine-resistant (MFR) strains. In addition, DMMB-PDT cytotoxicity was assessed on mammalian cells.

The thesis was divided into five chapters, each chapter representing one scientific manuscript related to the objectives outlined above.

3. CHAPTER ONE

3.1 *In vitro* activity of NPs and NONPs

3.2 EXPERIMENTAL SECTION

3.2.1 Nitrosation of free or encapsulated MSA

The synthesis and characterization of free (NP) or encapsulated S-nitroso-MSA, henceforward named S-nitroso-MSA and NONP were carried out in our previous assays and can be found elsewhere.[57] Free or encapsulated MSA (50 $mmol \cdot L^{-1}$) was nitrosated by adding the same quantities of sodium nitrite ($NaNO_2$) leading to form either free (NP) or encapsulated S-nitroso-MSA, named S-nitroso-MSA and NONP, respectively. The formation of both compounds was confirmed by the S-NO group absorption bands at either 336 nm (ε =980.0 $L \cdot mol^{-1} \cdot cm^{-1}$) or at 545 nm ($\varepsilon$ =18.4 $L \cdot mol^{-1} \cdot cm^{-1}$) using the UV-Vis spectrophotometer (Agilent 8454, Palo Alto, CA, USA).

3.2.2 Parasite culture

Leishmania (L.) amazonensis (MHON/BR/73/2269, transgenic line expressing luciferase) provided by Prof. Silvia R. B. Uliana (University of São Paulo). Promastigotes were harvested at 25°C in M199 media (Sigma-Aldrich, USA) supplemented with 10% fetal bovine serum (FBS, GibcoTM Invitrogen Corporation, USA) and 0.25% hemin (Sigma-Aldrich, USA) with pH 7.2.[58] Amastigotes were extracted from lesions of infected BALB/c mice.

3.2.3 Activity of NONPs on Leishmania promastigotes

Leishmania promastigotes were treated with different concentrations ranging from 25-200 µM of NONPs and NPs for 24 h at a density of $5x10^6$ per well. The molar concentrations refer to the molar concentrations of MSA for NPs, and S-nitroso-MSA for NONPs. Cells viability was determined using luciferase assay. (One Glo Luciferase Assay System, Promega Corporation, USA). Luciferin was added to

wells five min prior the spectrophotometer analysis (Spectramax M4, Molecular Devices, USA). Thereafter, parasites at $1x10^5$ were treated with concentrations NONPs and NPs at 25-400 µM and bioluminescence signal was assessed on a daily basis for 5 days.

3.2.4 Cytotoxicity assays on macrophages

All the experiments were carried out in agreement with the Brazilian Federal Law 11,794, Decree 6,899 and on the Normative Resolutions published by the National Council for the Control of Animal Experimentation (CONCEA) and approved by the Ethic Committee on Animal Use of the IPEN-CNEN/SP under the protocol number 189/17.

Bone marrow-derived macrophages (BMDM) from BALB/c mice were extracted and cultured during 7 days in RPMI 1640 medium (15 mM HEPES, 2 g of sodium bicarbonate/L, and 1 mM *L*-glutamine) and supplemented with 20% FBS and 20% *L*-929 cell conditioned medium (LCCM).[59]

Activity of both compounds was carried out by seeding cells ($8×10^4$) on 96-well plates 24 h before experiments. Thereafter, cells were incubated with increasing concentrations (0-400 µM) of NONPs and NPs for 24 and 48 h. Then, viability was assessed using MTT, using 30 µL at 5.0 mg/mL (3-[4,5-dimethyl-2-thiazolyl]-2,5-diphenyl-2H-tetrazolium bromide; Sigma-Aldrich, USA) kept at 37°C for 4 h followed by the addition of 30 µL of 20% (w/v) sodium dodecyl sulfate (SDS). The optical density was evaluated by a spectrophotometer (Spectramax M4, Molecular Devices, USA) at 595 nm and 690 nm. Results were normalized and plotted as percentage.

Immunofluorescence staining was carried out using $2×10^5$ cells plated on glass coverslips in 24-well plates. Treatment was performed at 400 µM NONPs and NPs 24 h, for 48h. Afterwards, cells were fixed by methanol, washed with PBS, and permeabilized/blocked with 0.1% Saponin (Sigma-Aldrich, USA) and BSA (bovine seric albumin, Sigma-Aldrich, USA) in TBS (tris-buffer saline). Macrophages were incubated with DAPI for 1 h at 10 µg/ml. Images were obtained with a fluorescence microscope (DMI6000B/AF6000, Leica, Germany) connected to a digital camera system (DFC 365 FX, Leica, Germany) and processed by ImageJ software.

3.2.5 Activity of NONPs on intracellular amastigotes

The activity of NONPs and NPs against amastigotes on infected macrophages was performed by seeding macrophages at 2×10^5 per each well onto coverslips in 24-well plates. Cells were infected with amastigotes extracted from lesions of previously infected BALB/c mice at multiplicity of infection= 5 for 1 h at 34°C. Afterwards, cells were washed and incubated in fresh medium overnight followed by the treatment at 400 μM concentration of either NONPs or NPs. After treatment, the cells were fixed with methanol and permeabilized/blocked with 0.1% Saponin and BSA in TBS. Coverslips were incubated for 2 h with rabbit polyclonal antibodies against *Leishmania*, followed by anti-rabbit IgG Alexa Fluor 488 (Molecular Probes, USA). Rat anti-mouse Lamp1 mAb (BD Biosciences, USA) was used to stain vacuolar-associated protein, being incubated for 2 h and then for 1 h with anti-rat IgG Alexa Fluor 568 (Molecular Probes, USA). Nuclei were stained with 10 μg/mlL DAPI for 1 h. Images were obtained with fluorescence microscopy and processed by ImageJ software.[60] Results were determined by counting 300 cells per coverslip and plotted as percentage of infected cells, number of intracellular amastigotes per infected macrophage and the infection index was also calculated following the formula:

$$\frac{\text{Number of amastigotes}}{\text{infected macrophages}} \text{ x \% infection}$$

3.2.6 Statistical analysis

All data are representative of at least three independent assays in triplicate, unless stated otherwise. Statistical analysis was performed using GraphPad Prism 6.0 software by one-way ANOVA followed by the Tukey post-test. Differences were considered statistically significant when $p< 0.05$.

3.3 RESULTS

3.3.1 NONPs decrease promastigotes of L. (L.) amazonensis

NPs inactivated nearly 65% of promastigotes at a concentration of 200 μM. Activity was enhanced by the treatment with NONPs, in which we observed a reduction of nearly 50% of the of parasites at 25 μM. At 75 μM, pproximately 85% of parasites were killed. At the highest concentration (200 μM) activity of NONPs was even clearer. However, after 3 days the remaining parasites were able to replicate again. Therefore, we treated this parasites at 400 μM concentration (Figure 3.1 A,B).

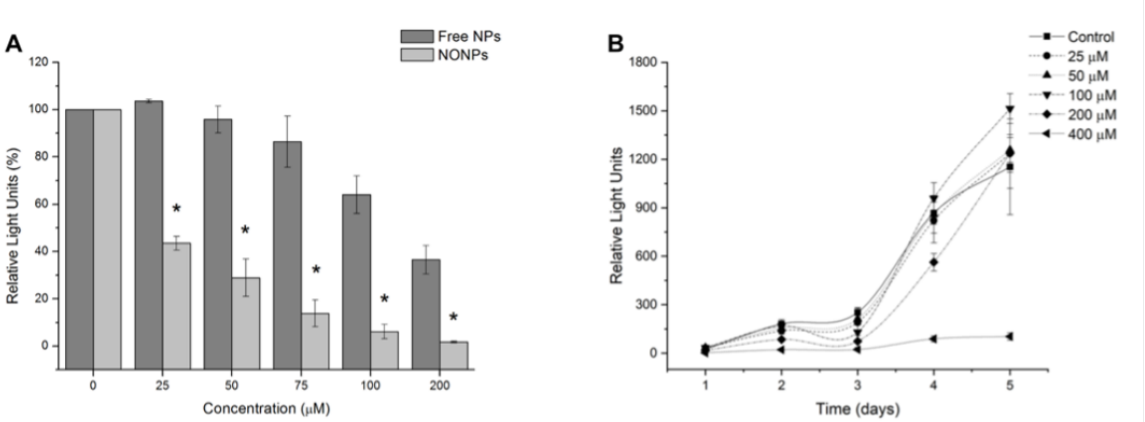

Figure 3.1: (A) Dose-response of NPs and NONPs under a wide range of concentrations (0 to 200 μM) against *L.(L.) amazonensis* promastigotes. (B) Promastigotes 5 days after treatment at different concentrations (0 to 400 μM) of NONPs determined by bioluminescence assay. Values show means ± SD (n=3).

3.3.2 Treatment with NONPs is not toxic to macrophages

MTT assay demonstrated no toxicity to macrophages regardless of NONPs concentrations (Figure 3.2). Indeed, the highest concentration of 3200 μM maintained cell viability in 75% even after 48 h. Macrophages morphology was similar between treated groups and untreated cells (Figure 3.2).

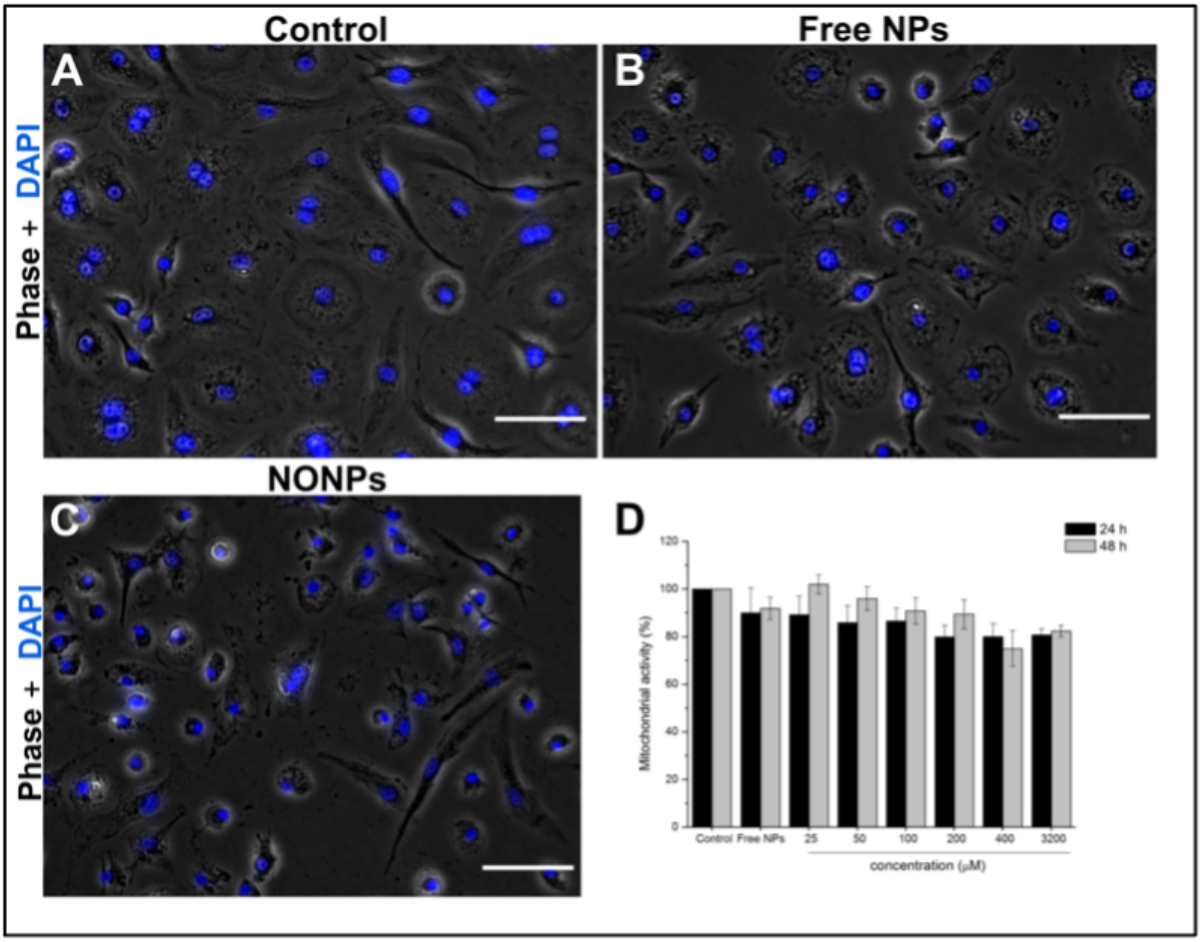

Figure 3.2: (A-C) Immunofluorescence representative images of BMDM treated with NPs and NONPs (400 μM). Blue fluorescence refers to nuclei stained with DAPI. (D) BMDM treated with increasing concentrations of NONPs (0 to 400 μM) and NPs (400 μM) for 24 h and 48 h. Mean values ± SEM of cell activity were assessed by MTT assay. No statistically significant differences were noticed (n=9).

3.3.3 Intracellular amastigotes of L. (L.) amazonensis are susceptible to NONPs

We assessed the anti-leishmanial effect of NONPs in intracellular amastigotes of *L. (L.) amazonensis* after 48-h after treatment. NPs decreased the number of intracellular parasites and infection index in nearly 21% and 33%, respectively. Conversely, NONPs inactivated around 47% and 56% the number of parasites and infection index, respectively. No significant difference in % of infection was found in comparison with the untreated control. (Table 3.1).

Table 3.1. Effectiveness of NPs and NONPs against intracellular amastigotes of *Leishmania (L.) amazonensis.* * Refers to statistically significant differences between NPs and NONPs. ** refers to statistically significant differences between control and NONPs ($p < 0.05$, n= 6).

	Number of intracellular amastigotes/infected macrophage	% Infection	Infection Index
Control	8.5±1.2	76.2±7.1	649.7±115.1**
NPs	6.7±0.2*	65.1±3.1	436.0±6.9
NONPs	4.5±0.4*	63.7±5.4	288.0±39.9**

The greater effectiveness of NONPs on intracellular amastigotes was observed within macrophages as displayed in Figure 3.3. Several amastigotes within parasitophorous vacuole (PV) were noticed after 48 h of infection in control group. Treatment with NPs reduced number of amastigotes inside PV compared to control. In contrast, NONPs treatment promoted a remarkable parasite burden decrease as well as a substantial PV reduction.

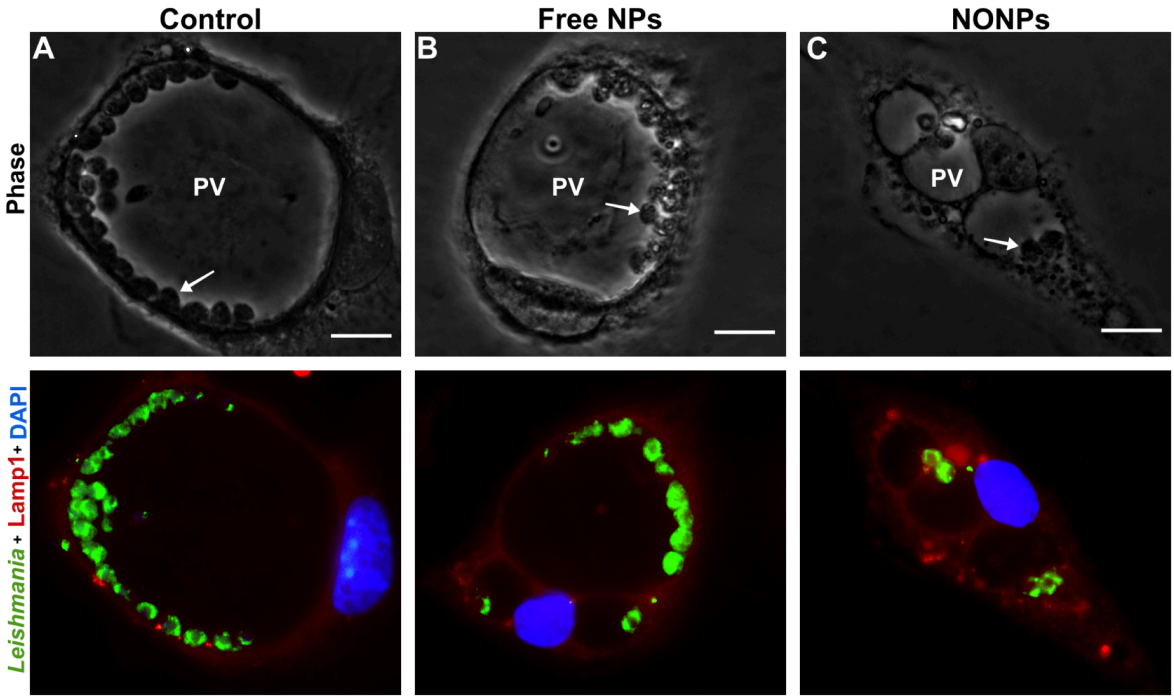

Figure 3.3: Immunofluorescence and phase representative images of infected macrophages. (A) Represents untreated control (B) Cells treated by NPs and (C) NONPs at 400 µM after a 48h incubation period. Blue fluorescence refers to DAPI staining. Green fluorescence shows parasites stained by rabbit polyclonal antibodies on amastigotes of *L. amazonensis*, then stained by by anti-rabbit IgG. Red fluorescence shows Rat anti-mouse Lamp1 mAb used to stain vacuolar-associated protein. Thereafter, anti-rat IgG was assessed. Images were analyzed by ImageJ software. Bars = 10 µm. Arrows shows amastigote inside macrophage (n=6).

3.4. DISCUSSION

This study demonstrated NONPs can inactivate promastigotes as well as amastigotes on infected cells of *L. (L.) amazonensis* with no toxicity to macrophages.

Chitosan is promising molecule to be used to encapsulate NO donors owing to characteristics as biodegradability, minimal toxicity, good bioavailability.[61] As a positive molecule, it is able to react with negative charged molecules.[62] Therefore, negative charge of parasites membrane can promote an antileishmanial activity, which observed when parasites were treated by NP, suggesting an antimicrobial potential for chitosan as well.[62] Nevertheless, the antileishmanial activity was

increases by NO donor encapsulated, thus suggesting the encapsulation on NO donors might have a synergism with chitosan properties.

NONPs did not demonstrate any toxicity to macrophages even at high concentrations. Additionally, NONPs are ideal to be used as a topical therapy, avoiding systemic toxicity.

At 200 μM we observed that parasite replicated again 3 days post -therapy (see figure 3.1). Therefore, we assumed that at 400 μM a greater reduction would be observed. As a result, we observed a sustained parasite inactivation even following 5 days, which is in agreement with literature, in which high concentrations of NO were necessary to provide an effictive activity.[63,64]

In terms of activity on macrophages, we can state that even though there was cellular viability decrease, still 80 % of cells were viable at high concentrations. In fact, NO donors, are normally toxic at high doses owing to to the free and spontaneous NO release.[41,61] Our results demonstrate that chitosan nanoparticles could be an attractive drug delivery system. In addition, the NO-loaded chitosan nanoparticles diminished mammalian cells toxicity, thereby promoting a sustained and slower NO release. As a result, no noticeable reduction in macrophages or cellular morphological alterations were detected at 400 μM.

At 400 μM we observed that 33% of amastigotes were reduced in one NONP dose. After 48h, a further reduction was detected, showing that around 50% of parasites were killed.

In fact, S-nitrosothiols are endogenous molecules with several biological functions, promoting different reactions, including transnitrosation and S-thiolation.[66] Transnitrosation comprise the reaction of nitrosothiols with a molecule or protein containing cysteine residues, thereby leading to cytotoxicity by an enzymatic inhibition.[67] Therefore, *Leishmania* cysteine proteinase activity is likely inhibited by NO-donors through transnitrosation reaction, thus resulting in parasite killing.[68] In addition, NO can react directly with parasites, thus affecting parasite survival as a consequence of mitochondrial respiratory chain disruption caused by iron depletion and aconitase inhibition.[68,69]

Promastigotes are more susceptible to NO than amastigote forms, mainly when it comes to *L. (L.) amazonensis species*, likely due to explained by their ability to live in the hostile environment within macrophages.[70] The amastigote stage of *L.*

(L.) amazonensis survive within large PVs during infections, and this is strongly related to virulence factors, ability to survive and proliferate inside the host cells.[71]

We observed a large number of amastigotes within a large PV in untreated control group, which suggests the infection is perpetuating.[15] Therefore, even though there was a parasite burden decrease after NP treatment, the PV size and morphology are similar to untreated cells. Conversely, NONP showed a significant PV size reduction and parasite burden reduction.

Small PVs are not able to sustain the parasite growth.[50] On the other hand, large PVs can dissolve the antimicrobial compounds like ROS and NO improving the amastigote survival.[50-51] Therefore, treatments that are able to reduce PVs size are advantageous to treat cutaneous leishmaniasis. Indeed, the PV size in this study brings further evidence that infection is resolving because of the sustained NO release rather than chitosan properties.[72]

In conclusion, we demonstrate the potential of NO donors encapsulated into chitosan nanoparticles to inactivate promastigote and amastigote forms de *L. (L.) amazonensis* without toxicity on macrophages. As this compound is formulated to treat CL, NONPs might be applied directly to the infected lesion by subcutaneous inoculation. We demonstrate this innovative and attractive nanoplatform as a non-invasive and promising therapy for cutaneous leishmaniasis.

4. CHAPTER TWO

4.1 *In vivo* activity of NONPs on infected BALB/c mice

4.2 EXPERIMENTAL SECTION

4.2.1 Parasite culture and in vivo infection

Promastigotes of *L. amazonensis* recombinant strain expressing the luciferase gene (La-LUC) were grown in M199 medium (Sigma-Aldrich, USA) supplemented with 10% heat-inactivated fetal bovine serum (Gibco Invitrogen Corporation, USA), hemin (0.005%) (Sigma-Aldrich, USA), HEPES (40 mM pH 7.4) (Sigma-Aldrich, USA), and penicillin/streptomycin 100 μg/mL (Sigma-Aldrich, USA). Parasites were incubated at 25°C until the stationary growth phase.

The animals were divided according to the concentration of NONPs applied, respectively: 2) NONPs 0.4 mM, 3) NONPs 1 mM, and 4) NONPs 2 mM. In the present work, the molar concentrations refer to the molar concentrations of S-nitroso-MSA for NONPs.

4.2.2 Treatment and disease progression

The synthesis and characterization of NONPs were carried out in our previous assays and can be found elsewhere.[73] On day 0, nitrosation of encapsulated MSA (50 mM) was performed and NONPs were kept in the fridge at 4 °C, protected from light for 60 min. Then, NONPs were dissolve in phosphate buffer saline (PBS) according to the concentrations used for each treated group (0.4 mM, 1 mM, and 2 mM). After nitrosation, mice were topically treated at one single dose by injecting 20 μL of NONPs in the infected paw. Afterwards, mice were monitored for the next 3 weeks to be evaluated parasite burden, lesion thickness, and pain score.

Parasite burden was assessed in real-time by analyzing luciferase activity using bioluminescence imaging (IVIS Spectrum; Caliper Life Sciences, USA). Three days prior to the therapy, imaging was performed to evaluate the presence of parasite burden in all animals. Thereafter, imaging was carried out at the day of treatment on a daily basis for 5 days. Then, parasite burden was performed once a week for the following 3 weeks.

Prior to luminescence, 100 μL of luciferin (VivoGlo, Promega Corporation, USA) at 75 mg/kg injected via intraperitoneally in each animal. Mice were then anesthetized with isoflurane (2.5% induction and 1.5% maintenance). Twenty-min after luciferin injection, images were obtained using 2 min of exposure time in a high-resolution mode, and total photon emission was analyzed over a region of interest and quantified using a living image software version 4.3.1 (Caliper Life Sciences). Results were obtained as photons/second/square centimeter/steradian (ph/sec/cm^2/sr).

Nociceptive sensibility was carried out using von Frey filaments, which are commonly used to evaluate pain upon a given mechanical stimulus. These stiff filaments with different forces were applied directly to the lesion and surrounding regions at 5 different forces: 10, 15, 26, 60, and 100 g. When we noticed a paw withdraw, we considered positive the response to the stimulus. Pain score was analyzed once a week for 3 weeks. Thereafter, a pain score (1 to 6) was set to detect hyperalgesia, in which scores 1 and 6 were considered the lowest and highest (severe) nociceptive sensibility, respectively, as shown in Table 4.1.

Table 4.1. Pain score for Von Frey filaments referred to force scale.

Pain Score	Force (g)
1	>100
2	60-100
3	26-60
4	15-26
5	10-15
6	<10

The lesion thickness was assessed by evaluating the differences between infected and contralateral non-infected paw with a caliper as follows in Eq. (2):

$$Lesion\ thickness\ (mm) = Pi - Pc \qquad \text{(Eq. 2)}$$

in which Pi is the infected paw and Pc is the contralateral uninfected one of the same animal.[38] The lesion was measured once a week for 3 weeks.

4.2.3 Statistical analysis

We used one-way ANOVA of repeated measures to compare outcomes of experimental groups over time. We used Tukey's test to assess statistically significant differences. Statistical analysis was carried out using GraphPad Prism 7 software and results were considered statistically significant when $p < 0.05$.

4.3 RESULTS

Results demonstrate the great activity of NONPs in the first 5 days post-treatment. Figure 4.1 displays the untreated group, showing that the parasite population underwent exponential growth, thus resulting in an average growth rate of one-log regarding the days - 3 and 5, respectively.

Conversely, a different trend was noticed on the animals receiving NONPs. Parasites demonstrated a slower growth between days - 3 and 1 at 0.4 mM and 1 mM, until reach a plateau in the 4th day. Afterwards, a less evident increase can be observed on the 5th day for both concentrations. Despite that, parasite load remained lower than control over this period, showing statistically significant differences between both treated groups and control. Indeed, NONPs activity appears to have dose-dependent response. This is clearer at 2 mM. Remarkably, at this concentration, NONPs reduced in 48.8 % the parasite burden 24h following treatment, keeping low until the 5th day. Consequently, there were differences statistically significant between the control and NONPs 2 mM group, in nearly 1.5-log (Figure 4.1A).

This can be confirmed by the increased bioluminescence signal in untreated control than treated groups. The red color at the center of the control's infected paw demonstrates a large number of parasites. In addition, the luminescence signal is brighter, and the distribution of light covers a larger area as observed to that of treated groups. In fact, animals receiving 0.4 mM and 1 mM showed similar signals in the 5th day post treatment. It is important to mention that no luminescent signal was observed on animals receiving NONPs at 2 mM, thus suggesting a successful outcome even at only one dose (Figure 4.1B).

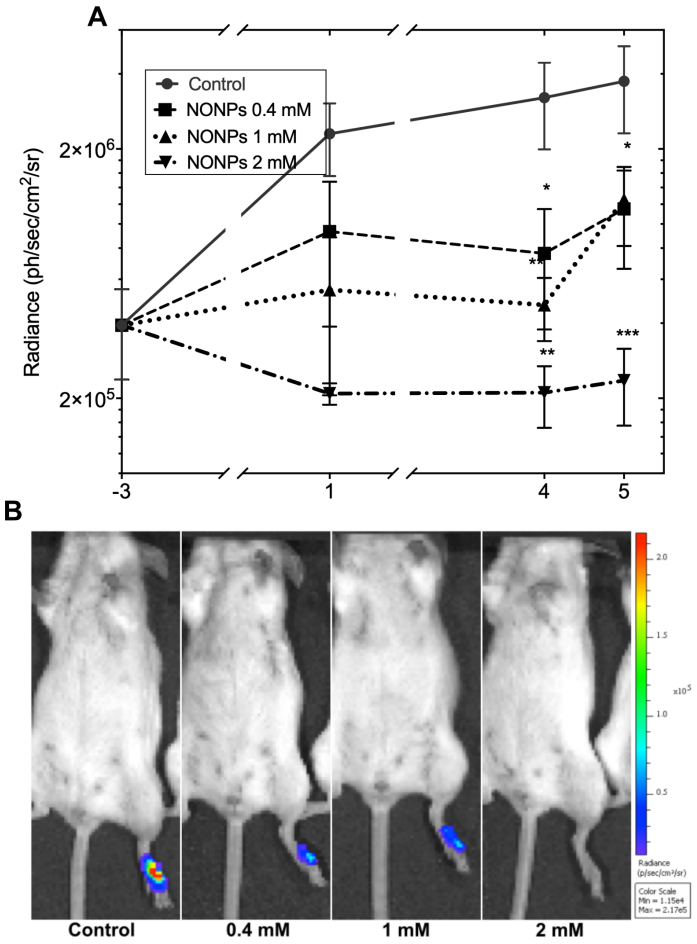

Figure 4.1. NONPs antileishmanial activity against La-LUC-infected BALB/c mice. (A) Values represent parasite burden mean ± SEM. Statistically significant differences observed between control and treated groups (* $p < 0.05$, ** $p< 0.01$, *** $p < 0.001$). (B) Bioluminescence images of untreated control and NONPs groups 5 days post-treatment. BALB/c mice were infected with $1x10^6$ La-LUC stationary promastigotes in the left paw. Treatments were carried out at three different NONPs concentrations (0.4 mM, 1mM, and 2 mM), in one single dose. Bar on the right side of "B" refers to a color scale representing light intensities expressed as photons/second/square centimeter/steradian (ph/sec/cm^2/sr). n = 4 animals/group.

Parasite burden was monitored for 3 weeks after therapy. Figure 4.2 shows the overall activity of NONPs. In animal treated with 0.4 mM and 1 mM we observed

that parasite burden reduced 64.9 % and 72.3% compared to untreated group, respectively, showing statically significant differences even after 21 days. Interestingly, the best results were achieved on animals treated at a 2mM concentration. Although after 5 days parasites were able to replicate, the growth rate was slower than those of control group, yet we observed a 1.5-log difference between. (Figure 4.2A).

Imaging also provided further substantial information regarding the long-lasting effects of NONPs. As shown in figure 4.2B, at the end of the experimental period, the control group showed an intense luminescence signal over the entire paw, while for 0.4 mM and 1 mM groups, luminescence is observed just at the center of the animal's paw. Moreover, the red colors surrounded by yellow-green ones suggest a high parasite burden in this region of untreated animals. Unlike control, NONPs at 0.4 mM and 1 mM presented only blue-green intensities, referring to a lower light signal. In contrast, bioluminescence signals were barely detected in a very specific area for the 2 mM group. Localized at the center of the paw, the blue-colored region clearly shows that the number of parasites was substantially lower compared to the other groups after 21 days.

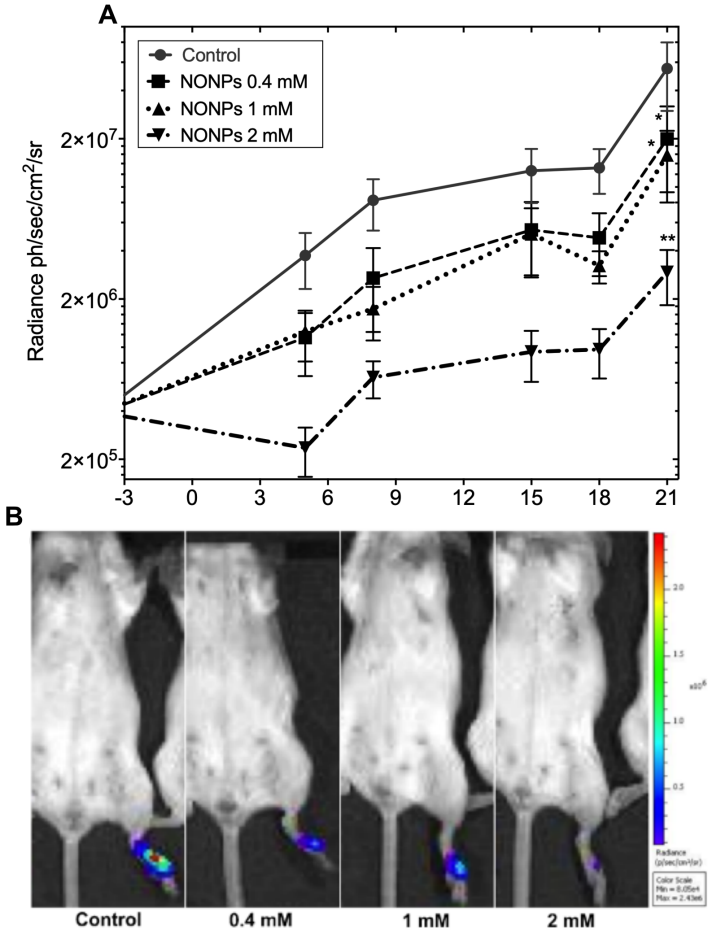

Figure 4.2. NONPs antileishmanial activity against La-LUC-infected BALB/c mice. (A) Values represent parasite burden mean ± SEM. Statistically significant differences observed between control and treated groups (* $p < 0.05$, ** $p< 0.01$). (B) Bioluminescence images of untreated control and NONPs groups 21 days post-treatment. BALB/c mice were infected with $1x10^6$ La-LUC stationary promastigotes in the left paw. Treatments were carried out at three different NONPs concentrations (0.4 mM, 1mM, and 2 mM), in one single dose. Bar on the right side of "b" refers to a color scale representing light intensities expressed as photons/second/square centimeter/steradian (ph/sec/cm^2/sr). n = 4 animals/group.

We also monitores pain score and lesion thickness. Lesion has approximately doubled in size 7 days after treatment in all groups: Control (0.5 mm to 0.95 mm), NONPs 0.4 mM (0.44 mm to 0.87 mm), NONPs 1 mM (0.42 mm to 0.76 mm) and NONPs 2 mM (0.43 mm to 0.7 mm). Except for NONPs 2 mM, a similar pattern was

identified in all groups over the experiment. The upward trend was further observed for control and NONPs 0.4 mM up to the end of the experiment, both showing lesion thickness of an average of around 1.1 mm (Figure 4.3A).

Nevertheless, after 3 weeks, lesions were smaller than control in groups NONPs 1 mM (0.95 mm) and NONPs 2 mM (0.25 mm), diminishing in 11.7% and 71.4%, respectively, compared to the 14th day. Indeed, animals treated by 2 mM had statistically significant differences, and lesion thickness resulted in values similar to a non-infected paw (Figure 4.3A).

Pain score demonstrated a similar trend in all groups. Seven days after therapy, groups treated with NONPs at 0.4 mM and 2 mM. Control and NONPs 1 mM presented a moderate sensibility with a score of 3 in the first week. However, we observed a severe (score 5) pain in all groups on the 14th and 21st days post-treatment. (Figure 4.3B).

We also assessed clinical presentation of animals over the course of the study. Figure 4.3c, displays the animals' paw after 3 weeks. Untreated animals presented a swollen paw. The redness of the skin indicates the presence of inflammatory process extending over the entire paw. We can also note the presence of a deep ulcer with a raised outer border and infiltrated plaques. Animals treated by NONPs at 0.4 mM had a similar clinical presentation. Although we might observe a pronounced edema, the ulcer was smaller, and no evident outer border was detected compared to control. Indeed, the same pattern was demonstrated towards NONPs 1 mM group. Despite the swollen paw, we may perceive a small ulcer. (Figure 4.3C).

In addition, clinical findings support the theory of a dose-dependent response. The remarkable outcome was more pronounced at 2 mM concentration group. The sustained NONPs effect led to a significant wound healing on animals of this group. Neither erythema nor infiltrated plaques were observed. We also did not find any signs of ulcer or edema. Indeed, the thickness is very similar to a healthy non-infected one (Figure 4.3C).

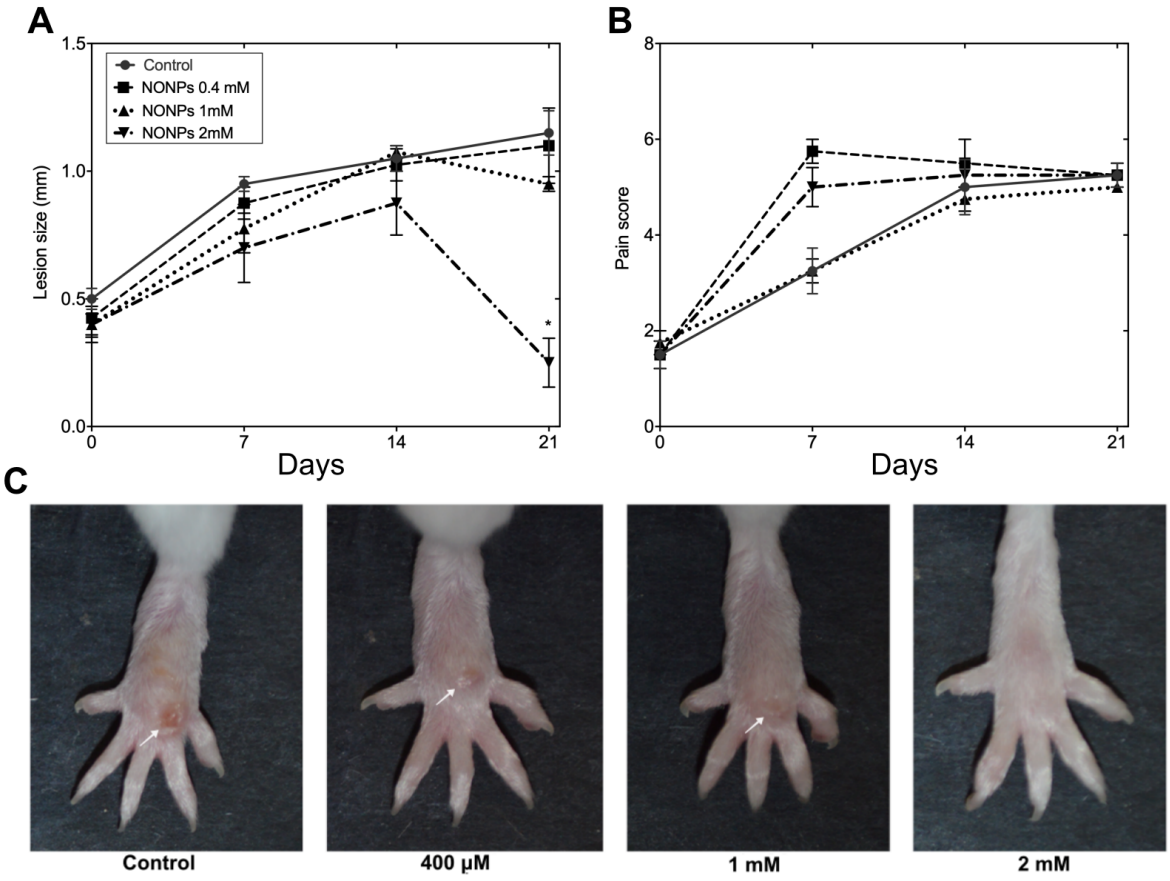

Figure 4.3. NONPs activity against La-LUC-infected BALB/c mice. Values represent mean ± SEM of (A) lesion thickness and (B) pain score. Statistically significant differences were observed between control and treated groups (* $p < 0.05$). (c) Clinical presentations of untreated control and NONPs groups 21 days post-treatment. BALB/c mice were infected with $1x10^6$ La-LUC stationary promastigotes in the left paw. Treatments were carried out at three different NONPs concentrations (0.4 mM, 1mM, and 2 mM), in one single dose. White arrows indicate ulcers developed during the course of infection. n = 4 animals/group.

4.4 DISCUSSION

The present work sought to evaluate the activity of NONPs to treat CL induced by La-LUC, which resulted in an *in vivo* dose-dependent effect. Additionally, at a 2 mM NONPs reduced significantly parasite burden and lesion thickness in one single dose. The positive effect was sustained for at least 21 days after therapy. Additionally, our data indicate that NONPs could be applied once a weekly.

We showed the successful synthesis, characterization, and encapsulation of S-nitroso-MSA into CSNPs to form NONPs. Afterwards, *in vitro* activity was assessed on La-LUC in both, promastigotes and intracellular amastigotes forms, resulting in an effective killing of parasites at 0.4 mM.[57]

Thus, we have been encouraged to carry on with *in vivo* experiments by starting with the same concentration of 0.4 mM. It is important to mention that free chitosan nanoparticles (without NO donor) did not promote great activity against parasites *in vitro*.[57] Therefore, we pursued *in vivo* experiments only with NONPs following the principles of the 3Rs (Replacement, Reduction, and Refinement) for animal experimentation.

As previously mentioned earlier, all concentrations of NONPs pdemonstrated activity on this *Leishmania* strain. Nevertheless, at 2 mM we observed a significant parasite burden (see figures 4.1 and 4.2) and lesion thickness (see figure 4.3A) decrease, thus resulting in a notable clinical cure (see figure 4.3C). In fact, *in vivo* studies involves several variables such as the higher number of parasites and barriers for the drug to target the local of infection.[74,75] In addition, the interplay between parasites and the host immune response is of great relevance.[75] Therefore, an increased therapeutic result would be expected at a higher dose *in vivo* compared to the conditions used for *in vitro* assays.

The susceptibility or resistance of mice to *Leishmania* infection is a interplay between the host immune response and *Leishmania* species.[22] Regarding animal models, BALB/c mice have been widely used to investigate of antileishmanial chemotherapy in preclinical trials.[22] Cutaneous leishmaniasis induced by *L. amazonensis* in this mouse strain is well known to induce a Th2-type response, thus resulting in increased susceptibility to infection. [22,74] In fact, BALB/c mice have a poor immune system. The aim of using this model for drug test lies on the purpose that if

the treatment is able to cure susceptible animals, so it will be effective to treat resistant ones.

The role of Th1/Th2 signaling pathways is of particular interest regarding CL and NO.[21] The production of NO is one of the major mechanisms related to *Leishmania* control.[76] In fact, a Th1 T cell response enables high levels of INF-γ to be released. INF-γ in synergism with tumor necrosis factor-alpha (TNF-α) and lipopolysaccharides activates infected macrophages, which upregulates iNOS to convert L-arginine into NO to kill parasites.[22,77] Conversely, Th2 T cell-mediated immune response induces the conversion of L-arginine to L-ornithine through the synthesis and activity of arginase.[77] Such pathway involves the production of polyamines, which is important for *Leishmania* survival in host cells.[77] As a result, the host is unable to control infection, hence resulting in large and chronic wounds.[78] [77] However, if this model promotes clinical cure in susceptible animals, it will also be good for immunocompetent ones.[74]

In this regard, NO has been investigates as an antimicrobial agent to treate leishmaniasis.[79] However, because of the gaseous nature and short half-life (1 to 5 s), exogenous administration of NO is very unlikely.[80] To overcome this, NO donors have been studited to promote a more controlled release.[81]

It has been shown the great susceptibility of *Leishmania spp.* to reactive nitrogen species (RNS). Indeed, RNS are of great importance over the role of the innate immune system.[61] Under physiological and pathophysiological conditions, NO as a signaling molecule, is able to react with distinct cellular constituents to form RNS, such as peroxynitrite ($ONOO^-$), nitrogen dioxide (NO_2), dinitrosyl iron complexes, and nitrosothiols. Each of these species has different targets and biological effects.[82]

The reaction of NO with zinc or iron metalloproteinase inhibits a wide range of different enzymes that results disturbing mitochondrial function.[82] In addition, peroxynitrite might target lipids and DNA replication.[83] The interplay of NO with cysteine thiols, thus promoting the generation of S-nitrosothiols (RSNOs) through S-nitrosylation. As a post-translational protein modification, such process might strongly affect a broad range of proteins.[84] All of these are possible mechanisms that have been reported by which NO may result in parasite death.[82]

RSNOs are endogenous classes of NO donors that have a relevant biological effect against pathogens. The exogenous administration of different low molecular weight RSNOs has been shown to promote positive effects *in vivo* over *Leishmania* inactivation, including in susceptible animal models.[85,86] In those studies, *in vivo* antileishmanial activity was achieved by multiple doses of NO donors in long-term treatment. On the other hand, we have successfully achieved an effective parasite burden and lesion size diminishing in one single administration at 2 mM. Such good response likely involves S-nitroso-MSA encapsulation into CSNPs.

From this perspective, our study indicates encapsulation of NO donors into chitosan nanoparticles increased the promosing activity of NO donors not only because of intrinsic NO activity but also because of chitosan antimicrobial properties, thus promoting in a long-term response.[39,87]

Other factors probably contributed to this successful outcome. The synthesis of nanoparticles with sodium tripolyphosphate resulted in a positively charged structure, which is very likely to interact with negatively charged *Leishmania* membranes.[39,88] Additionally, it has been reported that small-sized nanoparticles with spherical morphology enhance NPs intracellular uptake by murine macrophages.[89] Indeed, it has been shown that chitosan is taken up by pinocytosis, accumulating within the parasitophorous vacuole (PV) in macrophages infected by *L. major* and *L. mexicana*.[39]

It worth noting that intralesional administration of NONPs has brought further benefits to the treatment since available drugs are systemic and potentially toxic to the host. Local therapy is very advantageous for allowing high drug concentration directly into the site of infection avoiding systemic toxicity.[39] Thus, there might be a short-term wound healing, improving as well patient's compliance.[90] Indeed, this route of administration was not invasive, showing it was well tolerated by animals.

However, we did not observe any improvement in terms of in pain score. In humans, pain is not a common symptom described by patients with CL.[91] However, *Leishmania* has been shown to induce pain in animal models, particularly mice. In chronic infections, there is releasing of inflammatory mediators, growth factors, and cytokines, resulting in increased hyperalgesia.[91]

Our results suggest that NONPs were not able to reduce pain score in those treated animals. This could be due to the dual function of NO.[91] Although NO has

several antimicrobial activitites, it also has a significant role in the inflammatory response.[26] NO can promote vasodilation in acute or chronic inflammation, increasing the sensitivity of peripheral nociceptors in response to a stimulus.[92]

Despite that, the good results observed here were very promising, even though the exact biological mechanisms by which NONPs control *Leishmania spp.* in the host remains unexplored. I this regard, the sustained effect accomplished by one treatment of NONPs on a susceptible animal model suggests a bright future for this drug. In addition, it appears that NONPs could be applied weekly and further studies are welcome to evaluate new protocols. Besides, NONPs are suitable for topical administration and could be easily combined with conventional systemic antileishmanials in lower doses. Therefore, we hope our findings encourage further works to implement this treatment in future clinical trials.

5. CHAPTER THREE

5.1 Photodynamic therapy: Light sources for PDT

5.2 EXPERIMENTAL SECTION

5.2.1 Parasites

Promastigotes of *L. major (*MHOM/IL/80 Fredlin) and *L. amazonensis* (MHOM/BR/73/M2269) were harvested in M199 medium (Sigma-Aldrich) supplemented with 10% heat-inactivated fetal bovine serum (FBS; Gibco™ Invitrogen Corporation), 40 mM HEPES pH 7.4 (Sigma-Aldrich), 2.5 mg/mL hemin (Sigma-Aldrich) and 10 mM Adenosine (Sigma-Aldrich), at 28°C.[40]

5.2.2 Phenothiazine-based APDT of *Leishmania spp*

APDT effectiveness on both parasites was performed by treating parasites with a wide range of concentrations of MB (0 -100 μM) (Sigma-Aldrich), NMB (0 -10μM) (Sigma-Aldrich), or DMMB (0-3000 nM) (Sigma-Aldrich). Leishmania species were plated into a 96-well plate at $1x10^6$ per each well in 200 μL and then and incubated with the respective dye (MB, NMB, or DMMB) for 10 minutes to allow the photosensitizer uptake by the parasites prior to illumination. Then, treatment was carried out by two different light sources (LED or OLED) in different 96-well plates. Light parameters were set as described in table 5.1. The OLEDs development can be found elsewhere.[93]

Activity against parasites in combination with the three dyes without irradiation was performed by the incubation of parasites in the dark for 2 h, at increasing concentrations of MB (0 -100 μM), NMB (0 -10μM), or DMMB (0-3000 nM). Untreated control groups treated with light (LED or OLED) in the absence of dyes were also analyzed with the same parameters as shown in table 5.1.

Thereafter, viability of parasite was determined by the addition of resazurin (Alamar blue, Sigma-Aldrich), which is a non-fluorescent dye that undergoes a cellular metabolic reduction and becomes very fluorescent in the presence of living cells. Briefly, at the end of each experiment, 10 μL of a stock solution (1.1 mg/mL), dissolved in PBS and filtered with 0.22 μm, was added in each well and incubated

for 5 h at 28°C.[41]Then, fluorescence intensity was obtained by using a plate reader (Gen5 Reader, BioTek) at λ_{exc} = 530 nm and λ_{em} = 590 nm. Results were then normalized and expressed as a percentage of live parasites.

Table 5.1. Light sources parameters for APDT.

	LED	OLED
Radiant exposure (J/cm^2)	50	50
Intensity (mW/cm^2)	20	6.5
Time (minutes)	41' 39''	128' 12''
λ (nm)	660 ± 12.5 nm	671 ± 140 nm

5.2.3 OLED-APDT light dose study of *L. amazonensis*

The efficiency of OLED-APDT was also determined by varying the radiant exposures. For this, the most susceptible species (*L. amazonensis)* was treated with several concentrations of DMMB, as this was the best dye. Leishmania cells were plated in 96-well plates as mentioned above and illuminated with OLED irradiation as shown in table 5.2.

Table 5.2. OLED-APDT exposure times at different radiant exposures.

Time	Radiant exposure (J/cm^2)
5' 7''	2
10' 15''	4
20' 30''	8
32'	12.5
64' 6''	25
128' 12''	50

After this, the irradiance provided by the OLED was decreased, and set to deliver 1.5 mW/cm^2. In this conditions, OLED-APDT was compared with LED at 8 J/cm^2 (20 mW/cm^2). OLED-APDT intensity was further reduced in order to deliver and irradiance of 0.7 mW/cm^2 under a very low radiant exposure set to deliver 2

J/cm^2. Afterwards, experimental set up was carried out as shown in tables 5.3 and 5.4. At the end of each experiment, cells viability assay was performed as described in section 5.3.

Table 5.3. LED and OLED-APDT parameters at radiant exposure of 8 J/cm^2.

	LED	OLED	OLED
Radiant exposure (J/cm^2)	8	8	8
Intensity (mW/cm^2)	20	6.5	1.5
Time	6’ 39’’	20’ 30’’	88’ 52’’

Table 5.4. OLED-APDT parameters at radiant exposure of 2 J/cm^2.

	OLED		
Radiant exposure (J/cm^2)	2	2	2
Intensity (mW/cm^2)	6.5	1.5	0.7
Time	5’7’’	22’ 14’’	47’ 36’’

5.2.5 Statistical analysis

Results were performed in triplicates and were assessed by two-way analysis of variance (ANOVA). Differences were considered statistically significant when $p < 0.05$.

5.3 RESULTS

The absorption spectra of all three phenothiazine photosensitizers: methylene blue (MB), new methylene blue (NMB) and 1,9-dimethylmethylene blue (DMMB) matched with both LEDs and OLEDs emission spectra as represented in figure 5.1.[93]

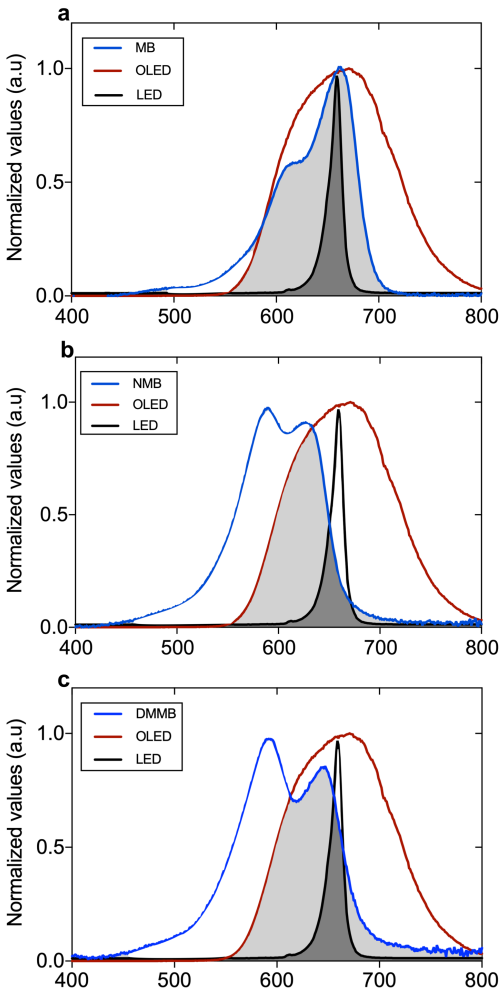

Figure 5.1: Emission spectra of OLED and LED and absorption spectra of (a) methylene blue (MB), (b) new methylene blue (NMB), and (c) 1,9-dimethyl-methylene blue (DMMB).

Either OLEDs or LEDs were very effective light sources for APDT, promoting parasites inactivation in the presence of three phenothiazines. In some conditions, the APDT activity promoted a better outcome for OLED-APDT (Figure 5.2). MB at 6.25 μM using LED-APDT reduced an average of 46.6±1.6% and 53.3±5.4% of *L. major* and *L. amazonensis* species, respectively. On the other hand, OLED-APDT promoted a killing response, reducing nearly 51.2±1.4% and 86.9±0.6% for the same *Leishmania* species. It is important to mention that regarding LED-APDT, there was an important dependence on MB concentration for both parasite species. A similar trend was identified when OLEDs were used to treat *L. major*. Nevertheless, this dependece was no longer noticed when *L. amazonensis* was irradiated by the

OLEDs, and a similar death rate was noticed in terms of the concentration range from 6.25 to 100 μM (Figures 5.2 a, d).

This trend was also noticed for NMB, as displayed in Figure 5.2 (b, e). in this case, we can clearly see that OLEDs have an increased effectiveness in comparion with the LEDs light sourced against both *Leishmania* species, mainly when treated at lower concentrations (Figure 2; b, e). In fact, we observed that and average of nearly 90.5±1.5% and 59.7±3.8% of *L. amazonensis* and *L. major* were reduced by OLED-APDT at 0.6 μM, which is greater when compared by the treatment with LED-APDT, in which we noticed that 58±1.5% of *L. amazonensis* and 13±3.1% of *L. major* were killed, respectively.

DMMB was found to be the most promising dye, however, LED-APDT and OLED-APDT promoted similar outcomes at the lowest and the highest concentrations (Figures 5.2 c, f). Indeed, we observed an inactivation of an average of 37.3±12.4% and 81.8±4.2% for *L. major* when treated by the LED-APDT at a concentration of 187 nM and 3000 nM*,* respectively. It is also possible to note that the death response for *L. major* promoted by the OLED was 42±4.5% at 187 nM and 82.5±0.4% at 3000 nM. In terms of *L. amazonensis* OLED-APDT was able to kill an average of nearly 86.4±0.9% and 92.9%±0.4% at 187 nM and 3000 nM, respectively, while 70.4±4.5% and 94±0.4% were inactivated at the same concentrations by LEDs treatment.

Indeed, *L. amazonensis* seems to be more susceptible to APDT in relation to *L. major* under all conditions, i.e., regardless of the photosensitizer or light source. In addition, we identified that DMMB to be the most potent dye, once it is capable of providing an effective death rate at very low (nanomolar) concentrations.

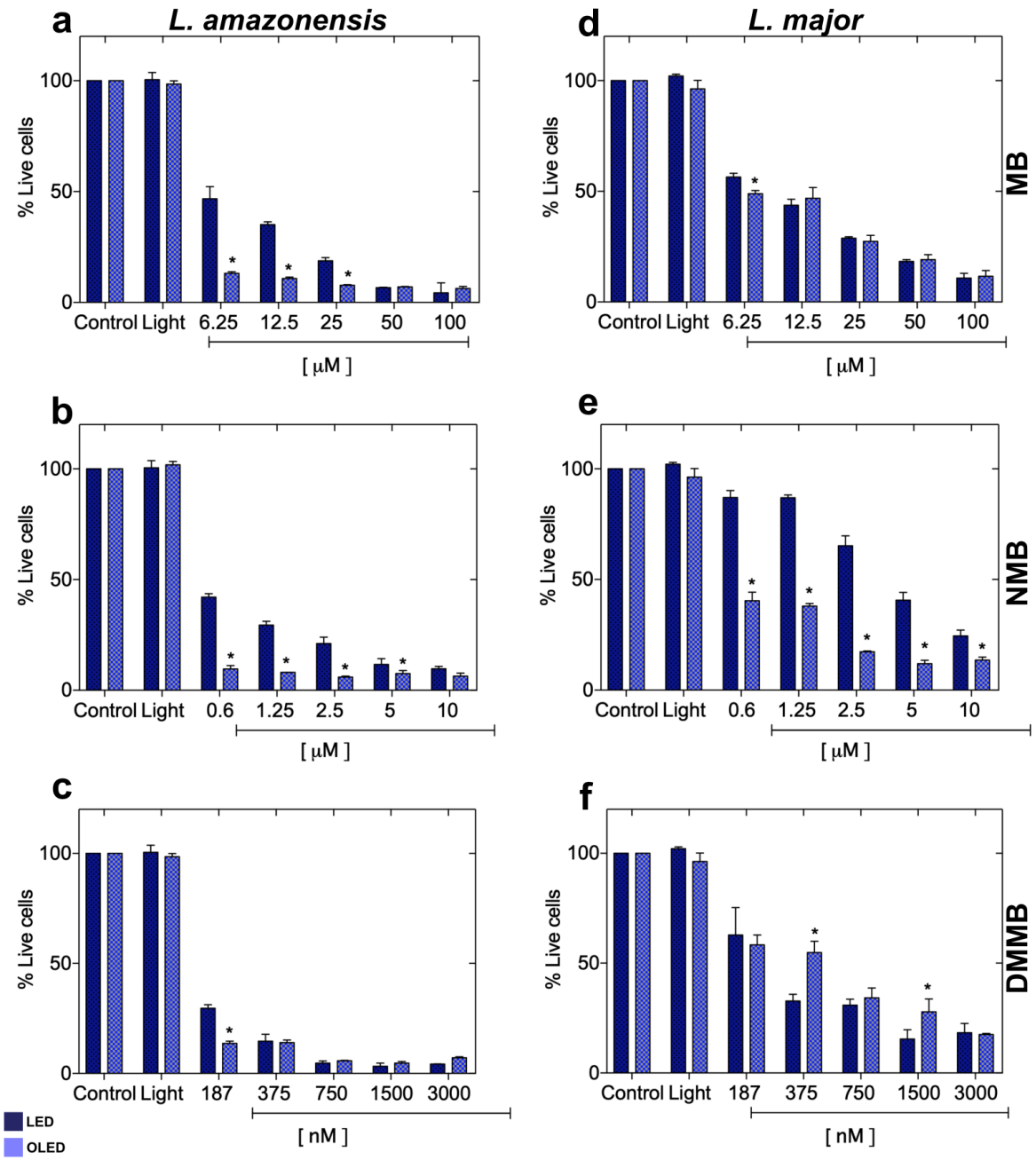

Figure 5.2: OLED and LED-APDT agains *L. major* and *L. amazonensis* promastigotes. Parasites were treated at 50 J/ cm^2 in the presence of increasing concentrations of MB (**a, d**); NMB (**b, e**) and DMMB (**c, f**). Values shown refers to the mean ± SD. Statistically significant differences observed between OLED and LED are marked with * ($p < 0.05$).

The most susceptible *Leishmania* species was found to be *L. amazonensis.* Therefore, we pursued out experiments by using this parasite species to evaluate

other APDT condition. For this, parasites were incubated with several concentrations of DMMB, using increasing radiant exposures of OLED APDT, ranging from 2 to 50 J/cm^2. In Figure 5.3a we can observe the DMMB dose-response curve fit at radiant exposures from 2 to 50 J/cm^2, determined by exposing parasites to 6.5 mW/cm^2 for a wide range of exposure time from 5 to 128 minutes (table 5.2). Our data demonstrate that there is no significant differencesin the killing response from 8 to 50 J/cm^2. Therefore, we assume the Leishmania parasites are probably killed in the first 20 minutes: 85.4±4.5% for 187 nM photosensitizer and 98.4±0.4% for 3000 nM, photosensitizer.

We reduced even further the OLEDs light intensity to 1.5 mW/cm^2, set to deliver a light dose of 8 J/cm^2, thereby resulting in an exposure time of approximately 90 min. We maintained the LEDs intensity at 20 mW/cm^2, and exposed parasites to the same light dose, hence resulting in and exposutre time of 6 minutes, as shown in table 5.3. In Figure 5.3b, we can clearly see that APDT was more effective for the OLED at the lowest concentration (187 nM), providing a significant parasite inactivation. The killing rate accomplished by OLED-APDT at 6.5 mW/cm^2 was nearly 86.5±4.9%, while at 1.5 mW/cm^2 we observed that 72.4±6.5% of cells were killed. In contrast, LED promoted 61.4±3.5% of parasites inactivation at 20 mW/cm^2. A similar pattern for the OLEDs used at low intensities being more effective than the LED source can be observed as well at the other concentrations.

Additionally, as displayed in Figure 5.3a, parasite load was inactivated significantly, for all the concentrations used for DMMB, even at the lowest light dose of 2 J/cm^2. Our results demonstrate 64.7±3.9% and 94.1±0.4% of cells inactivated when treated by DMMB at the lowest and highest concentration. Thus, we used these data as the basis to move forward and optimize OLED-APDT. For this we reduced even further OLED intensity to 0.7 mW/cm^2, using a light dose of 2 J/cm^2, thereby resulting in an exposure time of nearly 50 minutes. We compared with other OLED-APDT conditions at different intensities, as described in table 5.3. Our data is demonstrated in Figure 5.3c, and the killing rate remains the same despite the reduced intensity. For example, 96.5±0.9% of cells were inactivated at a photosensitizer concentration of 1500 nM, suggesting the pronounced impact of OLED as a potential tool to be used for antileishmanial therapy.

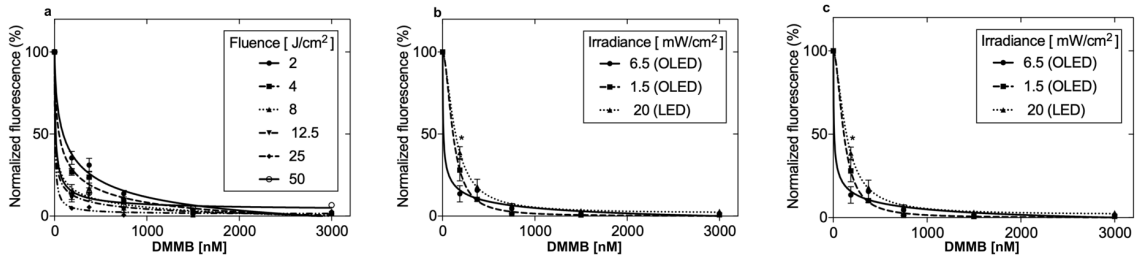

Figure 5.3. Promastigotes of *L. amazonensis* treated with either LED or OLED-APDT in the presence of increasing concentrations of DMMB. a) OLED at different radiant exposures and intensity of 6.5 mW cm^{-2}. b) OLED at 8 J cm^{-2} and intensities of 6.5 and 1.5 mW cm^{-2}. LED-APDT was per- formed at the same radiant exposure and intensity of 20 mW cm^{-2}; c) OLED-APDT at 2 J cm^{-2} and different intensities (0.7, 1.5 and 6.5 mW cm^{-2}). Values shown represent the mean ± SD (* denotes statistically significant differences between LED and OLED-PDT).

5.4 DISCUSSION

In the present study we demonstrated that OLED are promising light sources for APDT of cutaneous leishmaniasis. We evaluated their effectiveness *in vitro* using three phenothiazine dyes. Our results show that both OLEDs and LEDs are able to kill both *L. major* and *L. amazonensis* regardless of the photosensitizer concentration.

MB is a photosensitizer that has been widely used in APDT owing to its absorption lying in the red region of the spectrum, presenting two absorption peaks at 609 and 660 nm (Figure 5.1). MB can also produce increased levels of ROS by two types of reaction, either by Type I, generating O_2^-, OH^- and H_2O_2, or by Type II, producing singlet oxygen in a quantum yield of approximately 0.44.[94] Regarding MB application, it has been shown to lead to promising results against several microbial cells, including bacteria, and fungi, including resistant cell lines.[95,96] As an antileishmanial compound, *in vitro* and *in vivo* studies show its potential, demonstrating not only its ability to decrease parasite load in preclinical studies but also to treat human patients with outstanding cosmetic outcomes.[51,97]

Nevertheless, the major APDT light sources are LED-based and even though they enable an illumination over a large region, this light source is unable to be delivered uniformly as a result of shadow formation. We also have demonstrated that OLEDs can be a new light source for PDT of *Leishmania* species that is at least as

effective as LEDs and offers further benefits. OLEDs are more compact, can be attachable, flexible, and provide a uniform light emission over a large region. Despite the lower OLED intensity resulted in a longer exposure time to accomplish the same light doses used for LED-APDT, this is not an issue as the OLEDs could also be worn as a light source and longer exposure time could provide more time for oxygen to diffuse to the area to be treated. Another characteristic is that OLEDs have a broader emission spectrum than LEDs, which gives good overlap with the absorption of all the photosensitizers (see Figure 5.1). The broader emission spectrum also suggests that OLEDs are able to excite properly monomers and dimers of MB at the same time. This could lead to Type I and Type II reactions, and so may enhance parasite inactivation.

Phenothiazinium dyes are cationic molecules that can interact better with the negatively charged *Leishmania* cellular membranes, rather than anionic or neutral compounds, which makes the very good candidates for APDT.[98] A considerable number of MB analogues, such as NMB and DMMB have emerged as new approaches to MB because of their increased lipophilicity, as well as their ability to generate 35% and 21% more singlet oxygen than MB.[94] Consequently, NMB has been shown to generate antimicrobial effects against different microbial cells, including *Streptococcus mutans* and *Candida albicans* biofilms *in vitro* and in animal models.[99]

In the present study, we have shown the good acitivity of NMB under red light illumination, in which we have been able to efficiently kill both *Leishmania* species at concentrations in about 100 times lower than those of MB. This promising effect was also more evident when cells were treated by OLED-APDT. As the NMB maximum absorption peaks is at 590 nm, with another peak at 630 nm, NMB only partially absorbs LED irradiation once the LED emission comprise of a narrow peak at 660 nm. On the other hand, a broader emission spectrum of the OLED can excite more properly the NMB, thereby resulting an increased killing response.

DMMB is a derivative of MB that has been demonstrated to be more resistant to photobleaching.[42,100] Moreover, it is more effective as observed in our results from the great improvement in the death rate of *Leishmania* species at low (nanomolar) concentrations (see Figures 5.2 e, f). As mentioned earlier, the improvement is owing to its increased lipophilicity (positive log P value), in contrast to the hydrophilic

features of MB (log P < 0).[101] Therefore, DMMB as a cationic lipophilic molecule is most likely to target and accumulate into the parasites mitochondrion. As *Leishmania* parasites comprise just one single large mitochondrion, we assume that APDT disturb the membrane potential resulting in an effective cellular inactivation.[100]

There have been very few reports so far in term of the phototoxic effects of DMMB, and most of them associated with its use as an antibacterial compound under LED-based light sources.[101] In this regard, our work is the first report of the use of DMMB against *Leishmania* species. We demonstrate here that both light sources significantly decrease the parasite's survival under DMMB application in a photosensitizer concentration-dependent way.

To assesses the activity of OLEDs we also exposed cells to lower intensities at the same radiant exposure (2 J/cm^2), hence promoting in effective inactivation even at low photosensitizer concentrations. We observed a very effective killing response by 20 minutes of illumination at 1.5 mW/cm^2. Irradiation for longer periods using 0.7 mW/cm^2 was slightly less effective (figure 5.3 c). This could be related to the light dose, since 2 J/cm^2 at 0.7 mW/cm^2 is not enough to completely surpass the antioxidant ability of *L. amazonensis*. We also observed that 20 minutes of exposure time at 8 J/cm^2 and at 6.5 mW/cm^2 gave very goods killing rate when compared with other intensities, mainly at low DMMB concentrations (figures 5.3a and 5.3b). Collectively, our results suggest that the use of an appropriate light dose in combination with a suitable intensity is necessary to determine the largest antileishmanial effect.

The activity of APDT depends on many variables such as the light parameters, the photosensitizer characteristics, and how it interplays with the parasites, the type of light source, wavelength and oxygen. *Leishmania* parasites contain superoxide dismutase, peroxidases, and a series of thiol-containing proteins that act as antioxidants for ROS generated by type I reactions.[102,103] Moreover, there are differences in the biological system for different species, including in the redox balance.[104] Our results show that *L. amazonensis* is killed more effectively than *L. major* can be explained by the latter containing peroxidases capable of scavenging high levels of H_2O_2, making it more tolerant of ROS.[105] Consequently, a Type II reaction is preferred to target *L. major* once there are not endogenous antioxidant defenses for singlet oxygen. In addition, this could also explain why DMMB was

more effective. It yields high levels of singlet oxygen promoted by type II reaction, therefore producing more oxidative stress in parasites in a short period, thus resuting in a faster killing rate at lower concentrations.

In conclusion, we have shown that OLEDs are very promising light sources for APDT. Most importantly, we have demonstrated in our study that they are very effective for antimicrobial PDT to inactivate two different strains of *Leishmani*a parasites. Moreover, it has been recently reported that all three dyes have no cytotoxicity to mammalian cells.[39] We also noticed that this great effect is obtained at low intensities and very low photosensitizer concentration. Our results suggest that OLED-APDT is a promising direction for ambulatory care of patients who suffer from cutaneous leishmaniasis, and should be further studied *in vivo* in preclinical trials.

6. CHAPTER FOUR

6. 1 Photodynamic therapy as a promising strategy to overcome drug resistance in cutaneous leishmaniasis

6.2 EXPERIMENTAL SECTION

6.2.1 Parasites

L. amazonensis WT (MHOM/BR/73/M2269) promastigotes were grown at 28°C in M199 medium (Sigma-Aldrich) supplemented with 10% heat-inactivated fetal bovine serum (FBS; Gibco™ Invitrogen Corporation), 40 mM HEPES pH 7.4 (Sigma-Aldrich), 2.5 mg/mL hemin (Sigma-Aldrich) and 10 mM Adenosine (Sigma-Aldrich).22 L. amazonensis MFR was selected from the reference strain M2269 (MF 150.3-1 line) as previously reported. MFR parasites were grown in the same media as WT, but in the presence of 150 μM of miltefosine (Sigma-Aldrich).

6.2.2 Miltefosine and PDT activity against WT and MFR L. amazonensis promastigotes

Miltefosine activity for WT and MFR L. amazonensis promastigotes was performed by the addition of serial dilutions of 100 μL of MF (0-500 μM) into a 96-well plate. Then, 100 μL of Leishmania promastigotes were seeded at a density of 1×10^6 per well to obtain a final volume of 200 μL. Miltefosine was incubated for 24 h at 28°C.

PDT activity against both strains was determined by the addition of serial dilutions of 100 μL of DMMB (0-3000 nM) into a 96-well plate. Parasites were then seeded at 1×10^6 per well in a final volume of 200 μL. Before irradiation, DMMB was incubated for 10 min (pre-irradiation time) to allow the photosensitizer uptake. Then, cells were irradiated using a red LED (660 ± 12.5 nm) in an irradiance of 20 mW/cm^2. Untreated parasites were used as a negative control in a different plate. Incubation of parasites with varying concentrations of DMMB without light was also assessed to evaluate the cytotoxicity of the photosensitizer in the dark.

For both assays, cell viability was assessed after treatment (24 h for miltefosine and directly after PDT). Briefly, 10 μL of a stock solution of resazurin (1.1

mg/mL) (Alamar blue, Sigma-Aldrich) was added to each well and incubated for 5 h at 28°C. Fluorescence intensity was determined by using a plate reader (Gen5 Reader, BioTek) at λex = 530 nm and λem = 590 nm. The half-maximal effective concentration (EC50) was obtained by sigmoidal regression analysis using GraphPad Prism 7.0 software.

6.2.3 Reactive oxygen species (ROS) detection

ROS production was measured using the indicator 2'-7'-dichlorodihydrofluorescein diacetate (DCFH-DA) (Abcam), a dye that evaluates total ROS in live cells.[22] *Leishmania* strains at a density of 1×106 per well were seeded into 96-well plates. Cells were treated with DMMB-PDT at 750 nM, delivering a dose of 50 J/cm2. Parasites were also incubated in the presence of DMMB at 750 nM without light. Untreated cells were used as a negative control and 25 μM H2O2 as a positive control. After treatment, 2 μL of a stock solution of DCFH-DA (1 mM) was added to each well and incubated for 45 min. Fluorescence intensity was determined using a plate reader (Gen5 Reader, BioTek) at λ_{ex} = 485 nm and λ_{em} = 530 nm.

6.2.4 Immunofluorescence microscopy

For immunofluorescence, 1×10^6 parasites per well were seeded into 96-well plates and treated (8 J/cm2, DMMB 750 nM). Cells were centrifuged at 1400 g for 10 min and gently washed in 1 ml PBS, followed by fixation with 4% paraformaldehyde for 20 min at room temperature. Afterward, cells were allowed to adhere to poly-L-lysine coated slides before staining with (i) DAPI: cells were fixed immediately after PDT and stained with DAPI (4,6-diamidino-2-phenylindole) for 5 min (2 μg/ml, diluted in PBS), in the dark, at room temperature; (ii) Nile red: the Nile red (Sigma-Aldrich) accumulation was assessed in two different moments: Directly after, and 1h after PDT. Cells were fixed and incubated with 10 μg/ml Nile red, in the dark, at room temperature, for 30 min and DAPI for 5 min; (iii) MitoTracker CMXRos: For mitochondrial labeling, cells were treated and incubated with MitoTracker CMXRos (Invitrogen) at 28°C, in a final concentration of 100 nM, for 2h. Experiments were also performed in two different time points: Immediately and 1h after PDT. Then, parasites were fixed and allowed to sediment and adhere to slides before staining with DAPI. All images were acquired with a fluorescence microscope (DeltaVision

Imaging System) connected to a digital camera system and processed by softWoRx image analysis software.

6.2.5 Lipid analysis

WT and MFR L. amazonensis promastigotes were harvested at a density of 1×108 cells/ml and treated with DMMB-PDT. After cells were treated, total lipid extraction was performed according to Bligh and Dyer method.[106] Cells were collected by centrifugation (800 x g, 10 min), washed, and resuspended with 100 μL of PBS and transferred to a glass tube. Then, 375 μL of chloroform:methanol 1:2 (v/v) were added and vortexed. Ten-μL of lipid internal standards SPLASH LIPIDOMIX Mass Spec Standard (Avanti Polar Lipids) were added to each sample followed by intense agitation for at least 15 min. Thereafter, 125 μL of chloroform was added and vortexed. Then, 125 μL of H2O was added and vortexed again to make the samples biphasic. Samples were centrifuged at room temperature (1000 g, 5 min) and the lower phase (organic) was transferred to a new glass tube, dried under nitrogen, and stored at 4°C.

Before the electrospray ionization-tandem mass spectrometry (ESI-MS-MS) analysis, 15 μL of 1:2 (v/v) chloroform:methanol and 15 μL of acetonitrile:isopropanol:water (6:7:2) were added to the sample, and lipids were resuspended. Phospholipids were analyzed using Absceix 4000 QTrap, a triple quadrupole mass spectrometer with a nanoelectrospray source.

Lipid analysis was determined in positive and negative ion modes using a capillary voltage of 1.25 kV. Tandem mass spectra scanning (MS/MS) (daughter, precursor, and neutral loss scans) were assessed using nitrogen as the collision gas, with collision energies between 35 and 90 V as previously described.[25] Each spectrum (m/z 600-1000) includes at least 50 repetitive scans. Glycerophospholipids, including phosphatidic acid (PA) and phosphatidylglycerol (PG), were detected by precursor scanning for m/z 153 in negative ion mode. Phosphatidylcholine (PC) in positive ion mode, parent-ion scanning of m/z 184. PI/IPC (phosphatidylinositol/inositol-phosphorylceramide) was detected in negative ion mode by parent-ion scanning of m/z 241. Phosphatidylethanolamine (PE) in

negative ion mode, parent-ion scanning of m/z 196 and phosphatidylserine (PS) in negative ion mode, neutral loss scanning of m/z 87.

Phospholipids identification was based upon previous Leishmania lipidomic analyses[107] and LIPID MAPS Lipidomics Gateway (http://www.lipidmaps.org). The concentration of each phospholipid class was obtained based on the corresponding internal standard from the SPLASH LIPIDOMIX Mass Spec Standard (Avanti Polar Lipids).

6.2.6 Statistical analysis

Data were obtained in triplicates. ROS production was analyzed by two-way analysis of variance (ANOVA) followed by the Bonferroni post-test. Lipid analysis was performed by one-way analysis of variance (ANOVA) followed by Tukey post-test. Differences were considered statistically significant when $p < 0.05$.

6.3. RESULTS

6.3.1 MFR promastigotes are more susceptible to PDT than the WT strain

Miltefosine activity against both WT and MFR strains was determined by the incubation of parasites in the presence of increasing concentrations of miltefosine (0-500 μM). The miltefosine concentration required to achieve a reduction of 50% (EC50) of MFR parasites was 5.5-fold higher (140.2 ± 3.6 μM) compared to the WT (25.5 ± 0.22 μM) strain (Figure 6.1A). DMMB-PDT was also assessed by varying the concentrations of DMMB (0-3000 nM), in which EC50 value was found to be 1.5-fold lower on MFR (34.6 ± 0.12 nM) compared to the WT (53.0 ± 0.11 nM). Indeed, PDT was very effective in killing both parasites, however, MFR phenotype was more susceptible to PDT-induced oxidative stress (Figure 6.1B). Additionally, our previous studies showed that the photosensitizer at high concentrations without light did not promote any cytotoxic effect to the parasites.[21]

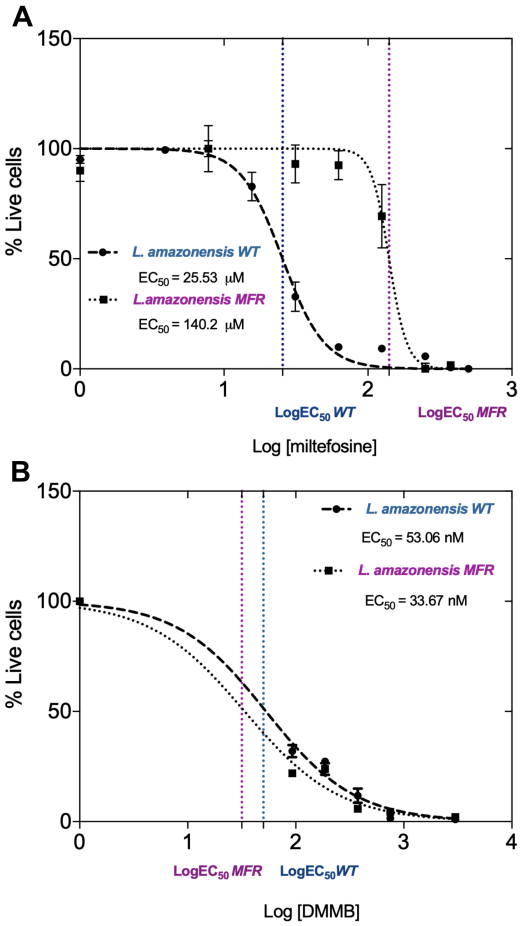

Figure 6.1: Susceptibility of WT and MFR L. amazonensis promastigotes to (A) miltefosine and (B) DMMB-PDT. Parasites were treated with PDT at 50 J/cm^2 and DMMB. Values represent mean ± SD.

6.3.2 PDT produces higher levels of intracellular ROS on MFR L. amazonensis strain

To measure the redox state of cells, ROS detection was determined directly after PDT. The H2DCFDA probe is a very sensitive method used to detect minor changes in the intracellular redox system promoted by oxidative stress. ROS levels were identified by an increase in fluorescence signal, as observed in figure 2. Low levels of ROS were produced over the WT and MFR untreated control (2739.7 ± 418.9; 2716 ± 175.8 AU, respectively). Moreover, DMMB 750 nM (without light) had similar values (2923.6 ± 684.1 for WT; 3630.3 ± 60.9 AU for MFR) with no significant differences between strains. The positive control group was assessed by the addition of H2O2 at 25 μM and showed a ~4-fold and ~6-fold increase in ROS production

over the WT (12.182 ± 121.6 AU) and MFR (16.118.3 ± 693.8 AU) strains compared to the negative control, respectively. Thus, the levels of ROS detected for the MFR strain were almost a third higher than for the WT. However, we perceived an overproduction of ROS following DMMB-PDT. There was a 14.6-fold and 18.5-fold increase upon fluorescence intensity over treated WT (38.410.6 ± 4202.6 AU) and MFR (50.489 ± 10.856.4 AU) cell lines, respectively, whereby the resistant strain produced 31.5 % more ROS produced compared to the WT.

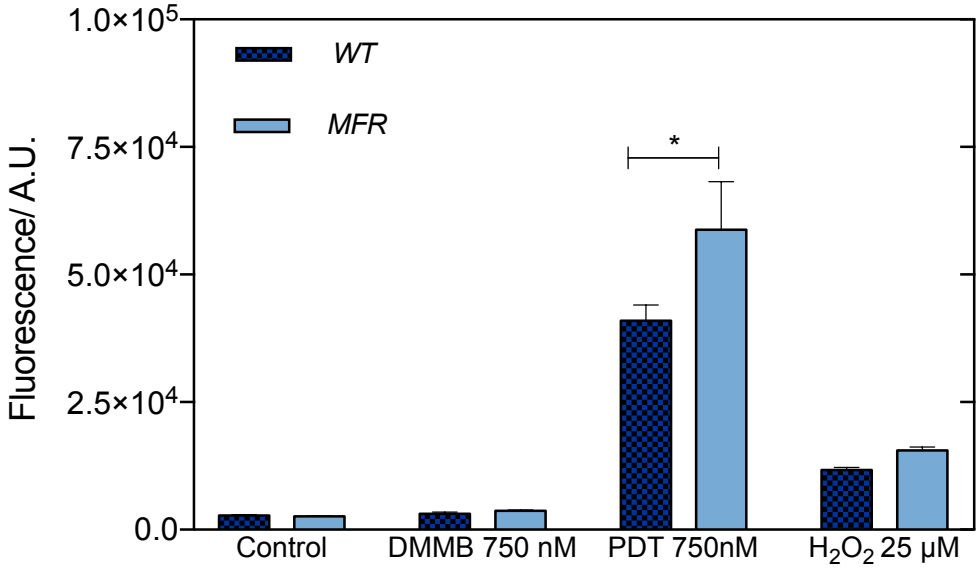

Figure 6.2: Total ROS production using the fluorescent probe H2DCFDA in WT and MFR *L. amazonensis* promastigotes. Parasites were treated with PDT at 50 J/cm^2 and DMMB at 750 nM. Untreated parasites were used as a negative control and 25 µM H_2O_2 as a positive control. ROS production was analyzed by two-way analysis of variance (ANOVA) followed by the Bonferroni post-test. The values shown represent the mean ± SD. * denotes statistically significant differences between strains when $p < 0.05$.

6.3.3 PDT does not affect DNA-containing organelles of treated promastigotes

We also investigated any immediate changes in the parasites DNA due to PDT. Cells were fixed and stained with DAPI (kinetoplast - mitochondrial DNA, and nucleus) directly after PDT treatment, followed by image analysis using high-resolution fluorescence microscope. Results show that both DNA-containing

organelles were well stained in all groups, resulting in a high-intensity signal with bright areas, mainly over kinetoplast. Indeed, no differences in staining were observed between both controls and PDT groups. Both treated cell lines revealed the same structures of a kinetoplast (bar-shaped) and nucleus (round) as untreated controls. Under these conditions, parasites did not differ in their morphological phenotype, including shape and size. No signs of DNA degradation, nuclear condensation, and/or fragmentation were observed (Fig. S6.1, available in the supplementary information (S) at the end of this chapter).

6.3.4 PDT promotes mitochondrial dysfunction on both WT and MFR phenotypes

Mitochondria of WT and MFR parasites were visualised by incubating with MitoTracker red (at 100 nM) for 2 h at two different time points: (i) Directly after, and (ii) 1h after PDT.

The general cell, morphology, i.e. elongated cell body and long flagellum extending out of the flagellar pocket were preserved in all groups for both time points. In both untreated controls, the dye was well retained after fixation, displaying a bright and well-defined red color over the single large mitochondrion across the entire cell (Figure 6.3 A, E). However, when treated by PDT, the loss of membrane integrity resulted in a reduced signal even immediately after treatment (Figure 6.3 B, F).

To further investigate the mitochondrial membrane potential at a later time course, MitoTracker staining was assessed 1h post-treatment. As a result, the same pattern was observed for untreated control, and parasites maintained their morphological features (Figure 6.3 C, G). However, unlike the first time point (immediately after PDT), no red fluorescent signal was detected for treated groups, suggesting a loss of mitochondria membrane potential, thus sustained mitochondrial dysfunction over the 2-hour labelling period. PDT treated cells only showed a very low light intensity, barely detectible (Figure 6.3 D, H). We also observed that there were no significant changes in the parasite's nucleus or kinetoplast, as detected by DAPI staining, after the 3-hour time period.

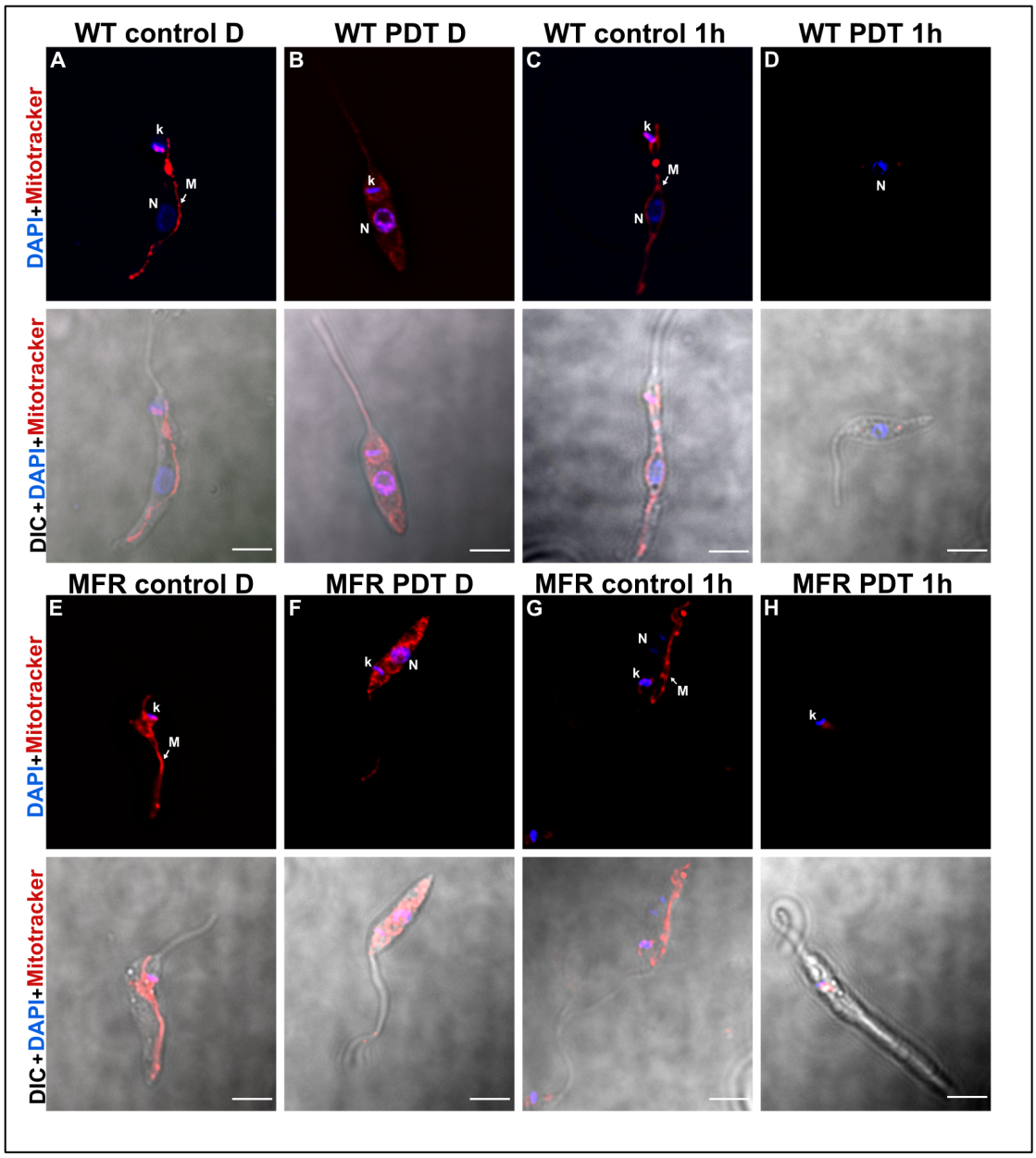

Figure 6.3. Differential interference contrast (DIC) and immunofluorescence staining images of WT and MFR *L. amazonensis* promastigotes treated with PDT at 8 J/cm^2 in the presence of 750 nM of DMMB. A and B refers to WT control and treated directly after PDT. C and D refers to WT control and treated 1 h after PDT. E and F refers to MFR control and treated directly after PDT. G and H refers to MFR control and treated 1 h after PDT. Nuclei were stained with DAPI (blue fluorescence) and mitochondria were stained with Mito tracker red (red fluorescence) directly after PDT. N = Nuclei; k = Kinetoplast; M = Mitochondrion. Scale bar = 5 µm.

6.3.5 PDT increases cytoplasmic lipid droplets of both WT and MFR phenotypes

The presence of intracellular lipid droplets (LDs) was investigated by staining with Nile Red directly after and 1 h after PDT. Subsequent fluorescence microscopy followed by image analysis shows a few small LDs were observed in untreated control groups of both cell lines, as expected under physiological conditions. For both untreated controls, the red points with low intensity over specific areas along the parasites' cytoplasm show the spherical shape of LDs (Figure 6.4 A, C, E, G).

However, the cellular stress in PDT treated parasites, both WT and MFR, caused an immediate and significant increase in the stained LD as well as LDs fusion, which is shown by the greater fluorescence intensity diffused across the cytosol (Figure 6.4 B, F). Indeed, 1 hour after PDT there was an abnormal accumulation of LDs in both strains, resulting in some large-sized globular structures, as shown in Figure 4 D and H.

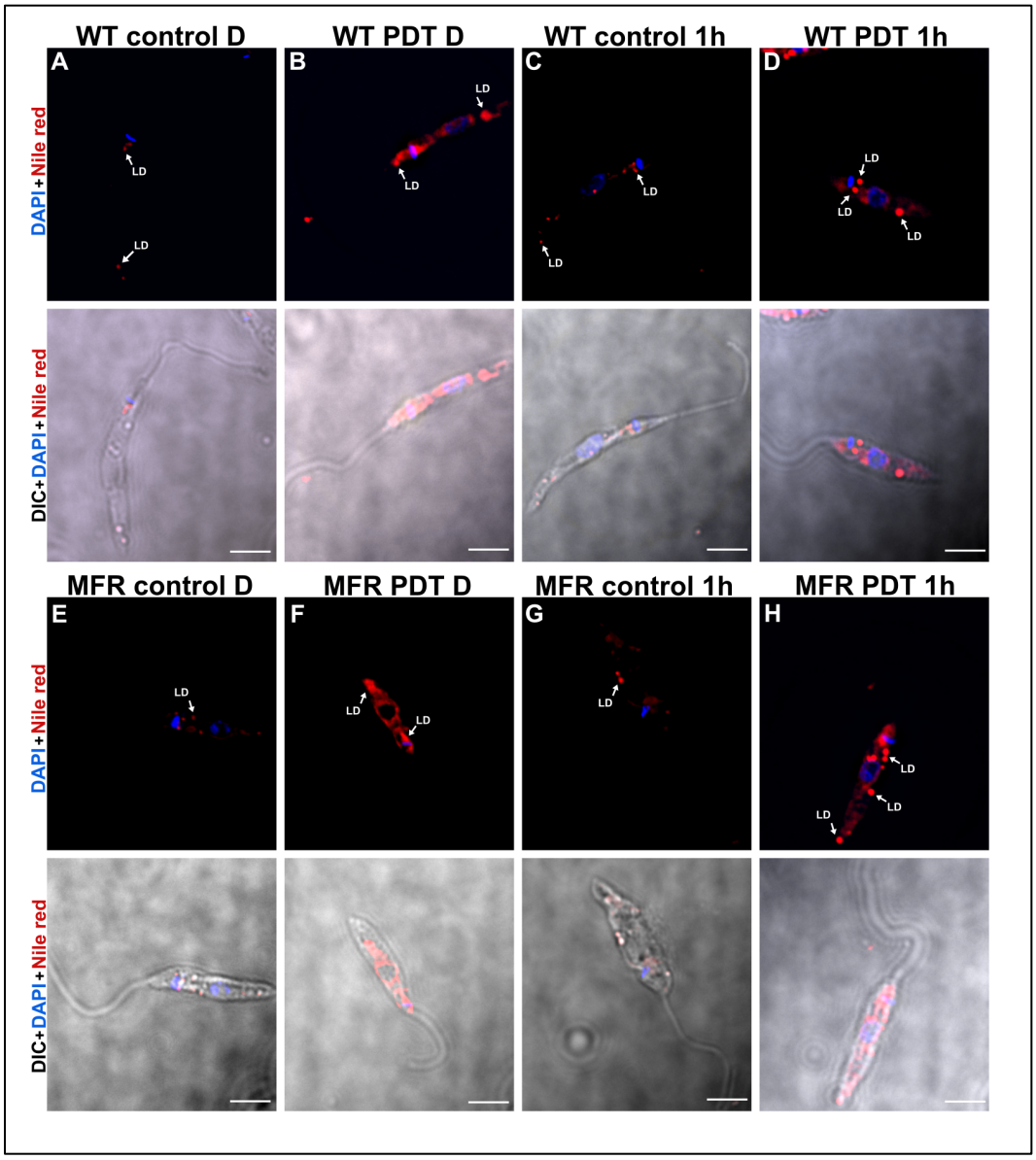

Figure 6.4 Differential interference contrast (DIC) and Nile Red and DAPI immunofluorescence staining, representative images of WT and MFR *L. amazonensis* promastigotes treated with PDT at 8 J/cm^2 in the presence of 750 nM of DMMB. A and B refers to WT control and treated directly after PDT. C and D refers to WT control and treated 1 h after PDT. E and F refers to MFR control and treated directly after PDT. G and H refers to MFR control and treated 1 h after PDT. Nuclei were stained with DAPI (blue fluorescence), and lipid droplets were stained with Nile red (red fluorescence) directly after PDT. LD = Lipid droplet. Scale bar = 5 µm.

6.3.6 Lipidomics analysis reveals a different lipid profile between the WT and MFR phenotypes

Lipidomics profile was evaluated using a triple quadrupole mass spectrometer fitted with a nano-electrospray source. Spectra were obtained from the total lipid extracts and evaluated in positive and negative ion mode for both WT and MFR *L. amazonensis*. As expected, many of the various glycerophospholipid species were observed as well as inositol-phospoceramide, in keeping with previous lipidomic analyses of other *Leishamania* species.[107-109] Phospholipid identities with the corresponding mass over charge (*m/z),* lipid components, and peaks obtained from high resolutions survey scan are specified in Figures 6.5 and 6.6 and Table S6.1. After normalization using non-natural internal standards, the identified lipid species, and their amounts in the various samples were calculated and are represented in a heat-map (Figure 6.6). The molecular species that showed statistically significant differences were plotted in bar graphs according to the corresponding phospholipid (PL) classes (Figures 6.5 and S6.2-S6.6).

ES-MS-MS negative ion spectra of inositol-containing PLs revealed some differences over phosphatidylinositol (PI) molecular species and minor changes of inositol-phosphorylceramide (IPC). Precursor ion scanning for *m/z* 241 identified that two of the most abundant PI species; 851 and 782 *m/z* (PI a-36:0) and (PI 30:0) were 2.2-fold and 1.6-fold higher for MFR than for the WT strain (Figure S6.2 B and E) respectively. Interestingly, for the *m/z* 935 (PI 42:8), one of the species produced in lesser amounts in WT, the abundance was found to be 3.4-fold higher for MFR (Figure 6.5D). While many of the other PI and IPC species showed no significant differences in their relative amounts (Figure 6.5B, C, Fig 6.6 and S6.2A, C, D, F and G).

Negative ion mode using the precursor scanning for *m/z* 196 allowed us to identify ethanolamine-containing PLs from total lipids extracted from WT and MFR. As well as diacyl PE species, the presence of ether (phosphatidylethanolamine) PE (alkylacyl PE and alkenylacyl PE), i.e. plasmalogens were detected (Figure 6.5, 6.6 and S6.4). The overall PE composition did not show major differences in the relative abundance of this PL class between WT and MFR. However, one of the most abundant plasmalogen PE species *m/z* 728 (PE a-36:2) showed significantly lower

levels in MFR, about 4 times compared to the WT. In contrast, *m/z* 701 (PE a-34:1), which is less abundant in the WT, is increased by 26% in MFR parasites (Figure 6.6 and S6.4).

Precursor ion scanning for *m/z* 153 in negative ion mode can also reveal the phosphatidic acid (PA) and phosphatidylglycerol (PG) species and their relative amounts. The dynamic pool of PA species is synthesized in very small numbers for both strains. Although they seem to be present in increased levels for MFR, but there is no statistically significant difference. PG is also normally a minor class of PLs and its synthesis follows the same trend as PA, with no relevant differences between the WT and MFR, even though some molecular species are present in smaller abundance on MFR parasites (Figure 6.5E-H, 6.6 and S6.3).

The PLs containing choline-based head groups were obtained in positive ion mode by precursor scanning for *m/z* 184. [M-H$^+$] ions of phosphatidylcholine (PC) revealed the presence of the main PLs subclasses, such as diacyl and alkylacyl (plasmanyl).

Lipid analysis showed that PC comprises the most abundant class of PLs in WT *L. amazonensis*. However, the differences between both strains revealed that the overall amounts of PC are substantially increased in MFR *L. amazonensis*, pointing out to 24 molecular species with higher amounts than in the WT strain. The main PC peaks includes *m/z* 734 (PC 32:0), *m/z* 760 (PC 34:1), *m/z* 785 (PC 36:2), *m/z* 788 (PC 36:1), *m/z* 811 (PC 38:4), *m/z* 812 (PC 38:3), *m/z* 832 (PC 40:7), *m/z* 834 (PC 40:6), *m/z* 861 (PC 42:6) (Figures 6.5M-P, 6.6 and S6.5).

Except for *m/z* 760, which was 1.6-fold increased, all other choline-containing PLs mentioned above doubled in PC abundance on MFR strain (Figures 6.6 and S6.5M). To be more exact, it was observed a 2.3-fold increase for the *m/z* 733, 811, 812, 861 PC species (Figures 6.6 and S6.5 L, W and V, F). Levels of PC contents were 2.5 times higher for the *m/z* 785 and 788 in MFR (Figures 6.6 and S6.5 Q and R). Other PC molecular species produced in lower quantities were also detected at higher levels on the MFR phenotype. There was a 1.6-fold increase for the *m/z* 758 (PC 34:2), while the *m/z* 756 (PC 34:3), *m/z* 790 (PC 36:0), *m/z* 808 (PC 38:5), and *m/z* 837 (PC 40:4) species doubled in abundance for MFR, with statistically significant differences compared to the (Figures 6.6 and S6.5 N-P, X). It was observed that *m/z* 738 (PC a-34:5) and *m/z* 839 (PC 40:3) PC levels were 2.5-fold

higher in MFR (Figures 6.6 and S6.5 A and Z). The PLs showing the peaks of *m/z* 772 (PC a-36:2) and *m/z* 777 (PC 36:6) had the greatest increase, resulting in a relative abundance 3.4 and 5.1 times higher for MFR than for the WT, respectively (Figures 6.6 and S6.5 D and S).

Abundance of ether linked PC species was also significantly greater for MFR resulting in a doubled amount of the species *m/z* 734 (PC 32:0), *m/z* 792 (PC a-38:6), *m/z* 794 (PC a-38:5), while *m/z* 774 (PC a-36:1) and *m/z* 776 (PC a-36:0) demonstrated a 4.8-fold and 7.7-fold increasing over the WT strain (Figures 6.6 and S6.5 B, C, G, H and L).

PS analysis was carried out in negative ion mode by scanning a neutral loss of *m/z* 87. The overall PS content revealed that this PL class composes a very small percentage of total PLs in WT *L. amazonensis*. Surprisingly, the PS composition of MFR showed a significant reduction in the levels compared to the WT. MFR line revealed decreased amounts in PS series (about 99%) for the peaks with values of *m/z* 801 (PS 38:9), *m/z* 828 (PS a-40:3), *m/z* 853 (PS 42:11), *m/z* 855 (PS 42:10), *m/z* 903 (PS 44:1) (Figures 6.6 and S6.6 A,B,D-F).It was observed around 95% decreasing for *m/z* 892 (PS 44:6), *m/z* 880 (PS 44:12), while the abundance of *m/z* 829 (PS 40:9) detected was 90% less for MFR (Figures 6.6 and S6.6 C,G and H).

6.3.7 PDT promotes a rapid lipid remodeling of WT and MFR phenotypes

Phospholipids were also analyzed after PDT for both strains by ESI-MS/MS, allowing the identification of several changes in phospholipid levels and thus presumably their metabolism. Negative ion mode using the precursor scanning for *m/z* 241 revealed that in PDT WT group there was a ~40% overproduction of *m/z* 808 (IPC 36:0) compared to untreated WT, while this difference was not observed in the MFR cells upon PDT. (Figure 6.6 and S6.2A). We also observed that the levels of several PI species increased (~2.5 fold) for both strains after PDT, i.e. *m/z* 878 (PI a-38:1), *m/z* 897 (PI a-40:6), while *m/z* 883 (PI 38:6) species had a 14.4-fold (PDT WT) and 12.7-fold (PDT MFR) (Figure 6.6 and S6.2 C,D,G).

The overall lipid alterations detected through negative mode ion scanning for *m/z* 153 revealed a downward trend in PA abundance for both PDT-treated parasites (Figure 6.6). In contrast, PG content was considerably enhanced after treatment in both strains. However, statistically significant increases were found in 6 species for

PDT WT, by 2.7-fold for *m/z* 821 (PG 40:7) and *m/z* 822 (PG 40:6). While a 4.7-fold and 6.1-fold increase for *m/z* 789 (PG 38:8) and *m/z* 853 (PG 42:5), respectively (Figure 6.6 and S6.3 E-H). Impressively, there were two species of which a remarkable increase by 12.3-fold and 14.9-fold was detected (*m/z* 759 - PG cyc-37:1, *m/z* 805 - PG 38:1, respectively) after PDT (Figure 6.6, and S6.3 A, B).

Although the overall abundance of PG seems to be higher over PDT MFR group, only 3 species were significantly different from their own control. As mentioned earlier, while *m/z* 805 (PG 38:1) and *m/z* 759 (PG cyc-37:1) showed the largest increase over PDT WT, a minor raise was detected for the same species on PDT MFR (by 3.3-fold and 6.4-fold, respectively) (Figure 6.6, and S6.3 A, B). Regarding *m/z* 789 (PG 38:8), both treated groups presented a similar raise by 4.7-fold (Figure 6.6, and S6.3 E). Notably, statistically significant reduction of 90% was detected in *m/z* 798 (PG 38:4) for both treated strains.

In terms of PE, we found significant changes over 18 PE lipid contents. Unlike the other two PL classes mentioned earlier, 5 PE species were consistently decreased in both treated groups. Particularly, after PDT, three major PE components, *m/z* 726 (PE a-36:3), *m/z* 728 (PE a-36:2) and *m/z* 729 (PE a-36:1) were reduced in 97.6%, 97.9% and 95.1% for the WT, while for MFR there was a reduction of 73.2%, 16.9% and 73.1% over the same PEs species, respectively (Figure 6.6 and S6.4 C-E). Other two less abundant species *m/z* 698 (PE a-34:3) and *m/z* 701 (PE a-34:1) also showed a significant decrease in about 90.2% and 87.4% over the WT and an average about 68% (for both PEs) over MFR strain (Figure 6.6 and S6.4 A, B). There was one particular alteration in *m/z* 714 (PE 34:2) with a significant decrease (by 55%) only for treated WT line (Figure 6.6 and S6.4 F).

The lipid remodeling induced by the oxidative stress became even more evident when multiple PEs species unusually produced, or commonly detected in very small amounts, consistently increased at relatively high levels after PDT. In both strains, 9 PEs species were considerably increased compared to each corresponding untreated control. All of these species showed higher levels in relative abundance for the MFR strain over the WT. From these, *m/z* 760 (PE 38:7) and *m/z* 762 (PE 38:6) presented the greatest increase upon PDT MFR group (by 53.9-fold and 55.9-fold, respectively), while PDT WT enhanced in 14.3-fold and 8.3-fold regarding the same PE species (Figure 6.6 and S6.4 K and L).

For PDT WT, we found that *m/z* 775 (PE 38:0) and *m/z* 854 (PE 44:3) PE contents were 5.5 times higher than WT untreated control. However, PDT MFR comprised even greater amounts of such species (8.7-fold and 19.1-fold) (Figure 6.6 and S6.4 I and Q). The same trend was also observed for the other species: The *m/z* 792 (PE 40:6), *m/z* 794 (PE 40:5) were increased by 10.1-fold (PDT WT), 13.9-fold (PDT MFR), 13.7-fold (PDT WT) and 17.9-fold (PDT MFR), respectively (Figure 6 and S4 M and N). Whilst there has been detected nearly 9-fold increase for PDT WT over 823 (PE 42:4), in MFR values shown were about 11 times higher after PDT (Figure 6.6 and S6.4 O). However, *m/z* 822 (PE 42:5) was the only case in which the relative abundance of this molecular species was higher for the WT (by 6.9-fold) than for MFR (by 5.2-fold) after treatment compared to their own control. However, no significant differences were found between both (Figure 6.6 and S6.4 P)

It is important to mention that 3 particular species significantly increased post-treatment only in MFR line - *m/z* 742 (PE 36:2) (by 3.3-fold), *m/z* 744 (PE 36:1) (by 4.2-fold), *m/z* 764 (PE 38:5) (by 14.8-fold), even though an upward trend was also detected in the WT (Figure 6.6 and S6.4 G, H and J).

Several alterations were detected over the pool of PC species by assessing precursor ion scanning *m/z* 184 in positive mode. Although various PC species demonstrated a tendency to increase in PDT WT group, only 2 of them were statistically significant different from WT untreated control - *m/z* 820 (PC a-40:6) and *m/z* 818 (PC 38:0), revealing an increase by 2.6-fold and 3.0-fold (Figure 6.6 and S6.5 J and T). We also noted a few decreases in other different PC species with 2 alterations statistically significant - *m/z* 834 (PC 40:6) and *m/z* 832 (PC 40:7), with a reduction of 74% in both species. Interestingly, these are two of the most abundant PC in WT cell line (Figure 6.6 and S6.5 B and C)

Remarkably, a different pattern between WT and MFR parasites was observed in response to PDT over choline-containing PLs. We found that 9 PC species were significantly increased in MFR parasites, while 13 species showed a substantial decrease after PDT. Interestingly, the most abundant PC species were substantially reduced after PDT, while the lower ones increased.

It was observed a 1.6-fold increase upon *m/z* 803 (PC 38:7) and *m/z* 823 (PC a-40:4) followed by 2.0-fold increase of *m/z* 800 (PC a-38:2), *m/z* 866 (PC 42:4) and *m/z* 867 (PC 42:3) species (Figure 6.6 and S6.5 F, I, Y and E). The biggest changes

were identified in 4 species - *m/z* 802 (PC a-38:1), *m/z* 820 (PC a-40:6), *m/z* 848 (PC a-42:7), *m/z* 818 (PC 38:0), showing a raise by 2.5-fold in these molecular species (Figure 6.6 and S6.5 J, T, K and T).

Regarding the reduced PC species, *m/z* 760 (PC 34:1) presented the lowest decrease in abundance (28%), followed by *m/z* 734 (PC 32:0) (34%), *m/z* 772 (PC a-36:2) and *m/z* 790 (PC 36:0), both reduced in 38% (Figure 6 and S5 L, D, M, P). PC species with *m/z* peaks of 788 (PC 36:1) and *m/z* 808 (PC 38:5) resulted in further decrease, on average by 50%, while *m/z* 811 (PC 38:4), *m/z* 839 (PC 40:3) and *m/z* 785 (PC 36:2) reduced in 55% (Figure 6 and S5 Q, R, W, X and Z). The *m/z* 812 (PC 38:3) showed a 60% reduction, whereas *m/z* 837 (PC 40:4), *m/z* 834 (PC 40:6) and *m/z* 832 (PC 40:7) revealed the most significant decrease, 70% lower in abundance compared to untreated MFR parasites (Figure 6.6 and S6.5 V, A, B and C).

The PS contents showed a great decrease in all species in the WT strain, with significant alterations in 6 species - *m/z* 853 (PS 42:11) and *m/z* 903 (PS 44:1) were reduced by 98%, while *m/z* 855 (PS 42:10), *m/z* 880 (PS 44:12) were found in 95% lesser amounts than WT control (Figure 6.6 and S6.6 D-F, H). In addition, we found that *m/z* 829 (PS 40:9) and *m/z* 801 (PS 38:9) PS species reduced in 82% and 89% (Figure 6.6 and S6.6 B and C). In contrast, PS content in MFR parasites increased after PDT, with 2 significant alterations - *m/z* 829 (PS 40:9) and *m/z* 892 (PS 44:6), resulting in abundance about 4 and 40 times higher than untreated parasites (Figure 6.6 and S6.6 B and G).

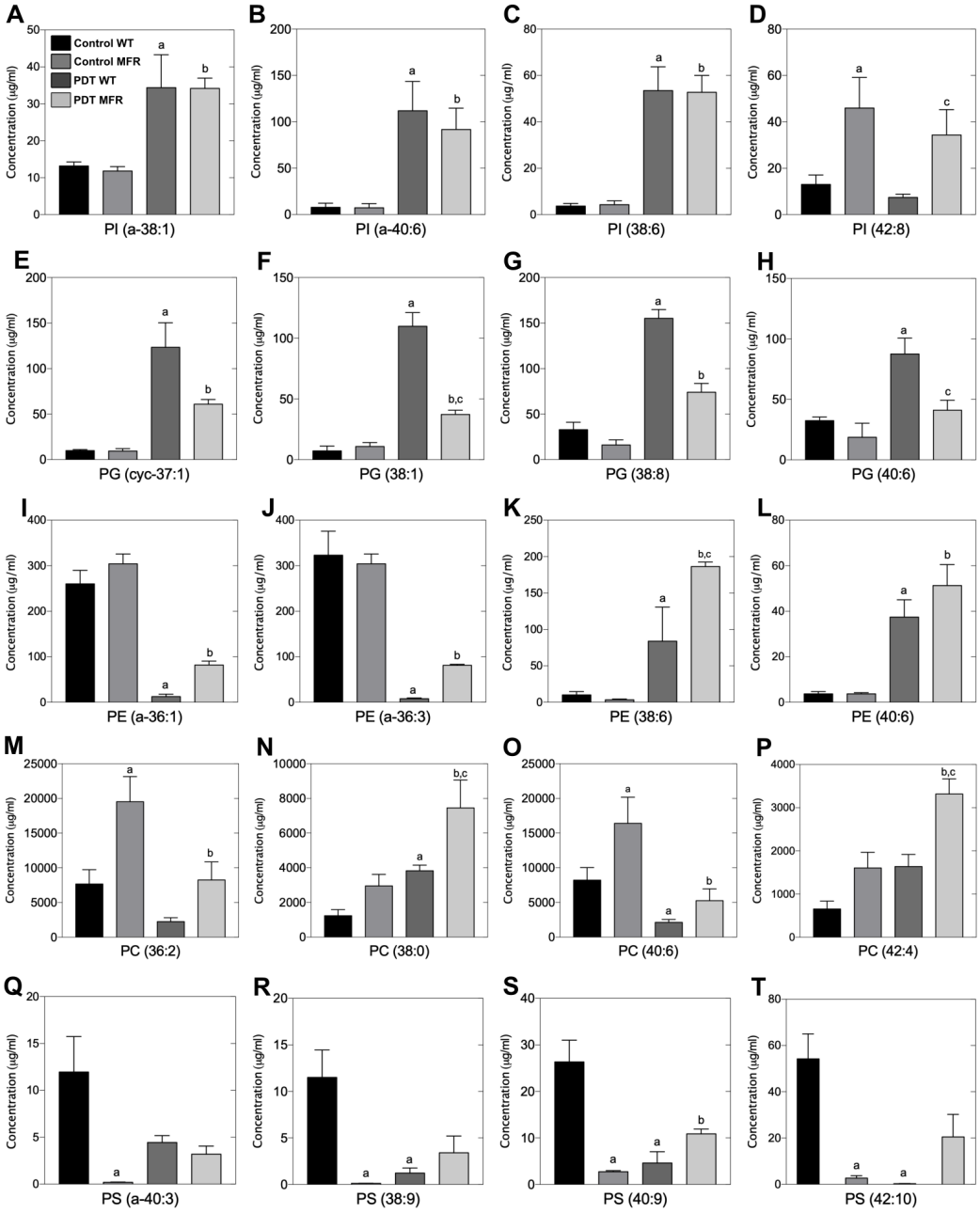

Figure 6.5. Phospholipid analysis of WT and MFR *L. amazonensis* promastigotes treated with PDT at 8 J/cm^2 in the presence of 750 nM of DMMB. A-T represents the concentrations of some molecular species of the corresponding untreated and treated WT and MFR strains. PL class (IPC, PI, PA, PG, PE, PC and PS) was analyzed and quantified according to its corresponding internal "SPLASH" standard. "a" denotes statistically significant differences of PLs species compared to Control WT. "b" denotes statistically significant differences of PLs species compared to Control MFR. "c" denotes statistically significant differences of PLs species between PDT WT and PDT MFR.

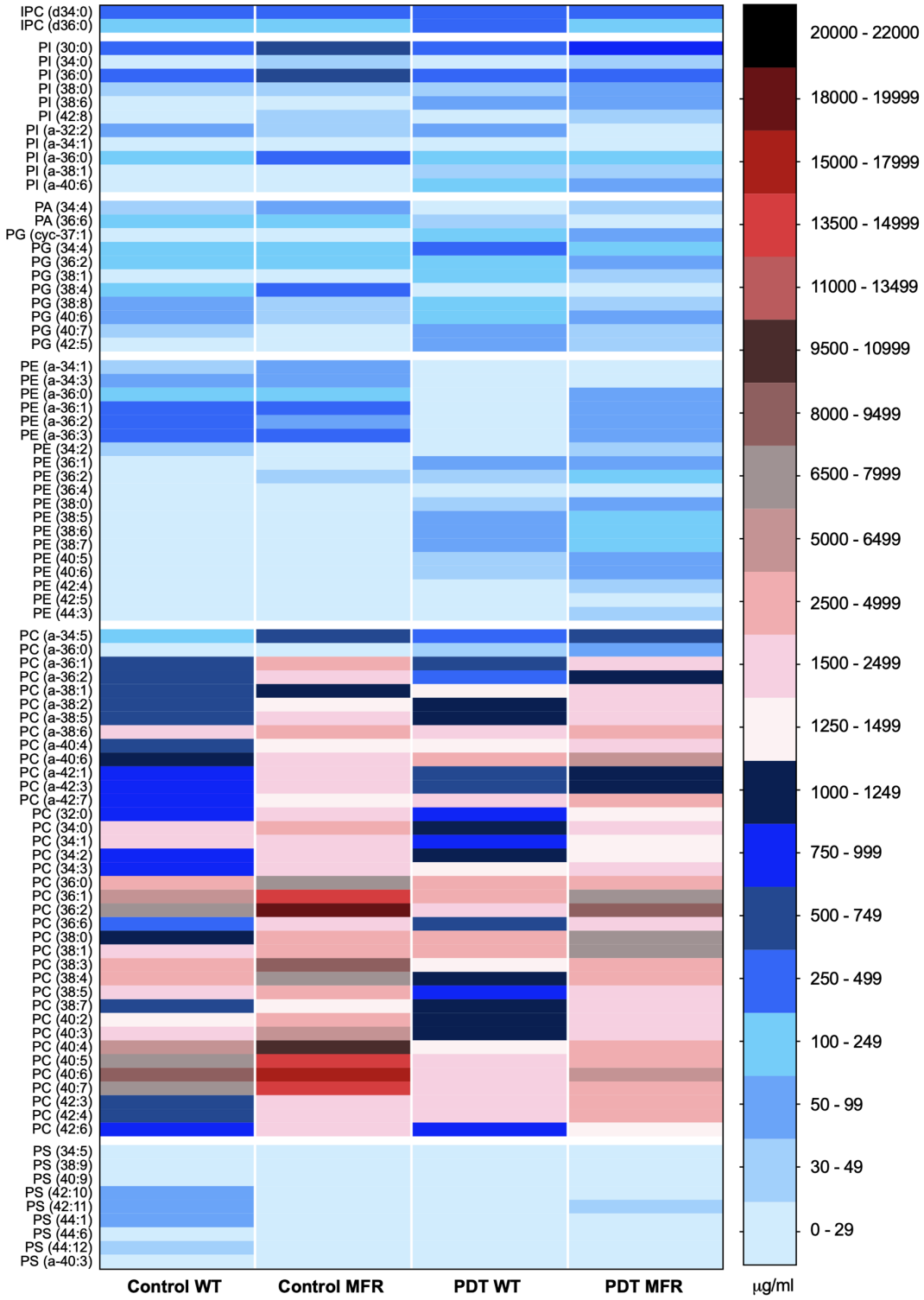

Figure 6.6. Phospholipid analysis of WT and MFR *L. amazonensis* promastigotes treated with PDT at 8 J/cm^2 in the presence of 750 nM of DMMB. Bar on the right side refers to a color scale of the concentration (µg/ml) of each molecular species related to the corresponding PL class (IPC, PI, PA, PG, PE, PC and PS). Each PL

class was analyzed and quantified according to its corresponding internal “SPLASH” standard.

6.4. DISCUSSION

The rise of antileishmanial drug resistance over the past decades has become one of the primary causes of leishmaniasis treatment failure. In recent years, increasing attention has been drawn to the use of PDT as a potential alternative to treat CL to prevent the widespread number of recurrence and unresponsive cases.

In our study, we have demonstrated that DMMB-PDT was very effective in the inactivation of both *L. amazonensis* promastigotes phenotypes (see Figure 6.1). Overall, *Leishmania* parasites are well equipped with an efficient antioxidant system, holding tryparedoxin, superoxide dismutase, thiols, and other peroxidases capable of maintaining their redox balance even in harsh conditions.[110] However, the oxidative stress produced played a significant role in parasite homeostasis (beyond the threshold levels), thereby resulting in cellular death. Remarkably, the accumulation of ROS at higher levels in MFR parasites resulted in their increased susceptibility to PDT compared to the WT strain (see Figure 6.2).

One of the major advantages of PDT is the potential to generate different types of ROS either by type I or type II reactions. Type I process is given by the transfer of charge (from the excited photosensitizer) to a substrate to form a radical (anion or cation), which may further react with oxygen and produce ROS, including H_2O_2, hydroxyl radical, and superoxide anions.[44] The triplet state photosensitizer may otherwise undergo the type II reaction and transfer energy to molecular oxygen, producing singlet oxygen, a highly reactive oxidizing agent.[53]

Both reactions are driven by the intrinsic characteristics of the photosensitizer, which in combination with a proper light source will determine the efficiency of the therapy.[43] In this regard, DMMB is very advantageous for exhibiting a long visible wavelength light absorption in the red region of the spectrum, producing a quantum yield of singlet oxygen around 70%.[53] Moreover, it is very unlikely to be reduced. Yet, the two additional methylene groups in DMMB make it very lipophilic with a positive log $P_{o/w}$ (+ 1.01), thereby it easily diffuses across the lipid bilayer of the plasma membrane.[111]

In addition, it has been shown that having a positive charge enables it to accumulate into the mitochondria (negatively charged inside).[111] As mitochondria are the main regulators of cellular energy production; irreversible mitochondrial depolarization jeopardizes oxidative phosphorylation and compromises adenosine triphosphate (ATP) synthesis. Thus, impaired mitochondrial respiration is a key factor involved in cell survival.[112]

Indeed, this is in agreement with our microscopic observations of mitochondrial labeling (see Figure 6.3). The diffusion of MitoTracker staining throughout parasite cytoplasm suggests that a disruption in mitochondria structural integrity and a loss of its membrane potential occurred directly after treatment. Because of the extensive photodamage, parasites failed to restore their mitochondrial function, thereby 1 h after irradiation no signs of the organelle were observed. Therefore, we assume that DMMB-PDT promoted a complete mitochondrial depolarization in both parasite strains as a consequence of low membrane potential, probably close to zero.

Another key point addressed was the increase of LDs in both treated phenotypes (Figures 4). Lipid droplets are storage organelles usually present in small numbers under physiological conditions.[36] They have long been known as energy reservoirs, mostly for neutral lipids such as triacylglycerol and sterols esters. In recent years, they have been recognized as independent dynamic organelles also involved in cellular homeostasis.[113] Lipid droplets can act beyond lipid metabolism and interact with other organelles such as mitochondria, endoplasmic reticulum, peroxisomes, and therefore play a pivotal role in the management of redox imbalance.[114]

LDs tend to accumulate under cellular stress conditions, protecting membranes from the peroxidation process. In the case of oxidative stress, the overproduction of ROS promotes rapid lipid peroxidation, which is very toxic to the cells due to the excess of fatty acids (FA) and their derivatives released.[114]In this way, lipid droplets can act as buffers and sequester and store the pool of free FA to prevent lipotoxicity, maintaining the redox state, and ensuring cellular survival.[114] The lipids stored can further be used as an energy source and supply gradually the FA necessary for posterior phospholipids synthesis.[113]

Therefore, our results suggest that the high yield of ROS PDT-induced promoted a significant lipid peroxidation in cellular membranes, especially in parasites mitochondria, which led to a loss of membrane potential and releasing of lipids to the cytosol. As a response to metabolic stress, LDs substantially increased, accumulating large amounts of free lipids as an attempt to protect and keep parasites homeostasis. Indeed, the association of LDs and mitochondrial metabolism are essential to prevent lipotoxicity and maintain parasite viability.[114] However, due to the lipid overload there was a dysfunction in LDs and they probably failed to regulate lipotoxicity and redox imbalance, which led to constant cellular stress resulting in parasite death.

To understand in more detail the role of lipid metabolism in *L. amazonensis*, we performed a comprehensive quantitative lipidomics analysis of both WT and MFR strains. Firstly, we compared the differences in lipid profile between both lines, and then we further evaluated their phospholipid alterations under oxidative stress conditions.

ES-MS-MS spectra demonstrated several differences over the lipid metabolism between both phenotypes, which could primarily explain the MF resistance mechanism in MFR *L. amazonensis*. The miltefosine resistance process has been related to a large reduction of drug internalization resulted from a defect in miltefosine transporter (MT) and its regulatory non-catalytic subunit Ros3.[115] Because of an impaired transport function, miltefosine can be expelled by cells even in high drug concentrations.[107] In fact, these genes are the major ones responsible for an inward translocation of miltefosine and PLs throughout the plasma membrane.[107,115] However, it has been previously reported that the MFR phenotype used in our study had a single point of mutation only in the MT gene, rather than both MT and Ros3.[115] In addition, there is growing evidence that MF resistance could also be correlated with other factors such as PL composition, FA and sterols metabolism.[116-118]

It has been reported that miltefosine-resistant *Leishmania donovani* species presented increased levels of PC content.[119] Likewise, our results demonstrate that the overall abundance of this PL class was substantially higher in the MFR phenotype compared to the WT counterpart. PC is the most abundant phospholipid class in eukaryotic membranes and its biosynthesis occurs via the CDP-choline

pathway, one of the two branches of the Kennedy pathway.[120] Briefly, choline is imported by cells and phosphorylated to phosphocholine via choline kinase. A second reaction involves the production of CDP-choline (via CTP:phosphocholine-cytidylyltransferase) followed by a final step, which is the formation of PC.[121]

Miltefosine belongs to the class of alkylphosphocholine drugs; therefore it acts as a phosphocholine analog, inhibiting the translocation of CTP:phosphocholine-cytidylyltransferase, and consequently PC synthesis.[122] Thus, the upregulation of PC observed in the MFR phenotype suggests an adaptive mechanism of parasites to overcome the inhibition of the CDP-choline pathway and promote their survival.

The second branch of the Kennedy pathway relies on the synthesis of PE, via the CDP-ethanolamine pathway.[120] PE is the second most abundant PL class in *Leishmania* parasites and it is closely related to PC synthesis. In fact, PC can be synthesized either by CDP-choline or by the conversion of PE to PC.[120] The alternative route for the synthesis of PC involves threefold methylation of PE, which is catalyzed by phosphatidylethanolamine N-methyltransferase.[120] Thus, we believe that the PE N-methylation pathway could be a possible reason for the significant decrease found in one of the most abundant PE species (PE a-36:2) upon MFR parasites.

Apart from this PE species, no further alterations were observed between MFR and WT phenotypes upon the overall abundance of PE. However, we assume that PE levels were maintained, because of PS decarboxylation, an alternative route used for PE biosynthesis. As *Leishmania* possesses orthologs of phosphatidylserine synthase and phosphatidylserine decarboxylase, PE could have been also generated from PS.[123] Since PS was found in lower abundance over MFR parasites compared to the WT, we hypothesize this pathway could be involved in such phospholipids alterations.

The analysis of inositol-containing phospholipids also revealed significant changes over some PI species in the MFR phenotype. One possible reason could be related to the MF mode of action, which involves the inhibition of phosphatidylinositol 3-kinase (PI3K)/protein kinase B (akt or PKB) pathway, which is essential for signal transduction and cell survival.[107] PI3K is a key protein responsible for phosphoinositides formation, thus the overproduction of PI species may have a role in the molecular mechanism underlying MF resistance developed by MFR parasites.

Phospholipids alterations promoted by oxidative stress were also noted in both phenotypes. The extensive lipid peroxidation mediated by PDT showed a rapid lipid remodeling as a consequence of significant damage in the parasite membrane. It is important to note that lipid peroxidation may cause severe changes in the lipid bilayer altering membrane permeability, fluidity, and structural integrity, thereby resulting in a subsequent cellular dysfunction.[124]

As previously mentioned, our findings suggested a significant mitochondrial oxidative damage, which is consistent with lipid alterations detected by ES-MS-MS. Cardiolipin is a mitochondria-exclusive phospholipid constituent, and its biosynthesis is related to PA and PG metabolism.[125] Initially, PA is converted to cytidinediphosphate-diacylglycerol (CDP-DAG), which is the precursor of PG. PG will then generate cardiolipin by the addition of another CDP-DAG molecule to PG.[126] PA and PG are minor PL classes present in *Leishmania* parasites membrane, however, tandem mass spectra revealed relevant changes over some species. Precursor ions scanning for m/z 153 in the negative mode pointed to an expressive reduction in PA species while PG species were greatly upregulated. Collectively, these data suggest that changes in these lipids' metabolism may have played a role in cardiolipin synthesis to overcome mitochondrial membrane damage.

Nevertheless, the overall PG synthesis was significantly greater in the WT strain than in the MFR phenotype. As a key molecule, PA can be either converted into CDP-DAG to form PI, PG, and cardiolipin, or it can be used as a precursor for DAG to form PC, PE, and PS.[127] Since MFR parasites are dependent upon high levels of PC, it is possible that PA was more involved in DAG pathway to form PC, rather than PG.

Drug-induced lipid alterations have been reported in several *Leishmania* species, mostly over PC and PE metabolism.[119] Indeed, the biggest lipid changes observed in our study were related to PC/PE classes, in which the most abundant species were significantly downregulated in both phenotypes. As these are the main PL classes containing polyunsaturated fatty acids, they are more susceptible to ROS, therefore prone to oxidation.[124] Alternatively, parasites underwent a rapid lipid remodeling in response to oxidative stress, producing other molecular species not usually detected under physiological conditions. Of note, the overproduction of PC

was more pronounced in MFR phenotype compared to the WT, probably due to their higher demand for this lipid class.

Interestingly, unlike in mammalian cells, most PE species in *Leishmania* are displayed in the form of plasmalogens, which in turn, should act as membrane antioxidants scavenging radical species.[127] However, those species were also significantly decreased, whereas the minor ones were greatly upregulated, suggesting that the amount of ROS produced was higher than the parasites ability to reduce oxidative stress.

Surprisingly, those upregulated PE species comprised a very long chain of fatty acids, which was also observed over the others PL classes. Indeed, it has been shown that the increase in the chain of fatty acids in *Leishmania* may have an important role underlying the cellular mechanism of protection, which has been previously reported for *Leishmania donovani*.[128] Long carbon chains enhance membrane rigidity and reduce its fluid properties, thereby preventing drug permeability into the plasma membrane. In addition, it is believed that longer fatty acids can be used as an energy source in parasites.[129] Therefore, our results suggest that the synthesis of phospholipids containing very long FA chains could have been a strategy developed by both *L. amazonensis* strains to help promote their survival.

The role of PE over *Trypanosomatidae* is very critical, because some parasite species are very sensitive to the decrease of PE levels, particularly upon the mitochondrial inner membrane.[120] Thus, we suggest that to compensate for the loss of PE content, levels of PS were also modulated after PDT via PS synthase and/or decarboxylase. However, both lines showed a different response under stress conditions. While PS amounts were substantially reduced in the WT parasites, MFR had some species increased.

PS is synthesized in the endoplasmic reticulum and is transported to mitochondria to produce PE.[130] Since levels of PE were decreased in the WT cells after PDT, we assume PS species were rapidly decarboxylated in mitochondria to form PE (via PS decarboxylase). On the other hand, as the relative abundance of PS was very low under normal conditions in the MFR phenotype, we hypothesize that PS synthesis (via PS synthase) was required to improve PE levels in mitochondria membrane upon oxidative stress.

Perturbations in PE content affect not only phospholipids in the membrane, but also result in proteins dysfunction, especially in those lipid-interacting proteins.[131] For example, glycosylphosphatidylinositol (GPI)-anchored proteins are inserted in the outer leaflet of the plasma membrane and are essential for parasite virulence and survival.[132] They are involved in membrane surface protection and cellular nutrition, and its biosynthesis relies on the addition of ethanolamine phosphate groups to PI (together with monosaccharides). It has been shown that levels of GPI are dependent on the synthesis of inositol in *T. brucei* bloodstream form.[133] Thus, changes in ethanolamine levels might also affect the modulation of PI as a consequence of damage in GPI anchors.[134] Indeed, our results suggest that PDT led to increased levels of some PI species as a result of changes in PE metabolism caused by the perturbations produced in the plasma membrane.

In conclusion, our results demonstrate that DMMB-PDT killed both, wild-type and miltefosine resistant strains effectively, promoting mitochondrial dysfunction via loss of membrane potential and lipid droplets accumulation with significant alterations over the lipid metabolism. Moreover, the MFR line showed to be more susceptible to oxidative stress than the WT strain, resulting in increased levels of ROS at very low nanomolar DMMB concentrations. Thus, DMMB-PDT could be a promising strategy to overcome the challenges of antileishmanial drug resistance for CL infections.

SUPPLEMENTARY INFORMATION

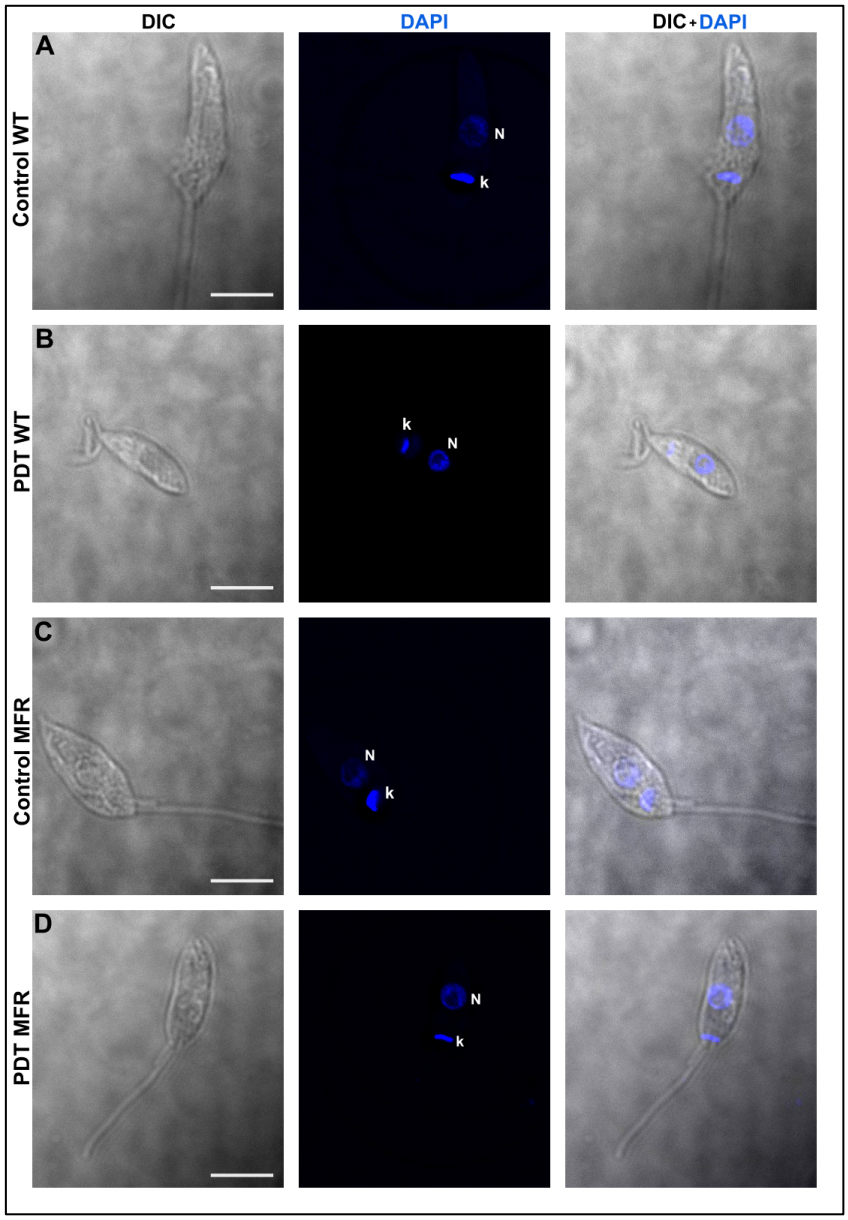

Figure S6.1. Differential interference contrast (DIC) and immunofluorescence staining images of WT and MFR *L. amazonensis* treated with PDT at 8 J/cm^2 in the presence of 750 nM of DMMB. Nuclei and kinetoplast were stained with DAPI (blue fluorescence) directly after PDT. N = Nuclei; k = Kinetoplast. Bar = 5 µm.

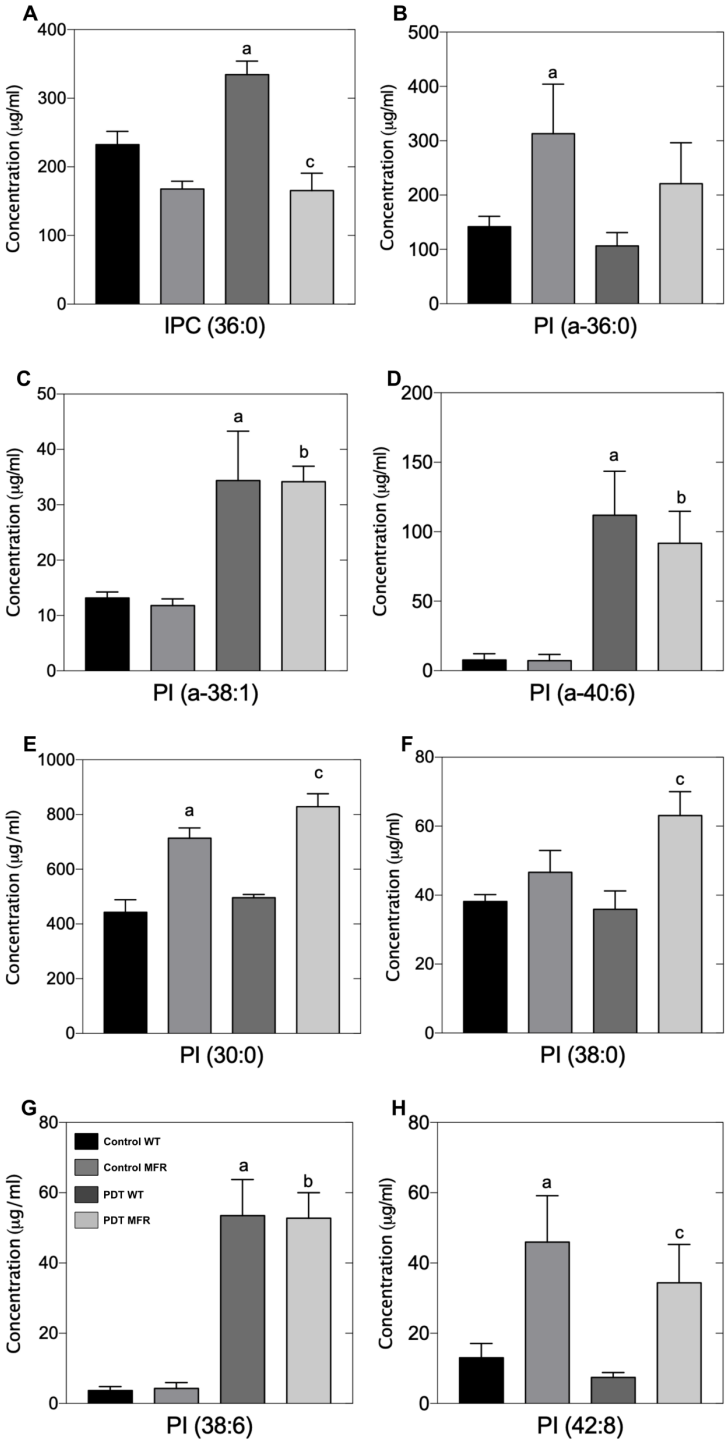

Figure S6.2. Inositol-containing molecular species of WT and MFR *L. amazonensis* promastigotes treated with PDT at 8 J/cm^2 in the presence of 750 nM of DMMB. Precursor ion scanning for *m/z* 241 detected [M - H]$^-$ PI and IPC ions from parasites total lipid extracts. A-H represents the concentrations of each individual molecular species of the corresponding untreated and treated WT and MFR phenotypes. “a”

denotes statistically significant differences of PLs species compared to Control WT. “b” denotes statistically significant differences of PLs species compared to Control MFR. “c” denotes statistically significant differences of PLs species between PDT WT and PDT MFR.

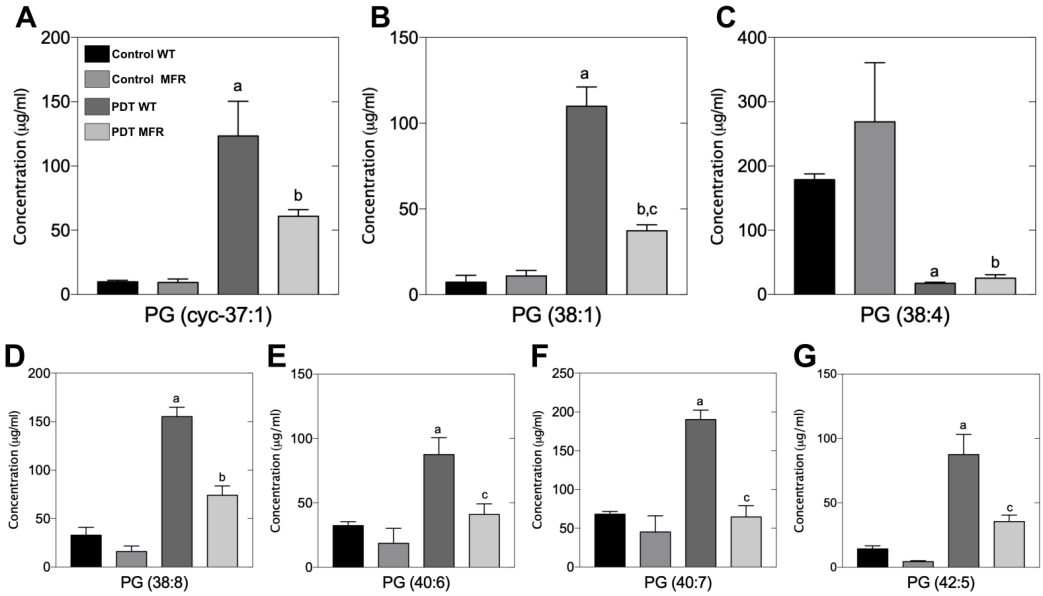

Figure S6.3. Phosphatidic acid (PA) and phosphatidylglycerol (PG) molecular species of WT and MFR *L. amazonensis* promastigotes treated with PDT at 8 J/cm^2 in the presence of 750 nM of DMMB. Precursor ion scanning for *m/z* 153 [M-H]$^-$ detected glycerophospholipids ions from parasites total lipid extracts.

A-G represents the concentrations of each individual molecular species of the corresponding untreated and treated WT and MFR phenotypes. “a” denotes statistically significant differences of PLs species compared to Control WT. “b” denotes statistically significant differences of PLs species compared to Control MFR. “c” denotes statistically significant differences of PLs species between PDT WT and PDT MFR.

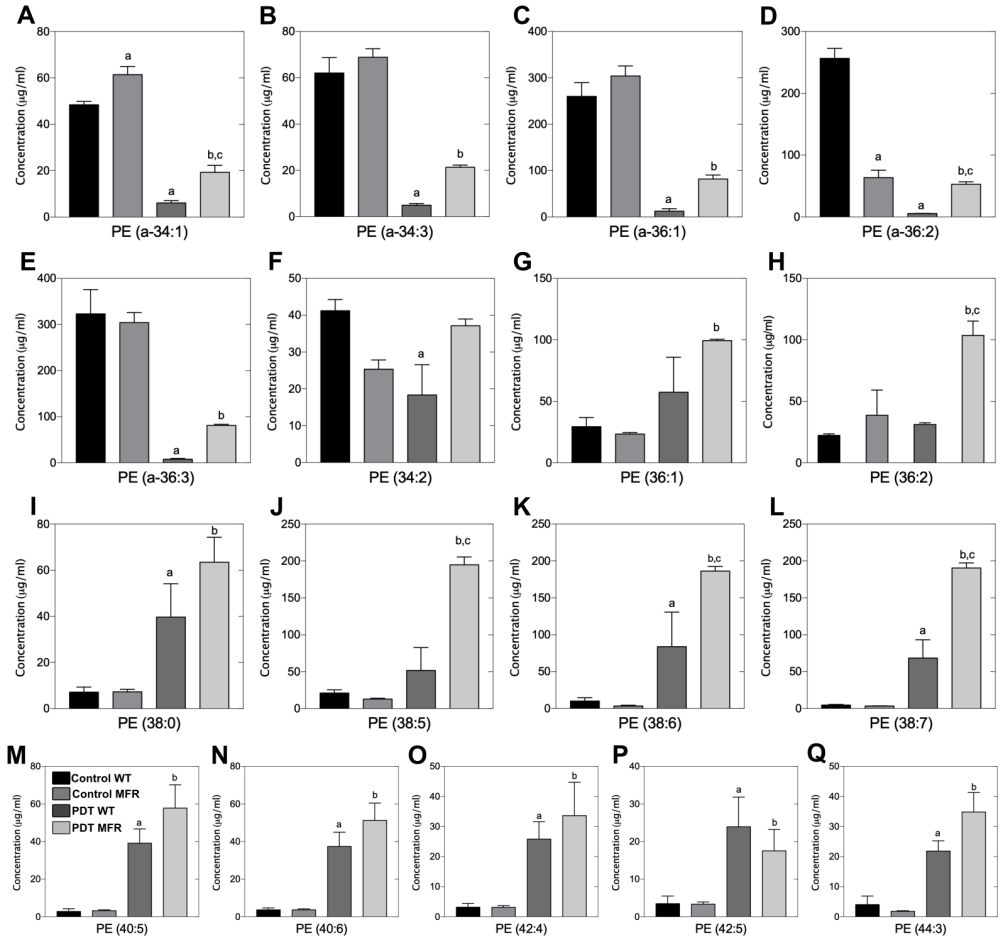

Figure S6.4. Phosphatidylethanolamine (PE) molecular species of WT and MFR *L. amazonensis* promastigotes treated with PDT at 8 J/cm^2 in the presence of 750 nM of DMMB. Precursor ion scanning for *m/z* 196 detected $[M - H]^-$ PE ions from parasites total lipid extracts. A-Q represents the concentrations of each individual molecular species of the corresponding untreated and treated WT and MFR phenotypes. “a” denotes statistically significant differences of PLs species compared to Control WT. “b” denotes statistically significant differences of PLs species compared to Control MFR. “c” denotes statistically significant differences of PLs species between PDT WT and PDT MFR.

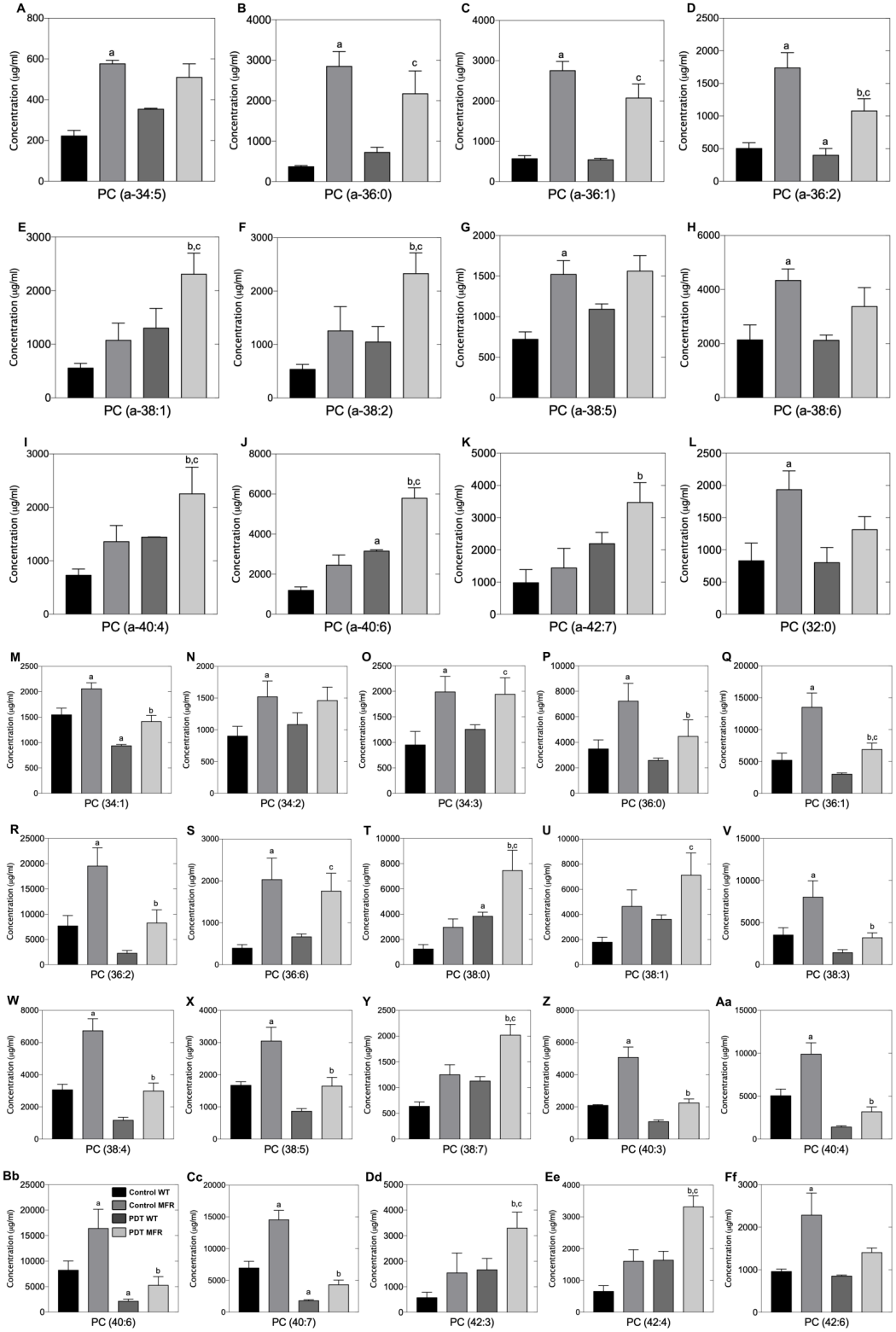

Figure S6.5. Phosphatidylcholine (PC) molecular species of WT and MFR *L. amazonensis* promastigotes treated with PDT at 8 J/cm^2 in the presence of 750 nM of DMMB. Precursor ion scanning for *m/z* 184 $[M + H]^+$ detected PI and IPC ions from parasite total lipid extracts. A-Ff represents the concentrations of each

individual molecular species of the corresponding untreated and treated WT and MFR phenotypes. “a” Denotes statistically significant differences of PLs species compared to Control WT. “b” denotes statistically significant differences of PLs species compared to Control MFR. “c” denotes statistically significant differences of PLs species between PDT WT and PDT MFR.

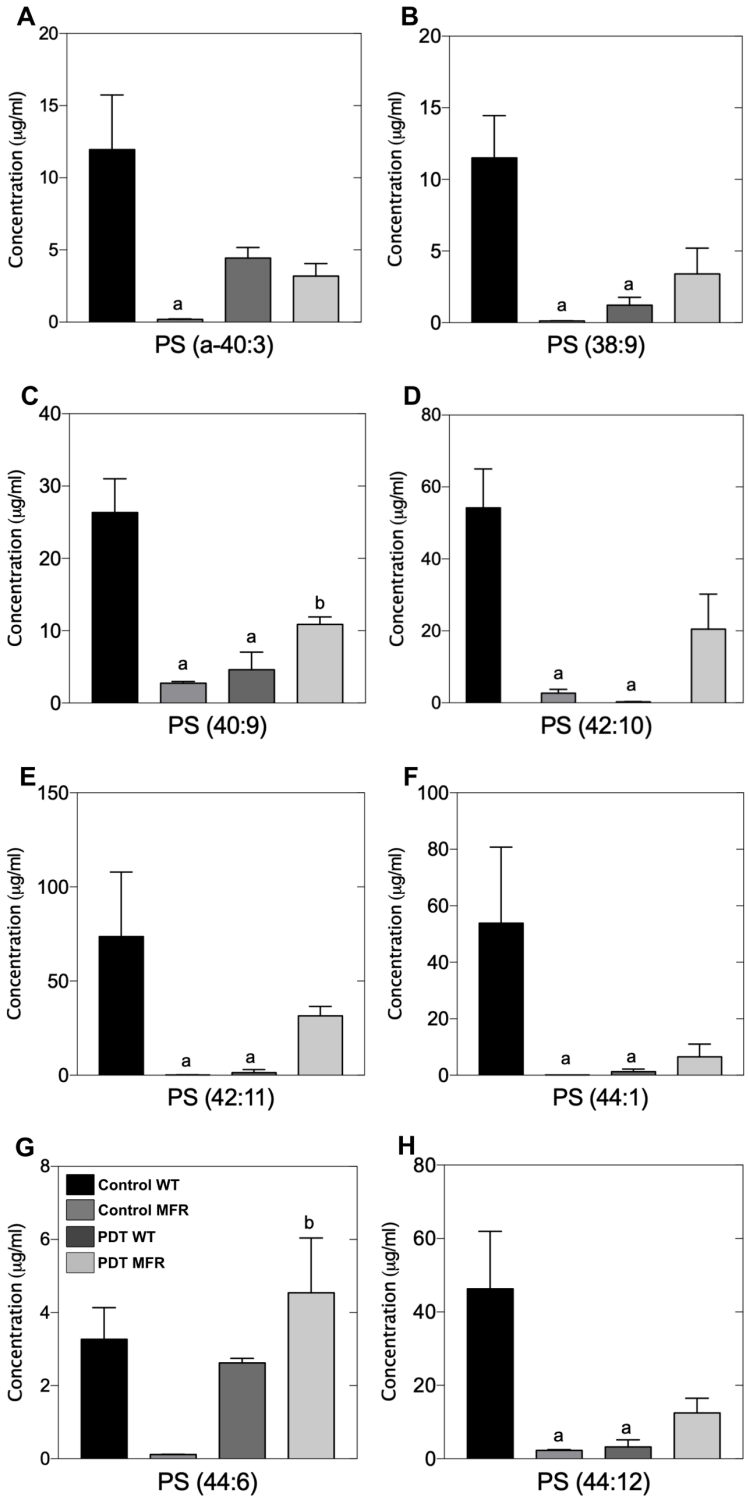

Figure S6.6. Phosphatidylserine (PS) molecular species of WT and MFR *L. amazonensis* promastigotes treated with PDT at 8 J/cm^2 in the presence of 750 nM of DMMB. Neutral loss scanning for *m/z* 87 detected [M - H]$^-$ PS ions from parasites total lipid extracts. A-H represents the concentrations of each individual molecular species of the corresponding untreated and treated WT and MFR phenotypes. "a"

Denotes statistically significant differences of PLs species compared to Control WT. “b” denotes statistically significant differences of PLs species compared to Control MFR. “c” denotes statistically significant differences of PLs species between PDT WT and PDT MFR.

Table S6.1. Mass spectrometric analysis of phospholipid species in *L. amazonensis*

INOSITOLPHOSPHOCERAMIDE (IPC)

m/z[a]	Lipid component[b]
778.4	IPC 34:1
780.2	IPC 34:0
806.6	IPC 36:1
808.7	IPC 36:0

PHOSPHATIDYLINOSITOL (PI)

m/z[a]	Lipid component[b]
782.0	30:0
810.9	32:0
793.9	a-32:2
822.7	a-34:1
836.9	34:0
851.1	a-36:0
865.0	36:0
878.9	a-38:1
883.0	38:6
893.0	38:0
897.5	a-40:6
935.4	42:8

PHOSPHATIDIC ACID (PA)

m/z[a]	Lipid component[b]
668.2	34:4
703.7	36:1
741.7	a-40:2

PHOSPHATIDYLGLYCEROL (PG)

m/z[a]	Lipid component[b]
742.4	34:4
759.4	cyc-37:1
774.3	36:2

789.9	**38:8**
798.8	**38:4**
805.7	**38:1**
821.7	**40:7**
822.4	**40:6**
853.0	**42:5**

PHOSPHATIDYLETHANOLAMINE SPECIES (PE)

m/z[a]	Lipid component[b]
698.7	**a-34:3**
700.6	**a-34:2**
701.6	**a-34:1**
714.7	**34:2**
715.8	**34:1**
726.8	**a-36:3**
728.8	**a-36:2**
729.1	**a-36:1**
731.2	**a-36:0**
738.7	**36:4**
740.6	**36:3**
742.5	**36:2**
744.5	**36:1**
760.2	**38:7**
762.3	**38:6**
764.8	**38:5**
775.0	**38:0**
792.1	**40:6**
794.4	**40:5**
796.3	**40:4**
798.3	**40:3**
822.1	**42:5**
823.1	**42:4**
854.1	**44:3**

[a] Observed $[M+H]^+$ or $[M-H]^-$ ions, mass over charge from survey scans as described in material methods.

[b] Peak identities refer to total number of carbon atoms and double bonds. a = (alkylacyl)

7. CHAPTER FIVE

7.1 DMMB-PDT *in vitro* activity against intracellular amastigotes of *Leishmania amazonesis* wild-type (WT) and miltefosine-resistant (MFR)

7.2 EXPERIMENTAL SECTION

7.2.1 Parasites

L. amazonensis WT (MHOM/BR/73/M2269) promastigotes were grown at 28°C in M199 medium (Sigma-Aldrich) supplemented with 10% heat-inactivated fetal bovine serum (FBS; Gibco™ Invitrogen Corporation), 40 mM HEPES pH 7.4 (Sigma-Aldrich), 2.5 mg/mL hemin (Sigma-Aldrich) and 10 mM Adenosine (Sigma-Aldrich). *L. amazonensis* MFR was selected from the reference strain M2269 (MF 150.3-1 line) as previously reported. Parasites were grown in the same media as WT in the presence of 150 μM of miltefosine (Sigma-Aldrich).

7.2.2 Cytotoxicity assay

7.2.2.1 DMMB-PDT cytotoxicity on fibroblasts and macrophages

NIH 3T3 mouse embryonic fibroblast cells were harvested in DMEM medium (15 mM HEPES, 2 g of sodium bicarbonate/L, and 1 mM L-glutamine) and supplemented with 20% FBS until reach 70 % of confluence, at 37°C.

RAW 264.7 (murine macrophage-like) were harvested in RPMI 1640 medium (15 mM HEPES, 2 g of sodium bicarbonate/L, and 1 mM L-glutamine) and supplemented with 20% FBS until reach 70 % of confluence, at 37°C.

For mitochondrial activity assay, 5×10^3 fibroblasts cells and 8×10^4 RAW 264.7 were seeded on 96-well plates 24 h prior to experiments. Before irradiation, DMMB (0-3000 nM) was incubated for 10 min (pre-irradiation time) to allow the photosensitizer uptake. Then, cells were irradiated using a red OLED (671 ± 140 nm) in an irradiance of 6.5 mW/cm^2. Untreated cells were used as a negative control in a different plate. Incubation of cells with varying concentrations of DMMB without light was also assessed to evaluate the cytotoxicity of the photosensitizer in the dark.

Miltefosine cytotoxicity was also carried out on RAW 264.7 macrophages. For this, 8×10^2 cells were seeded on 96-well plates 24 h prior to experiments. Miltefosine

activity was performed by the addition of serial dilutions of MF (0-500 μM), for 48 h at 37°C.

Cell viability was evaluated by MTT. Briefly, after treatment, the cells were incubated with 30 μL of MTT (at 5.0 mg/mL) (3-[4,5-dimethyl-2-thiazolyl]-2,5-diphenyl-2H-tetrazolium bromide; Sigma-Aldrich, USA) and maintained at 37°C for 4 h. The reaction was stopped by adding 50 μL of DMSO to each well and the optical density was measured in a spectrophotometer (Spectramax M4, Molecular Devices, USA) at 595 nm using a reference wavelength of 690 nm. Results were expressed as a percentage of mitochondrial activity compared to control. The half-maximal effective concentration (EC50) was obtained by sigmoidal regression analysis using GraphPad Prism 7.0 software.

7.2.2.2 Miltefosine and DMMB-PDT activity on intracellular amastigotes of WT and MFR

RAW 264.7 cells (8×10^4) were plated on glass coverslips in 24-well plates 24 h prior experiments and then infected with promastigotes of both strains at a multiplicity of infection (MOI) = 10 for 4 h, at 34°C. Cells were washed and incubated in fresh medium for 24 h. Infected cells were the treated with either miltefosine (0-50 μM) or DMMB-PDT at 8 J/cm^2 and varying DMMB concentrations (0-750 nM).

After 48 h, parasites were quantified using optical microscopy. For this, the cells were fixed with methanol, washed with PBS, and stained with Giemsa. Results were determined by counting 100 cells per coverslip and expressed as percentage of infected macrophages and average number of amastigotes per macrophage. The infection index was also calculated following the equation:

$$Infection\ index = \frac{\text{Number of amastigotes}}{\text{infected macrophages}}\ \text{x}\ \%\ \text{infection}$$

7.3 RESULTS

7.3.1 DMMB-PDT is not toxic to mammalian cells

Our results demonstrate that the photosensitizer did not promote cytotoxic effects neither on NIH 3T3 fibroblasts nor on RAW 264.7 cells when incubated with DMMB in the dark, regardless of the photosensitizer concentration (Figure 7.1A). However, mitochondrial metabolic changes were observed when cells were treated with PDT. We noticed alterations in cells viability depending on the light-dose as well as the photosensitizer concentration. The lowest and intermediate light doses (2 and 4 J/cm^2) promoted a slight reduction in fibroblasts at 750 nM, and a further decrease at 1500 and 3000 nM. Nevertheless, 75% of cells showed mitochondrial activity even at higher photosensitizer concentrations (Figures 7.1 B and C). At the highest radiant exposure (8 J/cm^2), 88% of cells were viable at 375 nM, whereas at the highest concentrations and same light dose we observed 75 % of cell activity (Figure 7.1 D). In all treated groups cells were properly adhered to the wells in the plates, showing that morphologic and phenotypic fibroblasts characteristics were maintained at all three light doses using a concentration of 750 nM, as displayed in Figure 7.2. No morphological alterations were noticed using only DMMB or just light at 8 J/cm^2 (Figure 7.2 B,C).

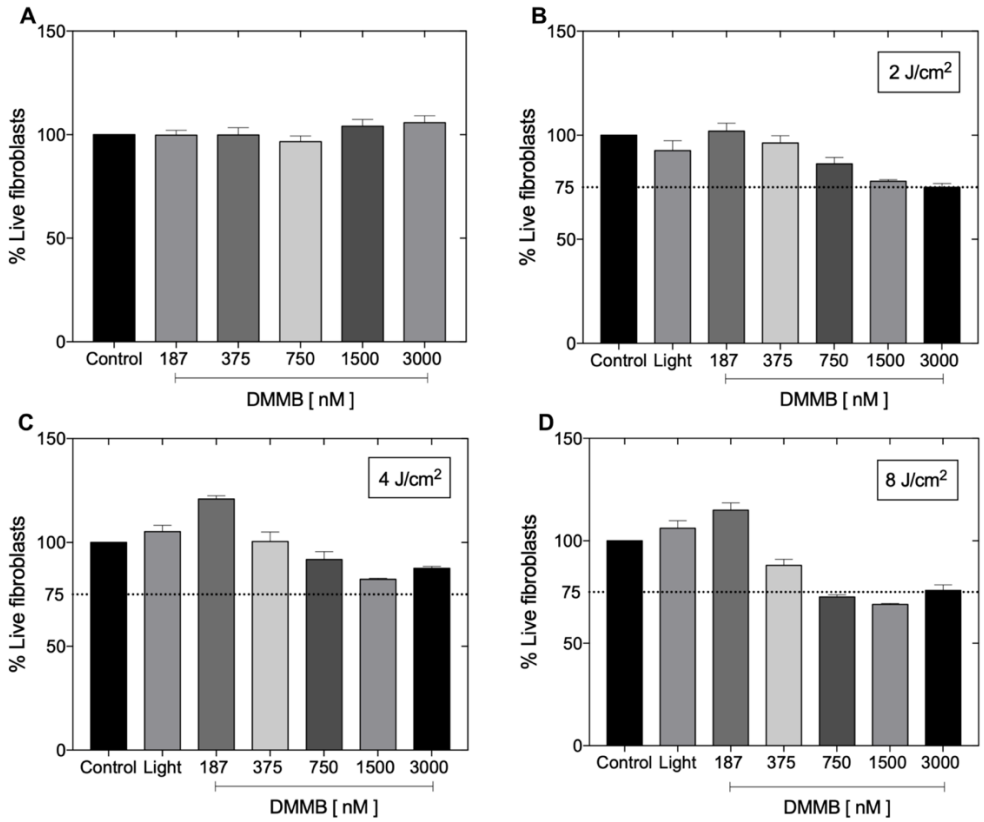

Figure 7.1: NIH 3T3 fibroblasts cells treated with increasing concentrations of DMMB (A) In the dark and at different radiant exposures (B) 2 J/cm^2, (C) 4 J/cm^2, (D) 8 J/cm^2. Mean values ± SEM of mitochondrial activity were determined by MTT assay (n=4).

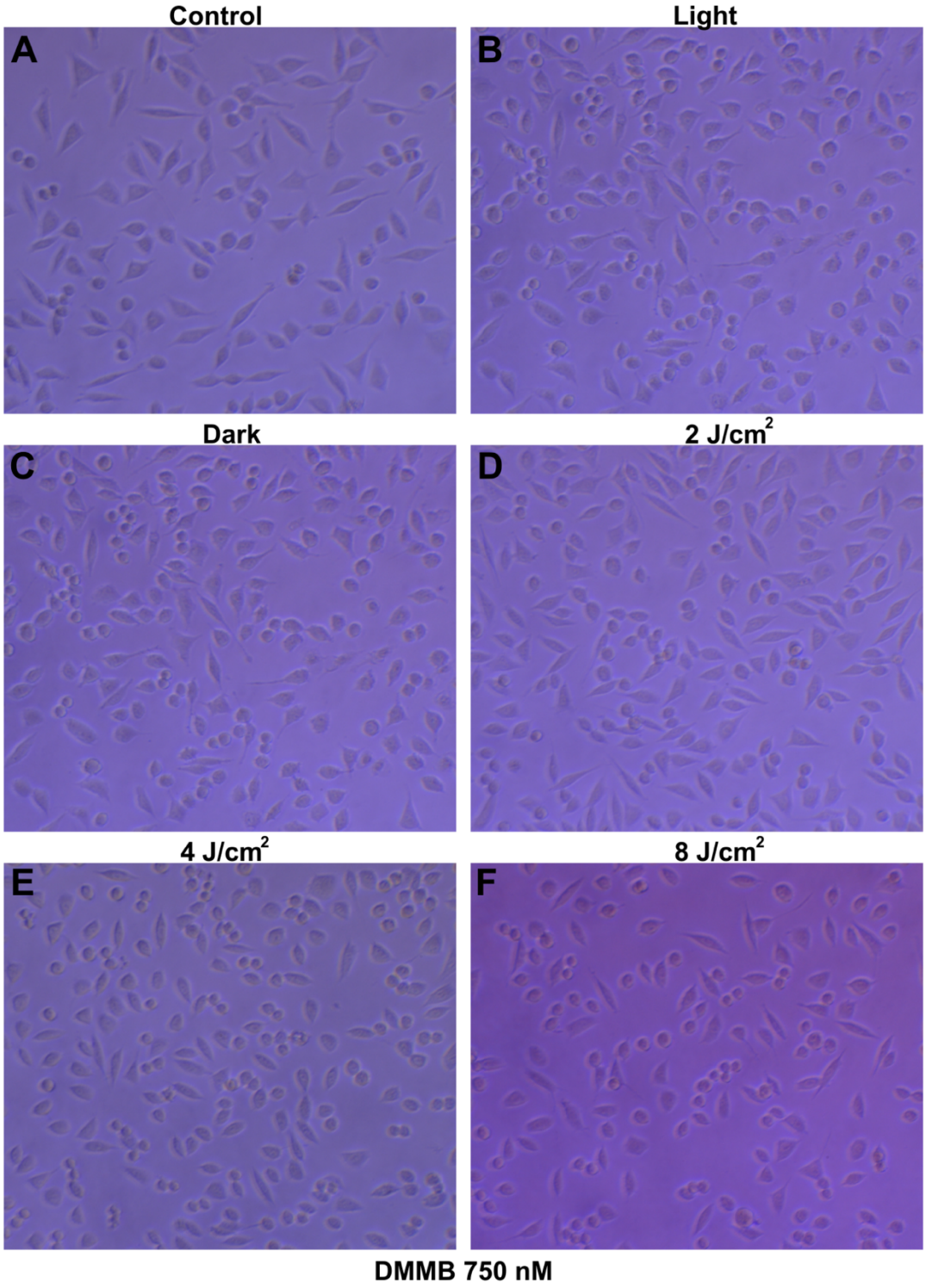

Figure 7.2: Representative images of NIH 3T3 fibroblasts cells treated with DMMB at 750 nM and different radiant exposures. (A) Untreated control, (B) Light at 8 J/cm^2, (C) DMMB in the dark, (D) DMMB-PDT at 2 J/cm^2, (E) DMMB-PDT at 4 J/cm^2, (F) DMMB-PDT at 8 J/cm^2.

A light dose and DMMB concentration-dependent effect was also observed when Raw 264.7 cells were treated by DMMB-PDT. Interestingly, at 750 nM no reduction in mitochondrial activity was observed at all light doses used, suggesting macrophages are more resistant to oxidative stress when compared to NIH 3T3 fibroblasts, except for the highest concentration (Figure 7.3). Cells were also properly adhered, covering all the surface on the bottom of the well plate in all groups. Yet, no morphological alterations were observed by optical microscopy, as shown in figure 7.4.

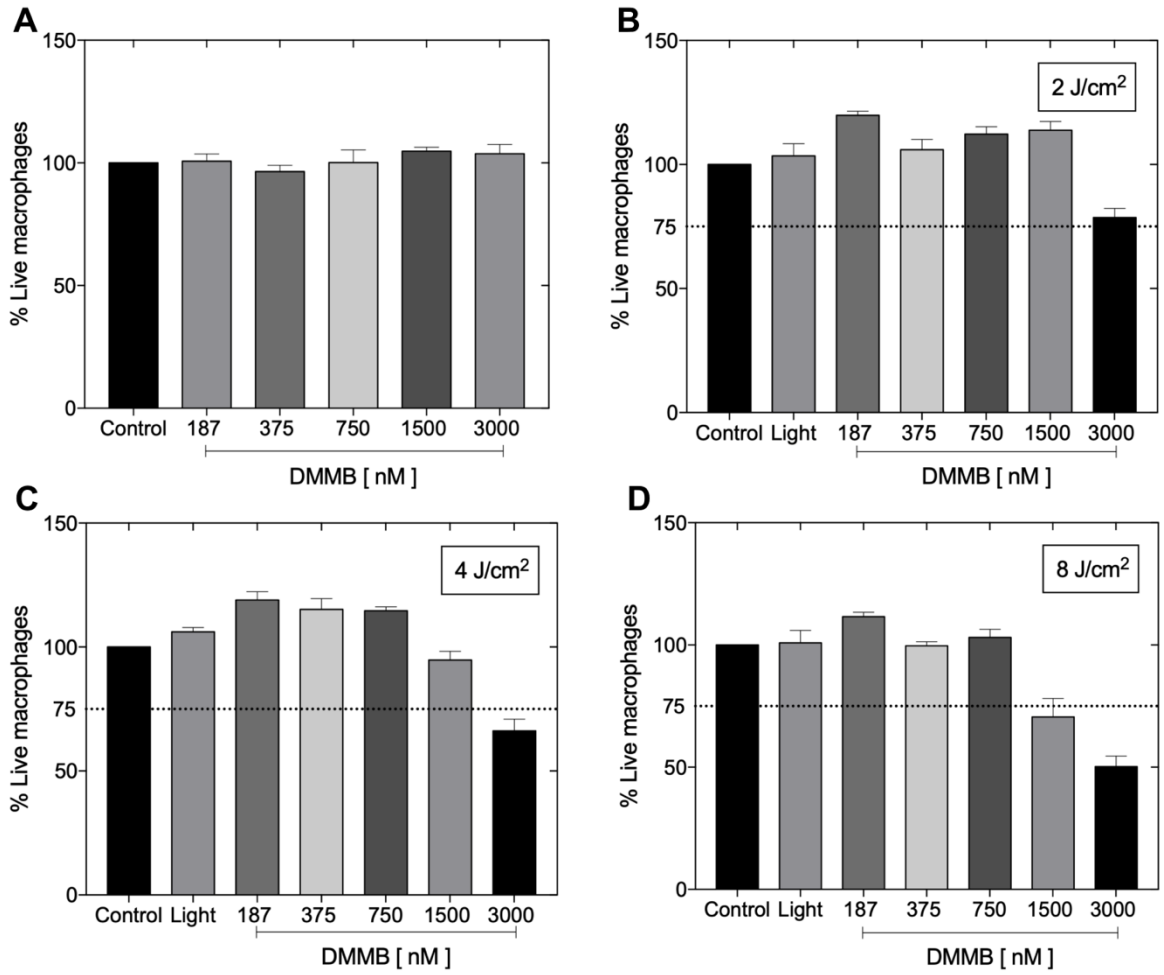

Figure 7.3: RAW 264.7 cells treated with increasing concentrations of DMMB (A) In the dark and at different radiant exposures (B) 2 J/cm^2, (C) 4 J/cm^2, (D) 8 J/cm^2. Mean values ± SEM of mitochondrial activity were determined by MTT assay (n=8).

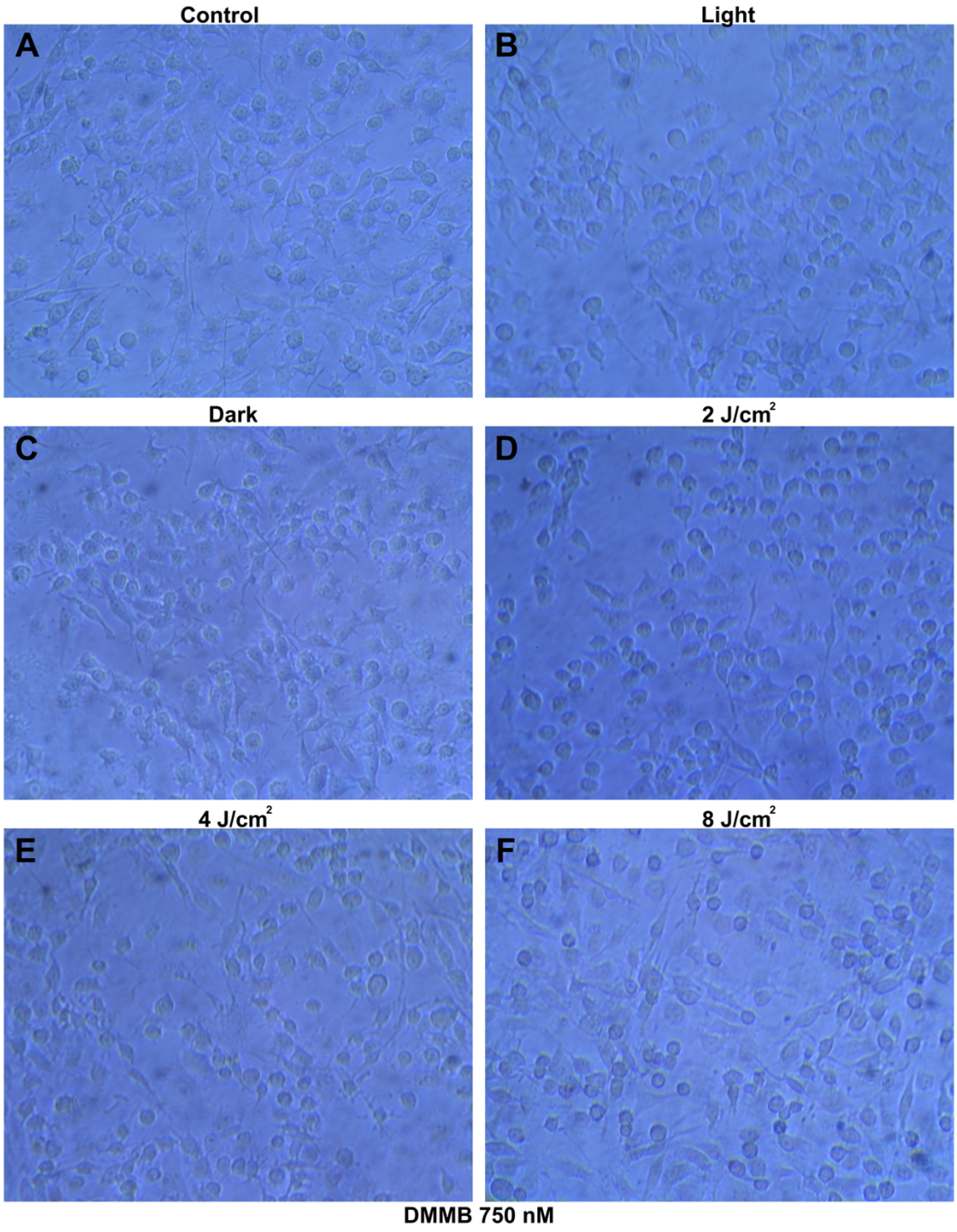

Figure 7.4: Representative images of Raw 264.7 cells treated with of DMMB at 750 nM and different radiant exposures (0,2,4 and 8 J/cm^2). (A) Untreated control, (B) Light at 8 J/cm^2, (C) DMMB in the dark, (D) DMMB-PDT at 2 J/cm^2, (E) DMMB-PDT at 4 J/cm^2, (F) DMMB-PDT at 8 J/cm^2.

Miltefosine cytotoxic activity was assessed on macrophages using increasing drug concentrations ranging from 0 to 500 µM. It was also noticed a dose-dependent effect in macrophages viability. MTT assay was performed after 48 h of incubation. CC_{50} value of miltefosine was 46.46 µM, and it was obtained by sigmoidal regression analysis (Figure 7.5 A). DMMB CC_{50} (1188 nM) was also calculated using the highest light dose (8 J/cm^2) (Figure 7.5 B).

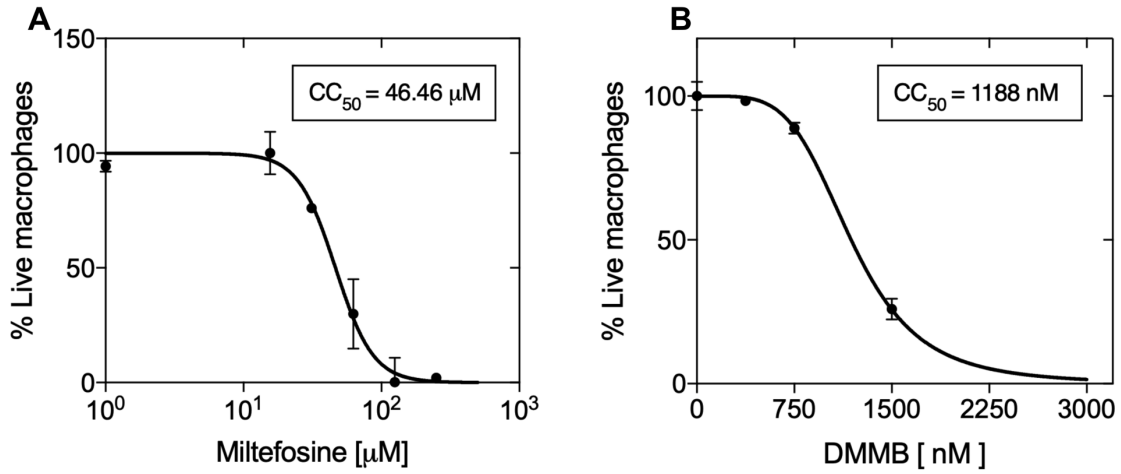

Figure 7.5: CC_{50} of macrophages treated with increasing concentrations of (A) miltefosine (0-500 µM) and (B) DMMB (0-300 nM) at 8 J/cm^2. Mean values ± SEM determined by MTT assay (n=3).

7.3.2 Intracellular *L. amazonensis* WT and MFR amastigotes are susceptible to DMMB-PDT

Macrophages were infected with promastigotes of *L. amazonensis* WT and MFR cell lines at MOI 10:1. Then, intracellular parasites of both strains were treated with DMMB-PDT or miltefosine. The experimental conditions used for both treatments were set from previous results determined from macrophages cytotoxicity assay.

Infected macrophages were treated with a radiant exposure of 8 J/cm^2 and DMMB concentrations ranging from 96 to 750 nM since these concentrations were not toxic to healthy macrophages. According to our results, we may observe that %

of infection was appropriate, showing nearly 80% of cells were infected by amastigotes of both strains (Figure 7.6 A and D). When parasites were treated by DMMB-PDT, we noticed that at the lowest concentration (96 nM) the % of infection was reduced in 47% and 38% in WT and MFR in comparison with their respective untreated controls. At 750 nM, a further reduction of 49% and 51% was observed for the WT and MFR. Indeed, only approximately 21% and 24% of cells were infected by WT and MFR in these conditions, respectively (Figure 7.6 A).

In contrast, parasites treated with miltefosine did not show significant improvement in the % of infection. Since miltefosine was toxic to macrophages at high doses (EC_{50} found was 46.46 μM), the highest concentration assigned was 50 μM. Although nearly 16% of intracellular WT amastigotes were reduced at a concentration of 50 μM, no statistically significant differences were observed. Indeed, statistical differences were observed between both strains at 50 μM, in which 79% of cells were infected by MFR, whereas the % of infection was around 61 % for the WT (Figure 7.6 D).

The number of amastigotes per infected macrophage was also significantly reduced in both cell lines treated by DMMB-PDT. Untreated controls presented similar numbers of intracellular amastigotes, accounting for an average of 15.7 and 12 parasites per infected macrophage for the WT and MFR lines, respectively. It was observed a DMMB concentration-dependent effect on the inactivation of both parasites. Surprisingly, even the lowest dose was able to reduce in 34 % (from an average of 15.7 to 10.4) and 15% (from an average of 12.3 to 10.5) the number of amastigotes/infected macrophage. DMMB-PDT at 750 nM inactivated nearly 79.2 % (from an average of 15.7 to 3.2) the WT amastigotes, whereas about 42.6 % (from an average of 12.3 to 5.2) of MFR parasites were inactivated in the same conditions (Figure 7.6 B).

When both parasites were treated with miltefosine, we noticed a decrease in about 28% in the number of WT parasites per infected cell (from an average of 8.7 to 6.2) at the lowest dose (6.25 μM), while at 50 μM, 48% (from an average of 8.7 to 4.5) of parasites were killed. However, miltefosine was not effective in inactivating the resistant parasites with the concentrations used (Figure 7.6 E).

The infective index represents the overall effectiveness of treatment, since it is calculated by the multiplication of both, the % of infection and the average number

of amastigotes/infected macrophage (see equation in section 3.2.3).

Both strains showed the same dose-dependent pattern when treated by DMMB-PDT, showing a reduction of WT and MFR around 65.0 % and 49.8% at the lowest concentrations on 96 nM, respectively. Remarkably, we observed that 94.5% of WT amastigotes were killed using 750 nM, while in MFR strain, 86.3% of parasites were inactivated in the same conditions (Figure 7.6 C).

There was 53.3% reduction in infection index when the WT parasites were treated with miltefosine at 50 μM, showing a significant difference compared to untreated control. However, as expected, miltefosine was not able to promote significant changes over the infection index in MFR strain (Figure 7.6 F).

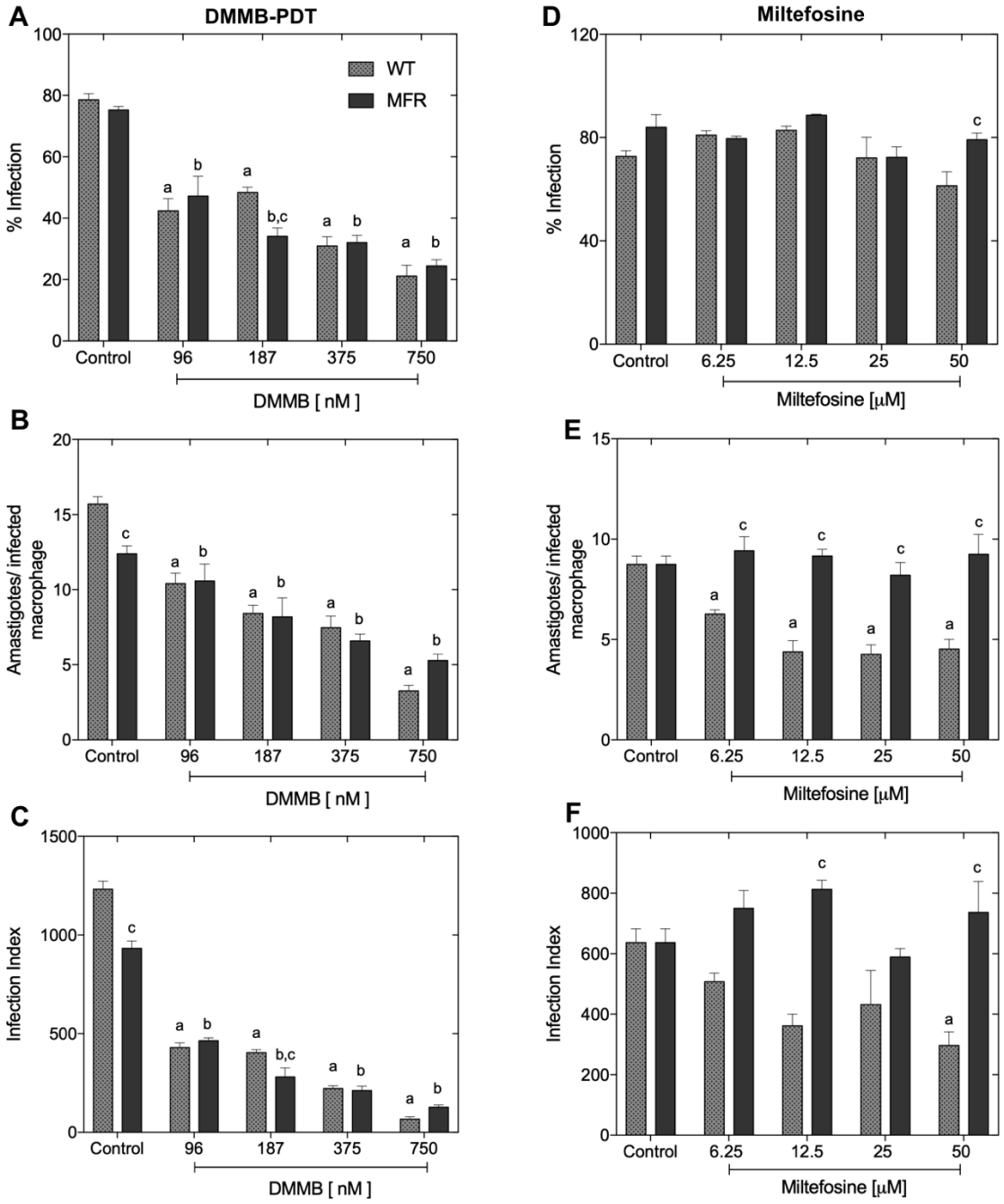

Figure 7.6: Activity of DMMB-PDT (0-750 nM) at 8 J/cm^2 and miltefosine (0 to 50 μM) on intracellular amastigotes of *L. amazonensis* WT and MFR. Results were determined by counting 100 cells per coverslip and expressed as percentage of infected macrophages and average number of amastigotes per macrophage. (A,D) Percentage of infection (B,E) Amastigotes per infected macrophage (C,F) Infection index. “a” denotes statistically significant differences between WT control and treated

groups. “b” denotes statistically significant differences between MFR control and treated groups. “c” denotes statistically significant differences between PDT WT and PDT MFR. ($p < 0.05$, n= 6).

By using a sigmoidal regression analysis, we calculated the EC_{50} of intracellular amastigotes of WT and MFR *L. amazonensis* treated with miltefosine or DMMMB-PDT. EC_{50} values of miltefosine for MFR amastigotes were not possible to calculate, however, for the WT, EC_{50} value obtained was 5.98 µM.

For the WT, DMMB EC_{50} value was 52.58 nM, while for MFR the half-maximal effective concentration was found to be 77.51 nM. Indeed, although both strains were effectively killed, WT line was more susceptible to DMMB-PDT than resistant parasites, suggesting that lower photosensitizer concentration is necessary to achieve the same killing rate (Figure 7.7).

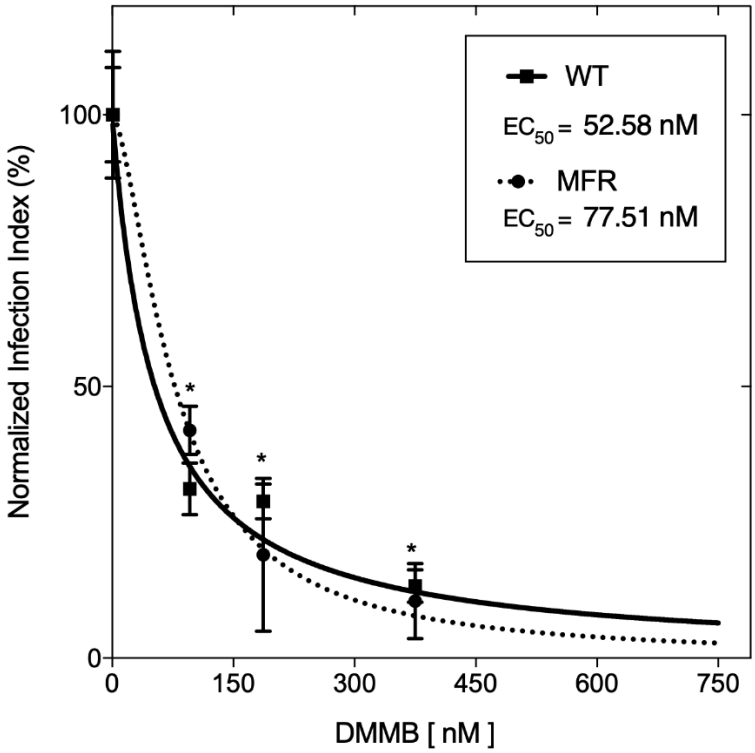

Figure 7.7: DMMB EC_{50} on intracellular amastigotes of WT and MFR *L. amazonensis* treated with DMMB-PDT at 8 J/cm^2. Mean values ± SEM. *denotes statistically significant differences between WT and MFR treated groups and their respective untreated control. (* $p < 0.05$, n = 6)

The selectivity index (SI) was determined by calculating the ratio of either miltefosine or DMMB cytotoxic concentration (CC_{50}) (obtained from macrophages MTT assay), and EC_{50} values.

$$SI = \frac{\mathrm{CC50}}{\mathrm{EC50}}$$

As shown in table 7.1, SI of miltefosine for the WT was 7.76, while for MFR parasites it was very low (> 0.92) since MFR intracellular amastigotes were not inactivated. Surprisingly, for DMMB-PDT, SI was very high for both lines, showing a higher value for WT (22.59) in relation to MFR (15.32).

Table 7.1. Selectivity index of intracellular amastigotes of WT and MFR *L. amazonensis* treated with miltefosine and DMMB-PDT at 8 J/cm^2, (n=6).

	Miltefosine Macrophages	**PDT macrophages**	**Miltefosine WT**	**Miltefosine MFR**	**PDT WT**	**PDT MFR**
EC_{50} Ama/Infec macrophage	N/A	N/A	5.98 μM	> 50 μM	52.58 nM	77.51 nM
CC_{50} macrophages	46.46 μM	1188 nM	N/A	N/A	N/A	N/A
Selectivity index (SI)	N/A	N/A	7.76	> 0.92	22.59	15.32

7.4. DISCUSSION

In the present work we have successfully demonstrated the potential of DMMB-PDT to inactivate *in vitro* intracellular amastigotes of both *L. amazonensis* WT and MFR strains.

Although we have observed a concentration and light dose-dependent cytotoxic effect of DMMB-PDT over fibroblasts and macrophages, the antileishmanial effective doses obtained were not toxic to these cells.

Fibroblasts are among the main cells of connective tissue and play a significant role in the synthesis of collagen fibers to support tissue repair, producing a new extracellular matrix.[135] It has been shown that fibroblasts stimulation and proliferation accelerated the wound healing process in BALB/c mice infected by *L. amazonensis*.[136] Therefore, a good fibroblast viability promoted by DMMB-PDT could keep the integrity of skin, and influence wound closure in the late inflammatory phase of infected patients, achieving a complete tissue repair in a short-term.

It is worth mentioning that since the disease develops ulcerated and destructive skin lesions, ideal topical treatments should be well tolerated by healthy skin cells with minor adverse effects, thus improving clinical aspects with smoother and less visible scars. There have been reports of PDT reducing significantly lesion size of different models of *Leishmania*-infected mice, hence promoting a better clinical aspect over CL lesions.[50,51] These results have been attributed to the modulation of inflammatory response, thus favoring clinical healing with an improved cosmetic outcome.[50]

In addition, it has been shown that red light sources have a deep penetration into tissue and stimulate fibroblast growth factors at the site of infection, thus inducing a rapid re-epithelization.[137] In this sense, our results show that DMMB-PDT could help promote wound healing with great potential to be a safe therapy suitable for topical administration.

Macrophages are phagocytic cells with protective functions against several pathogens. Activated macrophages are able to produce reactive species promoting parasite killing and control of CL infection. However, they are the main host cells for *Leishmania,* which can subvert antimicrobial macrophage defenses, hence surviving

in harsh conditions.[138] Therefore, infected macrophages are the major targets for the development of new therapeutic strategies.

Nevertheless, ideal treatments should be selective for parasites over the host cells, preventing photodamage over non-infected macrophages. This selective toxicity includes the uptake and distribution of drugs within infected cells as well as its accumulation into the PV.[138] In this regard, PDT has the advantage of dual selectivity, in which the photosensitizer can specifically target intracellular organelles, and yet, light can be delivered directly onto the desired lesion, resulting in a promising and potent local therapy to treat infectious diseases.[139,140]

Several cationic photosensitizers have shown selectivity against Gram (-) bacteria.[139,140] The cationic photosensitizer chlorin e6 showed a selective uptake of bacteria compared to mammalian cells (by 5-20-fold), therefore promoting a targeted antimicrobial PDT.[141] Because of a greater volume of mammalian cells compared to bacteria's, the amounts of ROS generated (in the same conditions) were less likely to diffuse across the entire mammalian cell and reach sensitive organelles than those in the case of bacteria.[141] Since amastigotes (approximately 1 to 4 μm in diameter) are much smaller than macrophages (approximately 20 μm in diameter), this could be one possible explanation for the good selectivity of DMMB-PDT in the present study.

The main targets of PDT include mitochondria, lysosomes and plasma membrane.[140] In this sense, the one single mitochondrion present in *Leishmania* makes this organelle a potential drug target for development of antileishmanial compounds.[142] As we have previously shown, DMMB-PDT leads to a mitochondrial dysfunction via loss of membrane potential, triggering parasites death. Yet, the lipid peroxidation observed by previous lipidomic analysis in the WT and MFR promastigotes suggested that plasma membrane could have been also oxidated. Thus, a rapid plasma membrane damage and mitochondria-targeted DMMB-PDT could as well elucidate such selectivity.

In addition, DMMB has been shown to accumulate into lysosomes of mammalian cells via endocytic pathways.[53] In this regard, the amastigote form of *L. amazonensis* species are well-known for surviving within large PVs, which are phagolysosome-like structures.[15] Therefore, it is very likely that DMMB uptake was

enhanced because of its physicochemical properties (such as lipophilicity), resulting in its accumulation into PVs, hence contributing to a localized photodamage.[101]

The multi-target characteristics of PDT make this technique an ideal candidate for the treatment of unresponsive patients, particularly those related to drug-resistant phenotypes. In this context, our results demonstrated that both WT and MFR intracellular amastigotes were very susceptible to DMMB-PDT, showing a high selectivity index in comparison to the standard oral drug miltefosine (see Table 1).

Our previous study demonstrated that MFR promastigotes were more susceptible to DMMB-PDT than the WT strain, showing DMMB EC_{50} values of 34 nM and 53 nM, respectively. Conversely, for intracellular amastigotes higher EC_{50} values were observed for both strains, where the WT strain (EC_{50} 52 nM) was found to be more susceptible to PDT than MFR cell line (EC_{50} 77 nM) (see Figure 7.7).

Differences in susceptibility could be related to the survival strategies needed for amastigotes to persist in macrophages under stress conditions.[23,138] It has been shown that amastigotes of *L. amazonensis* are more resistant to reactive species than promastigotes, thus suggesting the intracellular form of parasites adapt to survive and replicate within activated macrophages, which includes developing antioxidant mechanisms to deal with oxidative stress.[23,70]

Indeed, it has also been previously reported that miltefosine-resistant amastigotes of clinical isolates of *L. donovani* were more tolerant to ROS than the WT strain, behaving similarly to a miltefosine-resistant strain laboratory-induced.[143] This suggests the drug resistant phenotype might have adopted strategies to overcome oxidative stress, thereby increasing expression of antioxidant defenses, such as trypanothione synthetase and tryparedoxin peroxidase when compared to *L. donovani* WT strain.[143]

Moreover, differences in energy metabolism, levels of proteases (i.e., increased cysteine proteinase activity of amastigotes) and surface molecules (such as gp63 and LPG) have been also extensively reported in both *Leishmania* stages.[138] Therefore, differences between promastigotes and amastigotes go beyond their morphological features. Indeed, biochemical and molecular changes may partly elucidate the variations in drug sensitivity between both forms.[138]

It is worth mentioning that drug sensitivity is also dependent on drug formulations, mechanism of action, *Leishmania* species and type of infected macrophages.[144] Thus, those variables should also be taken into account for development of new antileishmanial approaches.

In conclusion, we have successfully demonstrated for the first time the potential of DMMB-PDT against intracellular amastigote forms of two *L. amazonensis* strains, including a miltefosine-resistant cell line. Our results indicate that our treatment effectively inactivated both strains without promoting cytotoxic effects to mammalian cells. Additionally, selectivity index of DMMB-PDT was much greater than that of miltefosine, suggesting it is a safe therapy to be applied. Thus, DMMB-PDT is a promising therapeutic strategy to treat CL. We hope to encourage future *in vivo* studies to investigate the best protocols in animal models.

8. CONCLUSION

In our study, we demonstrate that either ROS or NO, both endogenous molecules, can effectively be administered exogenously as potential strategies to target CL. Both treatments promoted significant inactivation of *Leishmania* parasites. Particularly, NONPs did not show any signs of adverse effects, nor even minimal scars, hence they are well tolerated in mice and have a great potential to be safely implemented in future clinical trials with the appropriate protocol.

PDT has been widely studied as a topical strategy against several *Leishmania* species, including in preclinical and clinical trials. However, here we show for the first time that PDT can also inactivate a drug resistant strain. Thus, it could be suitable for unresponsive cases to current drugs. Nevertheless, DMMB-PDT activity still needs to be addressed over *in vivo* studies, in order to demonstrate whether it could effectively overcome the antileishmanial drug resistance issue.

In conclusion, both topical therapies that generate ROS and NO could improve the immune response in those patients that have undergone macrophage inactivation, and therefore are unable to produce both reactive species.

PUBLICATIONS

Cabral, F.V., Souza, T.H.S., Sellera, F.P., Fontes, A., Ribeiro, M.S., *Towards effective cutaneous leishmaniasis treatment with light-based technologies. A systematic review and meta-analysis of preclinical studies.* Journal of photochemistry and photobiology B, Biology **2021;** 221: 112236. https://doi.org/10.1016/j.jphotobiol.2021.112236.

Cabral, F.V., Sabino, C.P., Dimmer, J.A., Sauter, I.P., Cortez, M.J. and Ribeiro, M.S. *Preclinical Investigation of Methylene Blue-mediated Antimicrobial Photodynamic Therapy on Leishmania Parasites Using Real-Time Bioluminescence*. Photochem Photobiol, 96, **2020**, 604-610. https://doi.org/10.1111/php.13188

Cabral F.V., Pelegrino, M.T., Sauter, I.P., Seabra, A.B., Cortez, M., Ribeiro, M.S. *Nitric oxide-loaded chitosan nanoparticles as an innovative antileishmanial platform,* Nitric Oxide, Volume 93, **2019**, Pages 25-33, https://doi.org/10.1016/j.niox.2019.09.007.

Cabral, F. V., Lian, C., Persheyev, S., Smith, T. K., Ribeiro, M. S., Samuel, I. D. W., *Organic Light-Emitting Diodes as an Innovative Approach for Treating Cutaneous Leishmaniasis.* Adv.Mater.Technol. **2021,**2100395. https://doi.org/10.1002/admt.202100395

Cabral, F.V, Pelegrino, M.T., Seabra, A.B., Ribeiro, M.S, *Nitric-oxide releasing chitosan nanoparticles towards effective treatment of cutaneous leishmaniasis*, Nitric Oxide, Volumes 113–114, **2021**, Pages 31-38. https://doi.org/10.1016/j.niox.2021.04.008.

Souza, T.H..S., Andrade, C.G., **Cabral, F.V**., Sarmento-Neto, J.F., Rebouças, J.S., Santos, B.S., Ribeiro, M.S., Figueiredo, R.C.B.Q., Fontes, A. *Efficient photodynamic inactivation of Leishmania parasites mediated by lipophilic water-soluble Zn(II) porphyrin ZnTnHex-2-PyP4+* Biochimica et Biophysica Acta (BBA) - General

Subjects, Volume 1865, Issue 7, **2021**, 129897, https://doi.org/10.1016/j.bbagen.2021.129897.

Dimmer J., **Cabral, F.V.,** Sabino, C.P., Silva, C.R., Núñez-Montoya, S.C., Cabrera, J.L., Ribeiro, M.S. *Natural anthraquinones as novel photosentizers for antiparasitic photodynamic inactivation, Phytomedicine*,Volume61,**2019,**152894. https://doi.org/10.1016/j.phymed.2019.152894.

Ramos Silva, C., **Cabral, F.V**., de Camargo, C.F.M., Núñez, S.C., Mateus Yoshimura, T., de Lima Luna, A.C., Maria, D.A. and Ribeiro, M.S. *Exploring the effects of low-level laser therapy on fibroblasts and tumor cells following gamma radiation exposure.* J. Biophoton, 9, **2016**, 1157-1166. https://doi.org/10.1002/jbio.201600107

Sellera, F. P., Sabino, C. P., **Cabral, F. V**., Ribeiro, M.S. *A systematic scoping review of ultraviolet C (UVC) light systems for SARS-CoV-2 inactivation.* Journal of Photochem and Photobiol. 2021,100068, https://doi.org/10.1016/j.jpap.2021.100068

Cabral, F.V., Sellera F.P., Ribeiro, M.S. *Methylene blue-mediated antimicrobial photodynamic therapy for canine dermatophytosis caused by Microsporum canis: a successful case report with 6 months follow-up. (In submission).* Photodiagnosis and photodynamic therapy.

CONFERENCE PAPERS

Ifor D. W. Samuel, Cheng Lian, Marta Piksa, Katarzyna Matczyszyn, Kou Yoshida, Saydulla Persheyev, Krzysztof Pawlik, **Fernanda Cabral**, Martha Ribeiro, Jose Lindoso, "OLEDs: Wearable light sources for medicine," Proc. SPIE 11475, Organic and Hybrid Sensors and Bioelectronics XIII, 114750C (22 August 2020); https://doi.org/10.1117/12.2569250

F. V. Cabral, M. T. Pelegrino, A. B. Seabra, and M. S. Ribeiro, "Could NO-releasing chitosan nanoparticles improve photodynamic therapy on cutaneous leishmaniasis?," in *Latin America Optics and Photonics Conference*, OSA Technical Digest (Optical Society of America, 2018), paper Tu4A.43. https://doi.org/10.1364/LAOP.2018.Tu4.43

C. R. Silva, C. F. M. Camargo, **F. V. Cabral**, M. S. Ribeiro, "Low-power laser irradiation did not stimulate breast cancer cells following ionizing radiation," Proc. SPIE 9695, Mechanisms of Photobiomodulation Therapy XI, 96950H (8 March 2016); https://doi.org/10.1117/12.2213506

AWARDS

2018 Innovation award: “NO-releasing chitosan nanoparticles to treat cutaneous leishmaniasis”- INOVA UFABC

2018 1st place in poster presentation - “Could NO-releasing chitosan nanoparticles improve photodynamic therapy on cutaneous leishmaniasis?”. OSA, Latin America Optics and Photonics Conference - LAOP.

2017 Honorable Mention - “NO-releasing chitosan nanoparticles associated to photodynamic therapy for *Leishmania amazonensis* inactivation. An in vivo study., 10th International Conference on Nanophotonics (ICNP).”

2017 Honorable Mention – “Antimicrobial photodynamic therapy combined with NO-loaded chitosan nanoparticles to treat cutaneous leishmaniasis”. Brazilian Society of Nuclear Biosciences (SBBN).

2016 Oral presentation honorable mention – Antimicrobial photodynamic therapy to cutaneous leishmaniasis in mice. Brazilian Society of Nuclear Biosciences. Federation of American Societies for Experimental Biology (FESBE).

2016 Poster presentation honorable mention– Antimicrobial photodynamic therapy to cutaneous leishmaniasis in mice. Brazilian Society of Nuclear Biosciences. Federation of American Societies for Experimental Biology (FESBE).

PATENT

Seabra, A.B. ; **CABRAL, F. V.** ; PELEGRINO, M. ; Ribero, M.S. ; MIOTTO, R. Chitosan nanoparticles containing S-nitroso-mercaptosuccinic acid (S-nitroso-MSA) to treat cutaneous leishmaniasis. 2018, Brazil. Number: BR10201800023. INPI – Brazilian National Institute of Industrial Property.

REFERENCES

1. Akhoundi M, Kuhls K, Cannet A, et al. A Historical Overview of the Classification, Evolution, and Dispersion of Leishmania Parasites and Sandflies. PLoS Negl Trop Dis; 2016.

2. Burza S, Croft SL, Boelaert M. Leishmaniasis. *Lancet (London, England)* 2018; **392**(10151).

3. initiative Dfnd. Cutaneous leishmaniasis | DNDi. 2020-01-06 2020. https://dndi.org/diseases/cutaneous-leishmaniasis/.

4. Croft SL, Olliaro P. Leishmaniasis chemotherapy--challenges and opportunities. *Clinical microbiology and infection : the official publication of the European Society of Clinical Microbiology and Infectious Diseases* 2011; **17**(10): 1478-83.

5. Chakravarty J, Sundar S. Current and emerging medications for the treatment of leishmaniasis. *Expert opinion on pharmacotherapy* 2019; **20**(10): 1251-65.

6. Ponte-Sucre A, Gamarro F, Dujardin JC, et al. Drug resistance and treatment failure in leishmaniasis: A 21st century challenge. *PLoS Negl Trop Dis* 2017; **11**(12): e0006052.

7. Scott P, Novais FO. Cutaneous leishmaniasis: immune responses in protection and pathogenesis. *Nature reviews Immunology* 2016; **16**(9).

8. Real F, Mortara R. The diverse and dynamic nature of Leishmania parasitophorous vacuoles studied by multidimensional imaging. *PLoS neglected tropical diseases* 2012; **6**(2): e1518.

9. Yanik M, Gurel MS, Simsek Z, Kati M. The psychological impact of cutaneous leishmaniasis. *Clin Exp Dermatol* 2004; **29**(5): 464-7.

10. Kevric I, Cappel MA, Keeling JH. New World and Old World Leishmania Infections: A Practical Review. *Dermatol Clin* 2015; **33**(3): 579-93.

11. Gurel M, B BT, Uzun S. Cutaneous leishmaniasis: A great imitator. *Clinics in dermatology* 2020; **38**(2): 140-51.

12. Torres-Guerrero E, Quintanilla-Cedillo M, Ruiz-Esmenjaud J, Arenas R. Leishmaniasis: a review. *F1000Research* 2017; **6**: 750.

13. Mann S, Frasca K, Scherrer S, et al. A Review of Leishmaniasis: Current Knowledge and Future Directions. *Current tropical medicine reports* 2021: 1-12.

14. Lainson R, Ready P, Shaw J. Leishmania in phlebotomid sandflies. VII. On the taxonomic status of Leishmania peruviana, causative agent of Peruvian 'uta', as indicated by its development in the sandfly, Lutzomyia longipalpis. *Proceedings of the Royal Society of London Series B, Biological sciences* 1979; **206**(1164): 307-18.

15. Wilson J, Huynh C, Kennedy KA, et al. Control of Parasitophorous Vacuole Expansion by LYST/Beige Restricts the Intracellular Growth of Leishmania amazonensis. PLoS Pathog; 2008.

16. Antoine J, Prina E, Jouanne C, Bongrand P. Parasitophorous vacuoles of Leishmania amazonensis-infected macrophages maintain an acidic pH. *Infection and immunity* 1990; **58**(3): 779-87.

17. Kaye P, Scott P. Leishmaniasis: complexity at the host-pathogen interface. *Nature reviews Microbiology* 2011; **9**(8).

18. Horta MF, Mendes BP, Roma EH, et al. Reactive Oxygen Species and Nitric Oxide in Cutaneous Leishmaniasis. *Journal of Parasitology Research* 2012; **2012**.

19. León B, López-Bravo M, Ardavín C. Monocyte-derived dendritic cells formed at the infection site control the induction of protective T helper 1 responses against Leishmania. *Immunity* 2007; **26**(4): 519-31.

20. Mills C, Kincaid K, Alt J, Heilman M, Hill A. M-1/M-2 macrophages and the Th1/Th2 paradigm. *Journal of immunology (Baltimore, Md : 1950)* 2000; **164**(12): 6116-73.

21. Kaye P, Scott P. Leishmaniasis: complexity at the host–pathogen interface. *Nature Reviews Microbiology* 2011; **9**: 604-15.

22. Dubie T, Mohammed Y. Review on the Role of Host Immune Response in Protection and Immunopathogenesis during Cutaneous Leishmaniasis Infection. *Journal of immunology research* 2020; **2020**.

23. Assche TV, Deschacht M, Luz Rd, Maes L, Cos P. Leishmania-macrophage interactions: insights into the redox biology. *Free radical biology & medicine* 2011; **51**(2): 337-51.

24. Cinelli M, Do H, Miley G, Silverman R. Inducible nitric oxide synthase: Regulation, structure, and inhibition. *Medicinal research reviews* 2020; **40**(1): 158-89.

25. Pessenda G, Silva Jd. Arginase and its mechanisms in Leishmania persistence. *Parasite immunology* 2020; **42**(7): e12722.

26. Tripathi P, Tripathi P, Kashyap L, Singh V. The role of nitric oxide in inflammatory reactions. *FEMS immunology and medical microbiology* 2007; **51**(3): 443-53.

27. Patel R, McAndrew J, Sellak H, et al. Biological aspects of reactive nitrogen species. *Biochimica et biophysica acta* 1999; **1411**(2-3): 385-400.

28. Hill BG, Dranka BP, Bailey SM, Jr JRL, Darley-Usmar VM. What part of NO don't you understand? Some answers to the cardinal questions in nitric oxide biology. *The Journal of biological chemistry* 2010; **285**(26).

29. Paiva C, Bozza M. Are reactive oxygen species always detrimental to pathogens? *Antioxidants & redox signaling* 2014; **20**(6): 1000-37.

30. Herb M, Schramm M. Functions of ROS in Macrophages and Antimicrobial Immunity. *Antioxidants (Basel, Switzerland)* 2021; **10**(2): 313.

31. Davidson RN, Yardley V, Croft SL, Konecny P, Benjamin N. A topical nitric oxide-generating therapy for cutaneous leishmaniasis. *Transactions of the Royal Society of Tropical Medicine and Hygiene* 2000; **94**(3).

32. Jowkar F, Dehghani F, Jamshidzadeh A. Is topical nitric oxide and cryotherapy more effective than cryotherapy in the treatment of old world cutaneous leishmaniasis? *The Journal of dermatological treatment* 2012; **23**(2).

33. Seabra A, Justo G, Haddad P. State of the art, challenges and perspectives in the design of nitric oxide-releasing polymeric nanomaterials for biomedical applications. *Biotechnology advances* 2015; **33**(6 Pt 3): 1370-9.

34. Nichols S, Storm W, Koh A, Schoenfisch M. Local delivery of nitric oxide: targeted delivery of therapeutics to bone and connective tissues. *Advanced drug delivery reviews* 2012; **64**(12): 1177-88.

35. Broniowska K, Hogg N. The chemical biology of S-nitrosothiols. *Antioxidants & redox signaling* 2012; **17**(7): 969-80.

36. Wang PG, Xian M, Tang X, et al. Nitric oxide donors: chemical activities and biological applications. *Chemical reviews* 2002; **102**(4).

37. Seabra AB, Duran N. Nanoparticulated Nitric Oxide Donors and their Biomedical Applications. *Mini reviews in medicinal chemistry* 2017; **17**(3).

38. Mohammed M, Syeda J, Wasan K, Wasan E. An Overview of Chitosan Nanoparticles and Its Application in Non-Parenteral Drug Delivery. *Pharmaceutics* 2017; **9**(4): 53.

39. Riezk A, Raynes JG, Yardley V, Murdan S, Croft SL. Activity of Chitosan and Its Derivatives against Leishmania major and Leishmania mexicana In Vitro. *Antimicrobial agents and chemotherapy* 2020; **64**(3).

40. Riezk A, Bocxlaer KV, Yardley V, Murdan S, Croft S. Activity of Amphotericin B-Loaded Chitosan Nanoparticles against Experimental Cutaneous Leishmaniasis. *Molecules (Basel, Switzerland)* 2020; **25**(17).

41. Lancheros CC, Pelegrino M, Kian D, et al. Selective Antiprotozoal Activity of Nitric Oxide-releasing Chitosan Nanoparticles Against Trypanosoma cruzi: Toxicity and Mechanisms of Action. *Current pharmaceutical design* 2018; **24**(7): 830-9.

42. Dai T, Huang Y, Hamblin M. Photodynamic therapy for localized infections--state of the art. *Photodiagnosis and photodynamic therapy* 2009; **6**(3-4): 170-88.

43. Hamblin MR. Antimicrobial photodynamic inactivation: a bright new technique to kill resistant microbes. *Curr Opin Microbiol* 2016; **33**: 67-73.

44. AP C, TN D, MR H. Mechanisms in photodynamic therapy: part one-photosensitizers, photochemistry and cellular localization. *Photodiagnosis and photodynamic therapy* 2004; **1**(4): 279-93.

45. Baptista MS, Cadet J, Di Mascio P, et al. Type I and Type II Photosensitized Oxidation Reactions: Guidelines and Mechanistic Pathways. *Photochem Photobiol* 2017; **93**(4): 912-9.

46. Hamblin M, Abrahamse H. Inorganic Salts and Antimicrobial Photodynamic Therapy: Mechanistic Conundrums? *Molecules (Basel, Switzerland)* 2018; **23**(12): 3190.

47. Aureliano DP, Lindoso JAL, de Castro Soares SR, Takakura CFH, Pereira TM, Ribeiro MS. Cell death mechanisms in Leishmania amazonensis triggered by methylene blue-mediated antiparasitic photodynamic therapy. *Photodiagnosis Photodyn Ther* 2018; **23**: 1-8.

48. Pinto JG, Martins JFS, Pereira AHC, Mittmann J, Raniero LJ, Ferreira-Strixino J. Evaluation of methylene blue as photosensitizer in promastigotes of Leishmania major and Leishmania braziliensis. *Photodiagnosis Photodyn Ther* 2017; **18**: 325-30.

49. Akilov OE, Kosaka S, O'Riordan K, Hasan T. Photodynamic therapy for cutaneous leishmaniasis: the effectiveness of topical phenothiaziniums in parasite eradication and Th1 immune response stimulation. *Photochem Photobiol Sci* 2007; **6**: 1067-75.

50. FV C, THDS S, FP S, A F, MS R. Towards effective cutaneous leishmaniasis treatment with light-based technologies. A systematic review and meta-analysis of preclinical studies. *Journal of photochemistry and photobiology B, Biology* 2021; **221**: 112236.

51. Cabral FV, Sabino CP, Dimmer JA, Sauter IP, Cortez MJ, Ribeiro MS. Preclinical Investigation of Methylene Blue-mediated Antimicrobial Photodynamic Therapy on Leishmania Parasites Using Real-Time Bioluminescence. *Photochemistry and photobiology* 2020; **96**(3).

52. Song D, Lindoso JA, Oyafuso LK, et al. Photodynamic therapy using methylene blue to treat cutaneous leishmaniasis. *Photomed Laser Surg* 2011; **29**(10): 711-5.

53. Martins WK, Santos NF, Rocha CS, et al. Parallel damage in mitochondria and lysosomes is an efficient way to photoinduce cell death. *Autophagy* 2019; **15**(2): 259-79.

54. Santos D, Crugeira P, Nunes I, Almeida Pd, Pinheiro A. A novel technique of antimicrobial photodynamic therapy - aPDT using 1,9-dimethyl-methylene blue zinc chloride double salt-DMMB and polarized light on Staphylococcus aureus. *Journal of photochemistry and photobiology B, Biology* 2019; **200**: 111646.

55. Collina GAd, Freire F, Barbosa VdS, et al. Photodynamic antimicrobial chemotherapy action of phenothiazinium dyes in planktonic Candida albicans is

increased in sodium dodecyl sulfate. *Photodiagnosis and photodynamic therapy* 2020; **29**: 101612.

56. Pereira LM, Mota CM, Baroni L, et al. Inhibitory action of phenothiazinium dyes against Neospora caninum. *Scientific reports* 2020; **10**(1): 7483.

57. Cabral FV, Pelegrino MT, Sauter IP, Seabra AB, Cortez M, Ribeiro MS. Nitric oxide-loaded chitosan nanoparticles as an innovative antileishmanial platform. *Nitric oxide : biology and chemistry* 2019; **93**.

58. Reimao JQ, Trinconi CT, Yokoyama-Yasunaka JK, Miguel DC, Kalil SP, Uliana SR. Parasite burden in Leishmania (Leishmania) amazonensis-infected mice: validation of luciferase as a quantitative tool. *J Microbiol Methods* 2013; **93**: 95-101.

59. Cortez M, Huynh C, Fernandes MC, Kennedy KA, Aderem A, Andrews NW. Leishmania promotes its own virulence by inducing expression of the host immune inhibitory ligand CD200. *Cell Host Microbe* 2011; **9**(6): 463-71.

60. Vos KD. Cell Counter. 2018.

61. Pelegrino MT SL, Watashi CM, Haddad PS, Seabra AB. Nitric oxide-releasing nanoparticles: synthesis, characterization, and cytotoxicity to tumorigenic cells - Dimensions. *Nitric oxide-releasing nanoparticles: synthesis, characterization, and cytotoxicity to tumorigenic cells* 2017; **19**(2).

62. Zhao D, Yu S, Sun B, et al. Biomedical Applications of Chitosan and Its Derivative Nanoparticles. *Polymers (Basel)* 2018; **10**(4).

63. Seabra AB, Kitice NA, Pelegrino MT, et al. Nitric oxide-releasing polymeric nanoparticles against Trypanosoma cruzi - IOPscience. 2015.

64. Mauel J, Ransijn A. Leishmania spp.: mechanisms of toxicity of nitrogen oxidation products. *Exp Parasitol* 1997; **87**(2): 98-111.

65. Menezes JPd, Saraiva EM, Rocha-Azevedo Bd. The site of the bite: Leishmania interaction with macrophages, neutrophils and the extracellular matrix in the dermis. *Parasites & Vectors* 2016; **9**(1): 264.

66. Schairer DO, Chouake JS, Nosanchuk JD, Friedman AJ. The potential of nitric oxide releasing therapies as antimicrobial agents. Virulence; 2012: 271-9.

67. Smith BC, Marletta MA. Mechanisms of S-nitrosothiol formation and selectivity in nitric oxide signaling. *Curr Opin Chem Biol* 2012; **16**(5-6): 498-506.

68. Gabriela Freitas Pereira de Souza, Jenicer K Yokoyama-Yasunaka, Amedea B Seabra, Danilo Cicconi Miguel, Marcelo Ganzarolli de Oliveira, Silvia Reni B Uliana. Leishmanicidal activity of primary S-nitrosothiols against Leishmania major and Leishmania amazonensis: implications for the treatment of cutaneous leishmaniasis. *Nitric Oxide* 2006; **15**(3): 209-16.

69. Lemesre J-L, Sereno D, Daulouède S, Veyret B, Brajon N, Vincendeau P. Leishmania spp.: nitric oxide-mediated metabolic inhibition of promastigote and axenically grown amastigote forms. *Experimental parasitology* 1997; **86**(1).

70. Henard C, Carlsen E, Hay C, Kima P, Soong L. Leishmania amazonensis amastigotes highly express a tryparedoxin peroxidase isoform that increases parasite resistance to macrophage antimicrobial defenses and fosters parasite virulence. *PLoS neglected tropical diseases* 2014; **8**(7): e3000.

71. Soong L. Subversion and Utilization of Host Innate Defense by Leishmania amazonensis. *Front Immunol* 2012; **3**.

72. Real F, Mortara RA, Rabinovitch M. Fusion between Leishmania amazonensis and Leishmania major parasitophorous vacuoles: live imaging of coinfected macrophages. *PLoS Negl Trop Dis* 2010; **4**(12): e905.

73. Cabral F, Pelegrino M, Seabra A, Ribeiro M. Nitric-oxide releasing chitosan nanoparticles towards effective treatment of cutaneous leishmaniasis. *Nitric oxide : biology and chemistry* 2021; **113-114**: 31-8.

74. Mears ER, Modabber F, Don R, Johnson GE. A Review: The Current In Vivo Models for the Discovery and Utility of New Anti-leishmanial Drugs Targeting Cutaneous Leishmaniasis. *PLoS neglected tropical diseases* 2015; **9**(9).

75. Sacks D, Noben-Trauth N. The immunology of susceptibility and resistance to Leishmania major in mice. *Nature reviews Immunology* 2002; **2**(11).

76. Wanasen N, Soong L. L-arginine metabolism and its impact on host immunity against Leishmania infection. *Immunologic research* 2008; **41**(1).

77. Gabriel A, Valério-Bolas A, Palma-Marques J, et al. Cutaneous Leishmaniasis: The Complexity of Host's Effective Immune Response against a Polymorphic Parasitic Disease. *Journal of immunology research* 2019; **2019**.

78. Olekhnovitch R, Bousso P. Induction, Propagation, and Activity of Host Nitric Oxide: Lessons from Leishmania Infection. *Trends in parasitology* 2015; **31**(12).

79. Davidson R, SL VY, Croft, Konecny P, Benjamin N. A topical nitric oxide-generating therapy for cutaneous leishmaniasis. *Transactions of the Royal Society of Tropical Medicine and Hygiene* 2000; **94**(3): 319-22.

80. Zhou X, Zhang J, Feng G, Shen J, Kong D, Zhao Q. Nitric Oxide-Releasing Biomaterials for Biomedical Applications. *Current medicinal chemistry* 2016; **23**(24).

81. Yu H, Cui L-X, Huang N, Yang Z-L. Recent developments in nitric oxide-releasing biomaterials for biomedical applications. *Medical gas research* 2019; **9**(4).

82. Fang FC. Antimicrobial reactive oxygen and nitrogen species: concepts and controversies. *Nature reviews Microbiology* 2004; **2**(10).

83. Stomberski CT, Hess DT, Stamler JS. Protein S-Nitrosylation: Determinants of Specificity and Enzymatic Regulation of S-Nitrosothiol-Based Signaling. *Antioxidants & redox signaling* 2019; **30**(10).

84. Hess DT, Matsumoto A, Kim SO, Marshall HE, Stamler JS. Protein S-nitrosylation: purview and parameters. *Nature reviews Molecular cell biology* 2005; **6**(2).

85. Butsch F, Lorenz B, Goldinger A, von Stebut E. Topical treatment with a two-component gel releasing nitric oxide cures C57BL/6 mice from cutaneous leishmaniasis caused by Leishmania major. *Exp Dermatol* 2016; **25**(11): 914-6.

86. Costa IS, de Souza GF, de Oliveira MG, Abrahamsohn Ide A. S-nitrosoglutathione (GSNO) is cytotoxic to intracellular amastigotes and promotes healing of topically treated Leishmania major or Leishmania braziliensis skin lesions. *J Antimicrob Chemother* 2013; **68**(11): 2561-8.

87. Esfandiari F, Motazedian M, Asgari Q, Morowvat M, Molaei M, Heli H. Paromomycin-loaded mannosylated chitosan nanoparticles: Synthesis, characterization and targeted drug delivery against leishmaniasis. *Acta tropica* 2019; **197**.

88. Sun Y, Chen D, Pan Y, et al. Nanoparticles for antiparasitic drug delivery. *Drug delivery* 2019; **26**(1).

89. Jiang L, Wang T, Webster T, et al. Intracellular disposition of chitosan nanoparticles in macrophages: intracellular uptake, exocytosis, and intercellular transport. *International journal of nanomedicine* 2017; **12**.

90. Garnier T, Croft S. Topical treatment for cutaneous leishmaniasis. *Current opinion in investigational drugs (London, England : 2000)* 2002; **3**(4).

91. Borghi SM, Fattori V, Conchon-Costa I, Pinge-Filho P, Pavanelli WR, Verri WA, Jr. Leishmania infection: painful or painless? *Parasitol Res* 2016.

92. Anbar M, Gratt B. Role of nitric oxide in the physiopathology of pain. *Journal of pain and symptom management* 1997; **14**(4).

93. Cabral FV, Lian C, Persheyev S, Smith TK, Ribeiro MS, Samuel IDW. Organic Light-Emitting Diodes as an Innovative Approach for Treating Cutaneous Leishmaniasis - Cabral - - Advanced Materials Technologies - Wiley Online Library. *Advanced materials technologies* 2021: 2100395.

94. Wainwright M. Dyes, flies, and sunny skies: photodynamic therapy and neglected tropical diseases - Wainwright - 2017 - Coloration Technology - Wiley Online Library. *ColorTechnol* 2017; **133**: 3-14.

95. Vincent IM, Weidt S, Rivas L, Burgess K, Smith TK, Ouellette M. Untargeted metabolomic analysis of miltefosine action in Leishmania infantum reveals changes to the internal lipid metabolism. *Int J Parasitol Drugs Drug Resist* 2014; **4**(1): 20-7.

96. Rampersad SN. Multiple Applications of Alamar Blue as an Indicator of Metabolic Function and Cellular Health in Cell Viability Bioassays. *Sensors* 2012; **12**(9): 12347-60.

97. Tardivo JP, Del Giglio A, de Oliveira CS, et al. Methylene blue in photodynamic therapy: From basic mechanisms to clinical applications. *Photodiagnosis Photodyn Ther* 2005; **2**(3): 175-91.

98. MN U, MC T, MA B. The role of the methylene blue and toluidine blue monomers and dimers in the photoinactivation of bacteria. *Journal of photochemistry and photobiology B, Biology* 2003; **71**(1-3).

99. Freire F, Ferraresi C, Jorge AO, Hamblin MR. Photodynamic therapy of oral Candida infection in a mouse model. *J Photochem Photobiol B* 2016; **159**: 161-8.

100. Wainwright M, Mohr H, Walker WH. Phenothiazinium derivatives for pathogen inactivation in blood products. *J Photochem Photobiol B* 2007; **86**(1): 45-58.

101. Wainwright M, Phoenix DA, Rice L, Burrow SM, Waring J. Increased cytotoxicity and phototoxicity in the methylene blue series via chromophore methylation. *J Photochem Photobiol B* 1997; **40**(3): 233-9.

102. Sampaio FJP, de Oliveira S, Crugeira PJL, et al. aPDT using nanoconcentration of 1,9-dimethylmethylene blue associated to red light is efficacious in killing Enterococcus faecalis ATCC 29212 in vitro. *J Photochem Photobiol B* 2019; **200**: 111654.

103. Ragas X, Dai T, Tegos GP, Agut M, Nonell S, Hamblin MR. Photodynamic inactivation of Acinetobacter baumannii using phenothiazinium dyes: in vitro and in vivo studies. *Lasers Surg Med* 2010; **42**(5): 384-90.

104. R M, S D, N X, et al. Trypanothione overproduction and resistance to antimonials and arsenicals in Leishmania. *Proceedings of the National Academy of Sciences of the United States of America* 1996; **93**(19).

105. Castro H, Tomás AM. Peroxidases of trypanosomatids. *Antioxidants & redox signaling* 2008; **10**(9).

106. BLIGH E, DYER W. A rapid method of total lipid extraction and purification. *Canadian journal of biochemistry and physiology* 1959; **37**(8): 911-7.

107. Vincent IM, Weidt S, Rivas L, Burgess K, Smith TK, Ouellette M. Untargeted metabolomic analysis of miltefosine action in Leishmania infantum reveals changes to the internal lipid metabolism. *Int J Parasitol Drugs Drug Resist* 2014; **4**: 20-7.

108. Williams R, Smith T, Cull B, Mottram J, Coombs G. ATG5 is essential for ATG8-dependent autophagy and mitochondrial homeostasis in Leishmania major. *PLoS pathogens* 2012; **8**(5): e1002695.

109. Negrão F, Abánades AD, Jaeeger C, et al. Lipidomic alterations of in vitro macrophage infection by L. infantum and L. amazonensis. *Molecular bioSystems* 2017; **13**(11): 2401-6.

110. Adak S, Datta AK. Leishmania major encodes an unusual peroxidase that is a close homologue of plant ascorbate peroxidase: a novel role of the transmembrane domain. *The Biochemical journal* 2005; **390**(Pt 2).

111. Bacellar I, Pavani C, Sales E, Itri R, Wainwright M, Baptista M. Membrane damage efficiency of phenothiazinium photosensitizers. *Photochemistry and photobiology* 2014; **90**(4): 801-13.

112. Zorov D, Juhaszova M, Sollott S. Mitochondrial reactive oxygen species (ROS) and ROS-induced ROS release. *Physiological reviews* 2014; **94**(3): 909-50.

113. Jarc E, Petan T. Lipid Droplets and the Management of Cellular Stress. *The Yale journal of biology and medicine* 2019; **92**(3): 435-52.

114. Olzmann JA, Carvalho P. Dynamics and functions of lipid droplets. *Nature reviews Molecular cell biology* 2019; **20**(3): 137-55.

115. Coelho A, Trinconi C, Costa C, Uliana S. In Vitro and In Vivo Miltefosine Susceptibility of a Leishmania amazonensis Isolate from a Patient with Diffuse Cutaneous Leishmaniasis: Follow-Up. *PLoS neglected tropical diseases* 2016; **10**(7).

116. Hefnawy A, Berg M, Dujardin J, Muylder GD. Exploiting Knowledge on Leishmania Drug Resistance to Support the Quest for New Drugs. *Trends in parasitology* 2017; **33**(3): 162-74.

117. Rakotomanga M, Saint-Pierre-Chazalet M, Loiseau P. Alteration of fatty acid and sterol metabolism in miltefosine-resistant Leishmania donovani promastigotes and consequences for drug-membrane interactions. *Antimicrobial agents and chemotherapy* 2005; **49**(7): 2677-86.

118. Rakotomanga M, Blanc S, Gaudin K, Chaminade P, Loiseau P. Miltefosine affects lipid metabolism in Leishmania donovani promastigotes. *Antimicrobial agents and chemotherapy* 2007; **51**(4): 1425-30.

119. Shaw C, Lonchamp J, Downing T, et al. In vitro selection of miltefosine resistance in promastigotes of Leishmania donovani from Nepal: genomic and metabolomic characterization. *Molecular microbiology* 2016; **99**(6): 1134-48.

120. Gibellini F, Smith T. The Kennedy pathway--De novo synthesis of phosphatidylethanolamine and phosphatidylcholine. *IUBMB life* 2010; **62**(6): 414-28.

121. Vance JE. Phospholipid synthesis and transport in mammalian cells. *Traffic (Copenhagen, Denmark)* 2015; **16**(1): 1-18.

122. Croft S, Seifert K, Duchêne M. Antiprotozoal activities of phospholipid analogues. *Molecular and biochemical parasitology* 2003; **126**(2): 165-72.

123. Moitra S, Pawlowic M, Hsu F, Zhang K. Phosphatidylcholine synthesis through cholinephosphate cytidylyltransferase is dispensable in Leishmania major. *Scientific reports* 2019; **9**(1): 7602.

124. Catalá A. Lipid peroxidation of membrane phospholipids generates hydroxy-alkenals and oxidized phospholipids active in physiological and/or pathological conditions. *Chemistry and physics of lipids* 2009; **157**(1): 1-11.

125. Dudek J. Role of Cardiolipin in Mitochondrial Signaling Pathways. *Frontiers in cell and developmental biology* 2017; **5**: 90.

126. Blunsom N, Cockcroft S. CDP-Diacylglycerol Synthases (CDS): Gateway to Phosphatidylinositol and Cardiolipin Synthesis. *Frontiers in cell and developmental biology* 2020; **8**: 63.

127. K Zhang, S.M. Beverley. Phospholipid and sphingolipid metabolism in Leishmania. *Mol Biochem Parasitol* 2010; **170**(2): 55.

128. Mathur R, Das R, Ranjan A, Shaha C. Elevated ergosterol protects Leishmania parasites against antimony-generated stress. *FASEB journal : official*

publication of the Federation of American Societies for Experimental Biology 2015; **29**(10): 4201-13.

129. Guarnizo SG, Tikhonova E, Zabet-Moghaddam M, et al. Drug-Induced Lipid Remodeling in Leishmania Parasites. *Microorganisms* 2021; **9**(4): 790.

130. Yang X, Liang J, Ding L, et al. Phosphatidylserine synthase regulates cellular homeostasis through distinct metabolic mechanisms. *PLoS genetics* 2019; **15**(12): e1008548.

131. Signorell A, Gluenz E, Rettig J, et al. Perturbation of phosphatidylethanolamine synthesis affects mitochondrial morphology and cell-cycle progression in procyclic-form Trypanosoma brucei. *Molecular microbiology* 2009; **72**(4): 1068-79.

132. McConville M. The surface glycoconjugates of parasitic protozoa: potential targets for new drugs. *Australian and New Zealand journal of medicine* 1995; **25**(6): 768-76.

133. Martin K, Smith T. The glycosylphosphatidylinositol (GPI) biosynthetic pathway of bloodstream-form Trypanosoma brucei is dependent on the de novo synthesis of inositol. *Molecular microbiology* 2006; **61**(1): 89-105.

134. Ferguson M, Brimacombe J, Brown J, et al. The GPI biosynthetic pathway as a therapeutic target for African sleeping sickness. *Biochimica et biophysica acta* 1999; **1455**(2-3): 327-40.

135. desJardins-Park H, Foster D, Longaker M. Fibroblasts and wound healing: an update. *Regenerative medicine* 2018; **13**(5): 491-5.

136. Miranda M, Panis C, Cataneo A, et al. Nitric oxide and Brazilian propolis combined accelerates tissue repair by modulating cell migration, cytokine production and collagen deposition in experimental leishmaniasis. *PloS one* 2015; **10**(5): e0125101.

137. Freitas Ld, Hamblin M. Proposed Mechanisms of Photobiomodulation or Low-Level Light Therapy. *IEEE journal of selected topics in quantum electronics : a publication of the IEEE Lasers and Electro-optics Society* 2016; **22**(3): 7000417.

138. Croft S, Yardley V. Chemotherapy of leishmaniasis. *Current pharmaceutical design* 2002; **8**(4): 319-42.

139. Hamblin MR, Hasan T. Photodynamic therapy: a new antimicrobial approach to infectious disease? *Photochem Photobiol Sci* 2004; **3**: 436-50.

140. Demidova T, Hamblin M. Photodynamic therapy targeted to pathogens. *International journal of immunopathology and pharmacology* 2004; **17**(3): 245-54.

141. Soukos N, Ximenez-Fyvie L, Hamblin M, Socransky S, Hasan T. Targeted antimicrobial photochemotherapy. *Antimicrobial agents and chemotherapy* 1998; **42**(10): 2595-601.

142. Fonseca-Silva F, Inacio J, Canto-Cavalheiro M, Almeida-Amaral E. Reactive oxygen species production and mitochondrial dysfunction contribute to quercetin induced death in Leishmania amazonensis. *PloS one* 2011; **6**(2): e14666.

143. Deep D, Singh R, Bhandari V, et al. Increased miltefosine tolerance in clinical isolates of Leishmania donovani is associated with reduced drug accumulation, increased infectivity and resistance to oxidative stress. *PLoS neglected tropical diseases* 2017; **11**(6): e0005641.

144. Croft SL, Sundar S, Fairlamb AH. Drug resistance in leishmaniasis. *Clinical microbiology reviews* 2006; **19**(1): 111-16.